Dissertation

Influenza virus hemagglutinin contains a cholesterol consensus motif required for efficient intracellular transport and lipid raft integration

zur Erlangung des akademischen Grades

doctor rerum naturalium

(Dr. rer. nat.)

im Fach Biologie

eingereicht an der

Lebenswissenschaftlichen Fakultät

der Humboldt-Universität zu Berlin

von

Diplom-Biologin Maren de Vries

Präsident der Humboldt-Universität zu Berlin

Prof. Dr. Jan-Hendrik Olbertz

Dekan der Lebenswissenschaftlichen Fakultät

Prof. Dr. Richard Lucius

Gutachter: 1. Prof. Dr. Andreas Herrmann

2. PD Dr. Michael Veit

3. Prof. Dr. Klaus Osterrieder

eingereicht: 18.08.2015

Datum der Promotion: 20.11.2015

Table of content

Zusammenfassung

Das Hämagglutinin (HA) der Influenzaviren wird während der Assemblierung in Cholesterin- und Sphingolipid-reiche Domänen (Rafts) der Plasmamembran rekrutiert. Vorangehende Studien konnten mittels Fluoreszenzresonanzenergietransfer eine Raft-Integration nachweisen, die von zwei Raft-Zielsignalen abhängig war; zum einen von drei S-acylierten Cysteinen in der zytoplasmatischen Domäne und zum anderen von hydrophoben Aminosäuren (VIL) am Beginn der Transmembrandomäne (TMD). Zudem zeigte sich ein möglicher Einfluss des VIL-Motives auf den intrazellulären Proteintransport. Um diese Annahme zu bestätigen, wurden HA Mutanten in Zellen exprimiert und ihre Ankunft im medialen und trans-Golgi verfolgt. In dieser Arbeit konnte eine Beteiligung des VIL-Motives am Transport bestätigt werden, jedoch nicht der S-Acylierungen. Zudem wurde eine generelle Abhängigkeit des Transportes von der Sphingolipidsynthese beobachtet. Da sowohl die Cholesterinsynthese als auch die Sphingolipidsynthese für den Transport von HA benötigt werden, habe ich die Hypothese aufgestellt, dass das VIL-Motiv in der Lage sein könnte, mit Raft Lipiden zu interagieren. Ein Sequenzvergleich ergab, dass kein Sphingolipid-Bindemotiv vorhanden ist, jedoch ein potenzielles Cholesterin-Consensus-Motiv (CCM, <u>W</u>/Y-I/V/<u>L</u>-<u>K</u>/R). Dieses Motiv wurde nur in der Sequenz von Gruppe 1 jedoch nicht Gruppe 2 HAs gefunden und umfasst das Leucin des VIL Motives. Tatsächlich ist die Mutation des Leucins aber nicht des vorangehenden Isoleucins für den verzögerten Transport verantwortlich. Untersuchungen weiter Einzel- und Mehrfachmutanten konnten eine Abhängigkeit des intrazellulären Transportes von einer möglichen Cholesterinbindung verifizieren. Zudem konnte auch ein zunehmender Effekt auf die Kinetiken vom medialen Golgi zum TGN beobachtet werden, welcher auch die Oberflächenexpression negativ beeinflusste. FLIM-FRET Analysen zeigten zusätzlich eine reduzierte Raft Assoziation der CCM-Mutanten mit Rafts an der Plasmamembran. Daher kann man spekulieren, dass HA mit Cholesterin interagiert, wodurch sein intrazellulärer Transport durch den Golgi und die Assoziation mit Rafts gewährleistet wird.

Schlagwörter: Influenza Virus, Hämagglutinin, Transport, Cholesterin-Consensus-Motiv

Summary

During assembly the hemagglutinin (HA) of influenza viruses is recruited to cholesterol- and sphingolipid rich domains of the plasma membrane (lipid rafts). Preceding studies using fluorescence resonance energy transfer showed that lipid-raft integration is dependent on two raft-targeting signals, three S-acylated cysteines located in the cytoplasmic tail and hydrophobic amino acids (VIL) in the part of the transmembrane region (TMR). Furthermore, they gave rise to the assumption that at least the VIL motif might also be important for the intracellular transport of the protein along the exocytic pathway. To verify this assumption, HA mutants were transiently expressed in cells and their arrival in the medial and trans-Golgi compartment was quantified. The observation regarding the involvement of the VIL motif, but not the S-acylation, was verified and a general dependency of HA´s transport on sphingolipid synthesis was detected. Since both cholesterol and sphingolipid synthesis are needed for the transport of HA, I hypothesized that the VIL motif might be able to interact with raft lipids. Sequence alignment revealed no sphingolipid-binding motif, but a putative cholesterol consensus motif (CCM, W/Y-I/V/L-K/R). This CCM is found only in the sequence of group 1 but not group 2 HAs and includes the leucine of the VIL motif. Indeed, mutation of the leucine, but not of the preceding isoleucine is responsible for the delayed transport. Investigation of further single and multiple mutations in the CCM verified a dependency of HA´s intracellular transport on the putative cholesterol-binding motif. Additionally the effect on the kinetics increased from the medial Golgi to the TGN also negatively effecting surface expression. Analysis by FLIM-FRET furthermore displayed a reduced association of HA with mutations in the CCM with lipid rafts at the plasma membrane. Therefore, it is speculated that HA associates with cholesterol, an interaction that facilitates its intracellular transport through the Golgi and association with lipid rafts at the plasma membrane.

Key words: Influenza virus, hemagglutinin, transport, cholesterol consensus motif

Abbreviations

AA	Amino acids
APP	Amyloid precursor protein
CCM	Cholesterol consensus motif
Cer	Cerulean
CG MD	Coarse-grained molecular dynamics
CHO	Chinese hamster ovary cells
CIP	Calf intestinal alkaline phosphatase
CLSM	Confocal laser scan microscopy
COPI	Coat protein complex I
CRAC	Cholesterol Recognition/ interaction Amino acid Consensus sequence
CRM1	Chromosomal maintenance 1
DMEM	Dulbecco's Modified Eagle Medium
DRM	Detergent resistant membrane
Endo-H	Endoglycosidase-H
ER, rER	Endoplasmatic reticulum
ESR	Electron spin resonance
FACS	Fluorescence activated cell sorting

FBS	Fetal bovine serum
FLIM	Fluorescence lifetime imaging microscopy
FPALM	Fluorescence Photoactivation Localization Microscopy
FPV	Fowl plague virus
FRET	Fluorescence resonance energy transfer
GalT	Galactose transferase
GFP	Green fluorescent protein
GlcNAc	N-acetyl glucosamine
GluCer	Glucosylceramide
GMPV	Giant plasma membrane vesicle
GPCR	G protein-coupled receptor
GPI	Glycosylphosphatidylinositol
GSL	Glycerosphingolipids
HA	Hemagglutinin
HAT	Human airway trypsin-like protease
HIV	Human immunodeficiency virus
HMG-CoA	3-hydroxy-3-methylglutary-coenzyme A
HRP	Horseradish peroxidase

IF	Immunofluorescence	PMT	Photomultiplier tube
IRF	Instrument response function	PS	Phosphatidylserine
LCP	Lipid cubic phase	QY	Quantum yield
M1	Matrixprotein 1	RE	Restriction enzyme
M2	Matrixprotein 2	RIPA	Radioimmunoprecipitation assay buffer
MDCK	Madin-darby canine kidney cells		
MEM	Minimal Essential Medium	RNA	Ribonucleid acid
NA	Neuraminidase	RSV	Respiratory syncytial virus
NDV	Newcastle disease virus	SDS-PAGE	Sodium dodecyl sulfate poly-acrylamide gel electrophoreses
NLS	Nuclear localization signal	SFV	Semliki-Forest virus
NMR	Nuclear magnetic resonance	SM	Sphingomyelin
NP	Nucleoprotein	SPAD	Single photon avalanche photo-diode
NS1, NS2	Non-structural protein 1 and 2		
PA	Polymerase acidic protein	SPT	Serine palmitoyltransferase
PB1	Polymerase basic protein 1	TCSPC	Time-correlated single-photon counting
PB2	Polymerase basic protein 2		
PBS	Phosphate buffered saline	TGN	Trans-Golgi-network
PC	Phosphatidylcholine	TMPRRS2	Transmembrane protease, serine
PCR	Polymerase chain reaction	TMR	Transmembrane region
PE	Phosphatidyletholamine	VLP	Virus-like particle
PFA	Paraformaldehyde	vRNP	Viral ribonucleoproteincomplex
BSA	Bovine serum albumin	VSV	Viscular stomatitis virus
PI	Phosphatidylinositol	WT	Wild type
		YFP	Yellow fluorescent protein

Amino acids

A	Ala	Alanine
C	Cys	Cysteine
D	Asp	Aspartic acid
E	Glu	Glutamic acid
F	Phe	Phenylalanine
G	Gly	Glycine
H	His	Histidine
I	Ile	Isoleucine
K	Lys	Lysine
L	Leu	Leucine
M	Met	Methionine
N	Asp	Asparagine
P	Pro	Proline
Q	Gln	Glutamine
R	Arg	Arginine
S	Ser	Serine
T	Thr	Threonine
V	Val	Valine
W	Trp	Tryptophan
X	Xaa	any random amino acid
Y	Tyr	Tyrosine

1 Introduction

1.1 Influenza viruses

1.1.1 Taxonomy

Influenza viruses, the Thogoto virus and the Isavirus belong to the family Orthomyxo-viridae. Viruses of this family are enveloped viruses with a single stranded, segmented RNA genome in negative orientation. We can distinguish three genera of influenza virus, influenza virus A, B and C. The classification is based on the serological differences of the nucleoprotein (NP) and the matrixprotein (M1). Additionally, influenza A viruses are further subdivided into subtypes due to the antigenic properties of their surface proteins hemagglutinin (HA) and neuraminidase (NA). So far 16 classical HA subtypes (H1-H16), 2 non-classical subtypes (H17 & H18), 9 classical NA subtypes (N1-N9) and 2 non-classical subtypes (N10, N11) have been described, whereby all classical subtypes can be found in wild birds, while the non classical subtypes are found in bats [1−4].

Orthomyxoviruses are transmitted mainly by aerosol transmission and infect, depending on the host, the respiratory tract (mammals) or the gastrointestinal tract (birds) Influenza A viruses have the broadest host range of all three influenza viruses infecting mammals like humans, swine, horses and wales as well as birds, whereby the primary host reservoir of influenza A viruses are wild aquatic birds [5]. Influenza B viruses could be isolated from humans and seals [6], whereas influenza C viruses infect human and swine [7,8].

1.1.2 Morphology and proteins

Influenza viruses have a pleomorphic shape with filamentous particles in field isolates and a spherical shape of about 100 nm diameter in cell culture. The virus particle has a lipid envelope that derives from the plasma membrane of the host cell [9]. Into the lipid envelope three viral proteins are embedded: mainly the two glycoproteins hemagglutinin (HA) and neuraminidase (NA) and to lower extent the matrix protein 2 (M2). Hemagglutinin is forming a homotrimer [10] and is responsible for the receptor bind-

ing and the fusion of the viral with the endosomal membrane [11,12], while neuraminidase is a homotetrameric complex and performs cleavage of the host cell receptor [13]. The two glycoproteins rise about 10 nm over the membrane [14]. Influenza C viruses posses only one surface glycoprotein the HEF, which combines the functions of the HA and NA [15,16]. Like NA, the M2 protein forms a homotetramer but functions as a proton channel [17–19]. By comparison, influenza B viruses have the NB protein [20] and influenza C viruses the CM2 protein [21]. The inner side of the lipid envelope is coated with the matrix protein 1 (M1). The segmented RNA genome associates over its full length with the nucleoprotein (NP) and segments form helical capsids by the annealing of complementary sequences at the 3'- respectively the 5'-end of the RNA [22,23]. Each encapsidated segment is coupled to the polymerase complex, which comprises the proteins PB1, PB2 and PA and binds the annealed complementary end region. The complex of the RNA, NP and the polymerase is called viral ribonucleoproteincomplex or vRNP and interacts with the M1 protein within the virus particle.
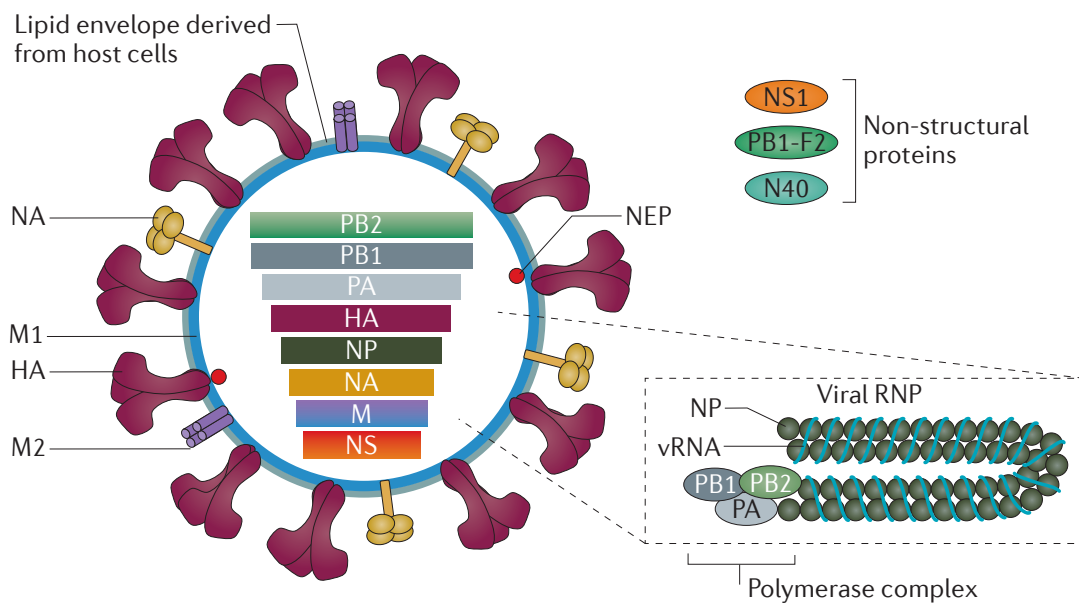
Figure 1-1: Schematic view of a typical influenza A virus particle, including the non-structural proteins and the structure of a model vRNP Reprinted by permission from Macmillan Publishers Ltd: [Nature Reviews Microbiology] [24], copyright 2011

Additionally, small copy numbers of the nuclear export protein NEP/NS2 are incorporated into the virion. The genome of influenza A viruses also encodes for several non-structural proteins, like the non-structural protein 1 (NS1), the PB1-F2 and N40. NS1 is translated from the unspliced mRNA of segment 7, while NEP/NS2 is translated from

a splice variant. NS1 has multiple functions by interacting with other proteins as well as with RNA, thereby antagonizing the cellular immune response and blocking the splicing, polyadenylation and export of cellular mRNAs (reviewed in [25]). PB1-F2 is translated by an alternate +1 open reading frame within PB1 and is a multifunctional protein with proapoptotic functions [26–29], the ability to deregulate the innate immune response [30,31], the ability to regulate polymerase activity [32,33] and an enhancing effect on secondary bacterial infection [34–36]. N40 is a truncated version of PB1 starting with the 5th start codon by leaky ribosome scanning and is important for the interdependent expression of PB1, PB1-F2 and PB1-N40 [37,38]. In the recent years, more proteins were discovered. Truncated variants of the PA protein [39] as well as an M2 variant [40] were found, but their function is still elusive. A +1 frame shift product of PA, the so-called PA-X protein, is the only one so far, being further characterized. It functions as an endonuclease being responsible for the degradation of cellular mRNA leading to a host cell shut off [41,42].

1.1.3 Replication cycle

Upon absorption of HA to its receptor α-2,6 or α-2,3 linked sialic acids (human receptor or avian receptor) [43,44] the virus is internalized into early endosomes. Interestingly, influenza viruses can enter by different routes. Either via clathrin-mediated endocytosis, clathrin- and caveolin-independent endocytosis [45] or macropinocytosis [46]. After internalization the virus particles are transported within the endosomes towards lysosomes, whereby fusion already occurs after acidification of the late endosome before reaching the lysosomes [47]. In detail, they are first transported in an actin dependent manner to the early endosomes, and then the endosomes are transported in a microtubule-dependent manner to the perinuclear region, where they are finally maturing to late endosomes. This is accompanied by the acidification of the lumen of the endosomes, which triggers a conformational change in the HA molecule, exposing the fusion peptide [48,49], which leads to the fusion of the endosomal and viral membrane. In addition, acidification of the endosome opens the proton channel M2 [19] leading to a decrease in pH inside the virion, facilitating the detachment of M1 from the vRNPs in order to release the vRNPs into the cytoplasm [50,51]. Due to their nuclear localization signals (NLS) the vRNP are then imported into the nucleus [52–

54]. Inside the nucleus, transcription begins by the RNA dependent RNA Polymerase complex of PB1, PB2 and PA. For the production of viral mRNA influenza viruses use the so-called "cap-snatching". PB2 binds to cellular caps [55,56], while PA "snatches" the cap via its endonuclease [57] activity and PB1 facilitates the actual synthesis of the viral mRNA from the vRNA [58]. Due to an uridin-rich stretch near the 5'end of the vRNA the polymerase stalls and polyadenylates the mRNA, allowing translation by cellular ribosomes [59,60]. Segment 7 and 8 additionally are spliced in the nucleus, each resulting in two mRNAs coding for M1 and M2, respectively NS1 and NEP/NS2. The mRNAs are then subsequently exported from the nucleus to the cytoplasm, where in the early stage of the infection the proteins of the polymerase complex, NP, NS1, NS2 and M1 are transcribed by free ribosomes. Due to their nuclear localization signals (NLS), they are transported back into the nucleus to perform their function in transcription and the formation of new vRNPS.
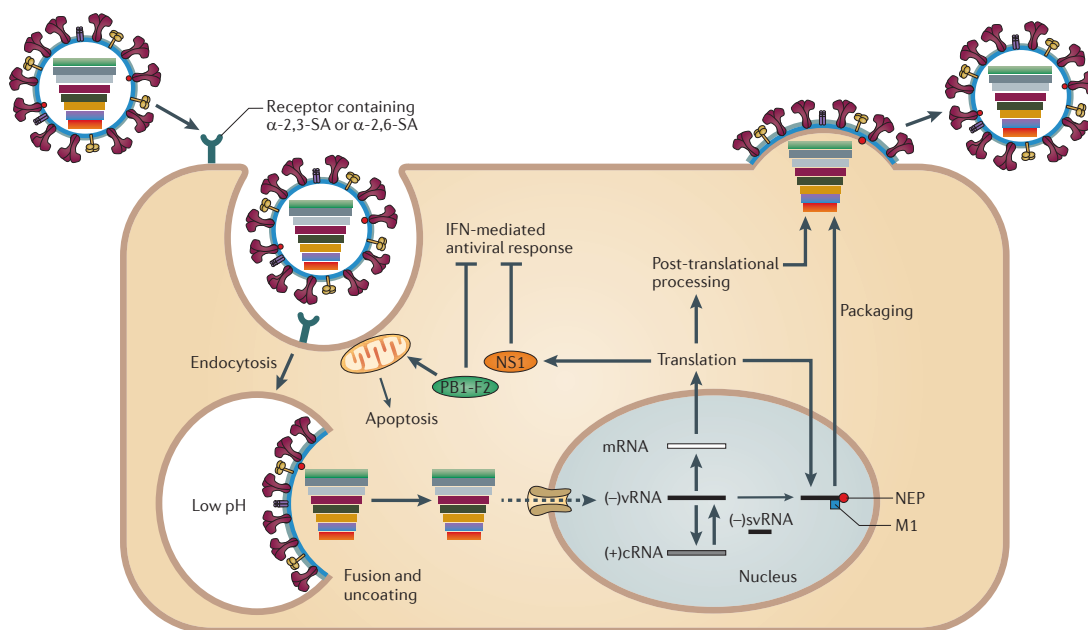
Figure 1-2: Replication cycle of influenza A viruses Reprinted by permission from Macmillan Publishers Ltd: [Nature Reviews Microbiology] [24], copyright 2011

HA, NA and M2 are translated by membrane bound ribosomes at the rough endoplasmic reticulum (rER), to be further transported to the plasma membrane along the exocytic pathway via the Golgi while being co- and posttranslationally modified. This includes glycosylation of HA and NA, and palmitoylation of HA [61] and M2 [62,63].

Besides mRNA, the polymerase complex also transcribes complementary RNA (cRNA) which serves as template for the synthesis of new full length viral RNA. The switch from mRNA to cRNA synthesis is thought to be initiated by small negative sense viral RNAs (svRNA) [64,65]. Newly synthesized vRNA then associates with NP and the polymerase complex to form new vRNP complexes, which then bind to M1 and NEP/NS2 to be exported from the nucleus by the cellular export factors Ran-GTP/CRM1 [66–69]. The exported vRNPs then bind to Rab11 on recycling endosomes in order to use the cellular transport system for vesicles, which in turn is using the microtubule system [70–73] for the transport to the plasma membrane. The assembly of new virions takes place at special membrane domains the so-called lipid rafts. HA and NA enrich in those domains [74–77], where they interact with M1 via their cytoplasmic tails [78–80], thereby leading the bound vRNPs to the site of budding. The right incorporation of the eight segments requires packaging signals, which are located at the 3' and 5' untranslated region of the gene segments and assure packaging of all eight needed segments [81–83]. The final scission of the virion is believed to be mediated by the viral M2 protein [84,85]. During the budding process, the neuraminidase cleaves off the sialic acids from the glycoproteins to avoid the agglutination of newly released viruses with each other and the reinfection of already infected cells. Not only is the neuraminidase important to cleave the bond between newly synthesized virions and the prior infected cell, it is also important for the entry in the airway. The ciliated airway epithelium is covered with mucines and cellular glycocalix on which sugars with terminal sialic acids are exposed, therefore leading to binding of influenza viruses before they are able to infect their target cells. Neuraminidase cleaves off these sialic acids as well, to enable the infection of the epithelium cells [86].

1.2 The glycoprotein hemagglutinin (HA)

1.2.1 Structure and function of HA

Hemagglutinin of influenza A viruses is a type I membrane protein with an ectodomain of about 525 amino acids (AA), a transmembrane region of 27 AA and a C-terminal domain of 11 AA. It forms a trimeric complex, which extends 135 Å from the membrane. In Figure 1–3 a monomer of HA is displayed. The precursor HA_0 is cleaved
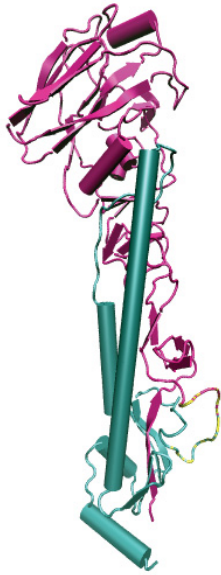
Figure 1–3: Chrystal structure of a HA monomer HA₁ in magenta, HA₂ in cyan, loop with cleavage site in yellow. Created with Visual molecular dynamics (VMD) 1.9.1 and POV-Ray 3.7.0 from PDB code 1HA0

during the replication cycle into its subunits HA$_1$ and HA$_2$ (displayed in magenta and cyan, respectively), that stay linked by a disulfide bond. This cleavage takes place at either a monobasic or multibasic cleavage site located in a loop at the base of the molecule (yellow). The cleavage site of HA$_0$ determines the pathogenicity of the virus in avian influenza. A monobasic cleavage site with a single arginine is cleaved by extracellular trypsin-like proteases [87], which limits the permissive cells to tissue expressing the suitable protease. In avian hosts, the replication is limited to the respiratory- and gastrointestinal tract, while in humans only cells of the respiratory tract can be infected. So far, the tryptase Clara in rat bronchiolar epithel Clara cells [88], the Factor Xa in embryonated chicken eggs [89,90] and HAT and TMPRRS2 in human bronchial tissue [91] have been described to perform the cleavage of monobasic HA. Contrary to monobasic cleavage sites, which can occur in all 16 classical HA subtypes, multibasic cleavage sites with the sequence R-X-K/R-R-G occur only in H5 and H7 subtype HAs and are cleaved by intracellular proteases like furin and PC6 already in the *trans*-Golgi network [92,93]. The ubiquitous presence of the proteases leads to a systemic infection of the host and therefore a severe course with a fatal outcome in infected poultry.

HA has several functions during the replication cycle. HA$_1$ mainly forms the globular head in which the antigenic variable parts and the receptor-binding site are located. The receptor binding site is build by specific secondary structures, the 190 helix (residues 188-195), that binds the upper part of the receptor, the 130 loop (residues 134-138), which binds the right side, the 220 loop (residues 221-228), which binds the left part and additional binding of Tyr 98, Trp 153, His 183 and Tyr 185 (H3 numbering) from the bottom [94]. The linkage of the terminal sialic acids, to which HA binds, determines the host specificity. While avian hosts mainly express α-2,3-linked sialic acids, humans express α-2,6-linked sialic acids in their upper respiratory tract and tra-

chea, which are the main entry routes for influenza viruses (see figure S2 in [93]). The expression of α 2,3-linked sialic acids in the lower respiratory tract is associated with fatal cases in humans with avian viruses like H5N1. Pigs for example, posses both receptor types in their airway and therefore can be infected by avian and human viruses at the same time and hence can serve as mixing vessels. In case of a double infection of one cell with two viruses it can lead to the formation of reassortant viruses, which then again exhibit features of both parental viruses and can lead to the formation of new pandemic virus strains [96]. HA_2 is forming the stem of the protein by a coiled-coil structure of the helices and comprises the transmembrane region and the cytoplasmic tail. The N-terminal end of HA_2 forms the fusion peptide after cleavage, which is the key player in the fusion of the viral membrane with the endosomal membrane during entry of the virus. By the influx of protons due to the M2-ion channel activity, HA undergoes a structural change, which finally leads to the exposure of the fusion peptide, which then integrates into the endosomal membrane [49]. By a second structural change the two membranes are brought in near proximity leading to hemifusion and finally full fusion of the two membranes [97]. The transmembrane region and the cytoplasmic tail have functions in the assembly of new virions, which will be described in more detail in the following parts.

1.2.2 Processing and transport of hemagglutinin

HA is synthesized as the precursor HA_0 at the rough endoplasmic reticulum (rER) due to its N-terminal signal peptide, which is cleaved off co-translationally. Processing of HA starts as well in the lumen of the rER with the attachment of a high-mannose core oligosaccharide consisting of two N-acetyl glucosamines (GlcNAc), nine mannoses and three glucoses to the amid nitrogen of the asparagine of the consensus sequence N-X-T/S, whereby X can be any amino acid except proline [98]. The glycosylation is needed for the proper folding of the peptide chain and thus for the trimerization of the fully translated protein [99–101]. Aberrant trimers with the wrong quaternary structure of the protein will be retained in the ER, which is true for approximately 10% of HA_0 [102]. After attachment of the core oligosaccharides, they are then further trimmed along the exocytic pathway. Initial trimming occurs still within the ER by cleaving off the three glucoses, which is followed in the *cis-* to medial-Golgi by cleavage of the

mannoses (except three) and the attachment of N-acetyl glucosamines resulting in a more complex oligosaccharide, which no longer can be cleaved by the endoglycosidase Endo-H. Since the N-acetyl glucosamine transferase is located in the medial Golgi, resistance of carbohydrates to Endo-H cleavage is a convenient and reliable tool to measure arrival of a glycoprotein in this compartment. In the *trans*-Golgi network finally galactose, fucose and sialic acis are attached, whereby sialic acids gets cleaved off directly by the neuraminidase, resulting in the fully glycosylated protein. FPV HA has seven glycosylation sites, five in its HA_1 subunit (Asn 12, 23, 28, 123 and 149) and two in HA_2 (Asn 406 and 478), whereby two of the seven glycosylation sites remain unprocessed [99,100]. But it needs to be stated, that the number and location of glycosylation sites are highly variable among subtypes.

Additionally, HA gets S-acylated at three cysteines [61], one fatty acid is located at the boundary of the TMR with the cytoplasmic tail and two in the cytoplasmic tail. Interestingly, depending on their location [103], the two cysteines in the cytoplasmic tail are palmitoylated, while the cysteine at the boundary to the TMR is mostly stearoylated [104], depending on the host [103]. The S-acylation is located between ER and *cis*-Golgi, whereby it is unknown if it occurs in the late ER, in the transport vesicles from ER to Golgi or in the *cis*-Golgi [105], due to the fact that trimerization is completed but not trimming of the carbohydrates.

Moreover, as described in 1.2.1 the highly pathogenic HA subtypes H5 and H7 are cleaved in the *trans*-Golgi network into their subunits HA_1 and HA_2 before they are transported to the plasma membrane, the site of assembly and budding. This cleavage is facilitated by the protease Furin. Furin itself is a protein, which undergoes proteolytic maturation before acquiring its full functionality. After synthesis in the ER the signal peptide is removed and the propeptide gets removed. After these cleavages furin enters the Golgi, where it gains full functionality. Within the TGN its carbohydrates acquire sialic acid and the fully matured protein gets enriched [106] via a retention signal [107]. Cleavage of HA occurs after acquisition of Endo-H resistant carbohydrates but before the attachment of galactose and sialic acids, therefore in the medial and *trans*-Golgi [106,108]. Despite its retention signal to the TGN, furin can also be transported to the cell surface and recycled via endosomes back to the TGN [107,109]

allowing late cleavage of HA within transport vesicles to the plasma membrane as well.
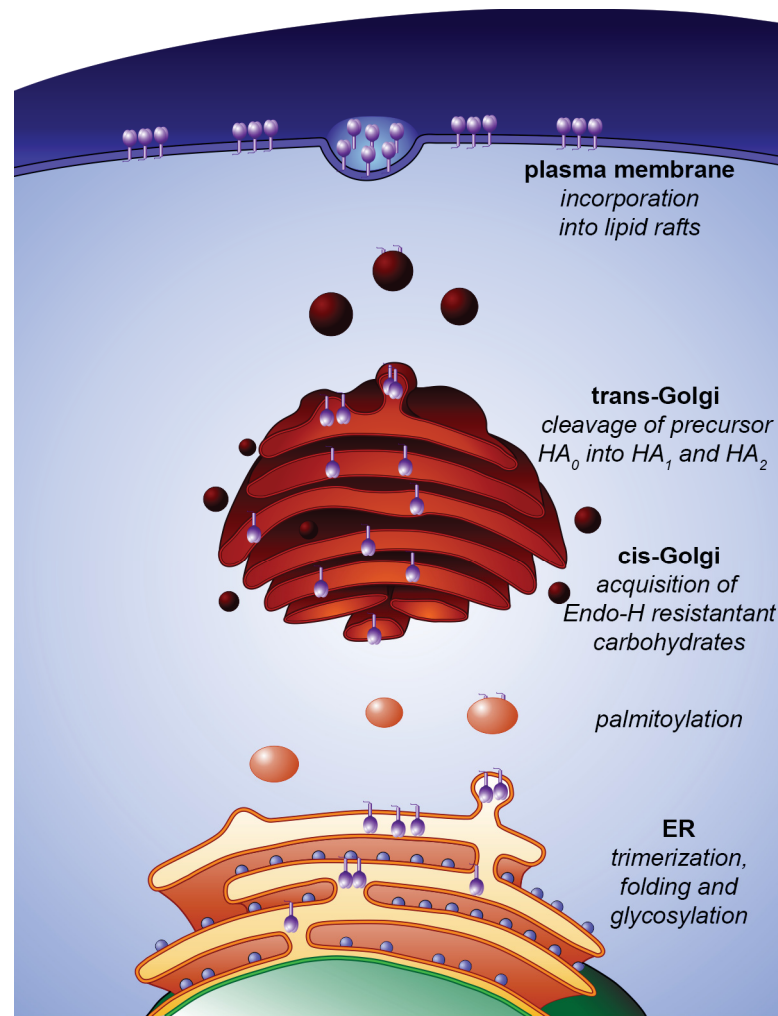
Figure 1-4: Transport of HA along the exocytic pathway. HA_0 is synthesized as the precursor HA_0 at the rough endoplasmatic reticulum (rER). After trimerization, folding and initial glycosylation it is palmitoylated on its way to the *cis*-Golgi, where it acquires its final glycosylation. Subsequently, the precursor HA_0 is cleaved by furin into its subunits HA_1 and HA_2 in the *trans*-Golgi. Upon transport to the plasma membrane it is incorporated into lipid rafts. Created with CorelDRAW.

1.2.3 Assembly

The assembly of influenza viruses is a multistep process, which involves several protein-lipid and protein-protein interactions. The function of hemagglutinin in this process is the definition of the budding zone by integration into so-called lipid rafts; specialized membrane domains that are enriched in sphingomyelin and cholesterol (see 1.4 for further details). HA and NA are targeted to the lipid rafts via internal raft-targeting signals and thus building the assembly site. The integration of these two gly-

coproteins is already sufficient to induce the budding process. As shown in transfected cells, co-expression of HA and NA or expression of HA and exogenous NA facilitate generation of VLPs (virus like particles) that are similar to virus particles in their size [110].

Once HA and NA determine the site of assembly, M1 is recruited to the assembly site in dependence on the presence of the cytoplasmic tails of HA and NA [110], where it builds the bridge between the glycoproteins and the internal virus components. It was shown that M1 binds membranes by several different weak interactions [111–113]. Additionally, by indirect methods interactions with HA and NA were detected [80,114,115]. As described in 1.1.3 M1 also binds the vRNPs, thereby leading them to the budding site. The interaction with M2 in contrast could be verified by co-immunoprecipitation experiments [116,117]. Interestingly, M2 is not only intrinsically targeted to the plasma membrane, but is also targeted to the assembly site by interaction with HA, as it is not integrated into lipid rafts but to the edge of them [118]. When all virus proteins are assembled at the budding site, M2 finally performs the scission of the particle, whereby it is also responsible for the filamentous particle shape that can be observed in human isolates [85,119].

1.3 Composition of cellular membranes

The first model of the structure of cellular membranes was postulated by Singer and Nicolson in 1972 by proposing the "fluid mosaic model" [120]. In this model, they describe for the first time that membranes have a lipid matrix in which proteins are integrated in a randomly distributed manner. This model has been revised and enhanced in many aspects. Not only are lipids not randomly distributed, but they can form lateral clusters in the membrane [121]. In addition, lipids show an asymmetry in their location between the inner and the outer leaflet. Besides, different cellular compartments like the ER and Golgi exhibit different lipid compositions. Most lipids are synthesized at the ER, like phospholipids (phosphatidylcholine PC, phosphatidylethanolamine PE, phosphatidylserine PS and phosphatidylinositols PIs) [122] and cholesterol [123].
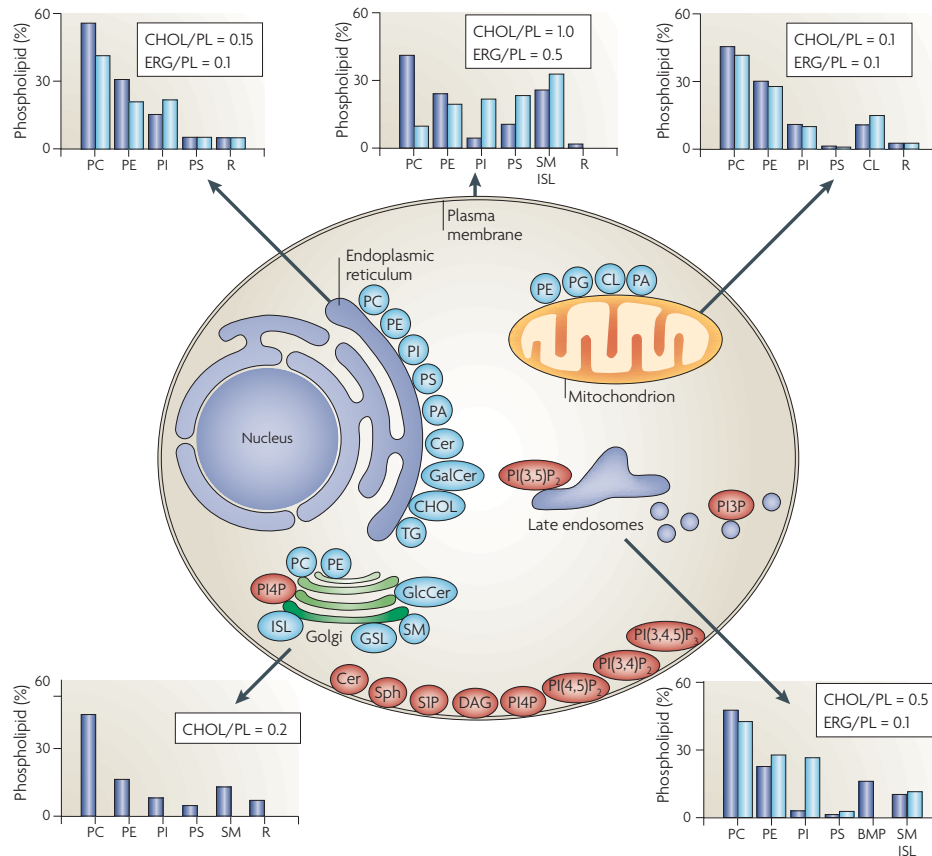
Figure 1-5: Lipid synthesis and steady-state composition of the different cell membranes

Sight of lipid synthesis is shown in the picture (major lipids in blue, signaling lipids in red). Lipid composition of the different membranes is displayed in bar graphs (mammals in blue, yeast in light blue). Reprinted by permission from Macmillan Publishers Ltd: [Nature Reviews Molecular Cell Biology], [124] copyright 2008

Although cholesterol synthesis starts in the cytoplasm by the conversion of acetyl-CoA to acetoacetyl-CoA, which then is condensed by the 3-hydroxy-3-methylglutaryl (HMG)-CoA synthase to HMG-CoA, the main steps of the synthesis of cholesterol are located to the ER and peroxisomes. HMG-CoA is reduced by the ER localized HMG-CoA reductase (still on the cytosolic site) to mevalonate, which then in turn gets metabolized to farnesyl-diphosphate by enzymes located in the peroxisome. Farnesyl-PP is then converted to squalene by the squalene synthase that again is located to the membrane of the ER. The squalene synthase is believed to obtain the substrate from the cytosol and release the hydrophobic product into the membrane. Following, squalene is transformed to lanosterol, which subsequently is converted to cholesterol. It needs to be stated that steps of the conversion of lanosterol to cholesterol is also believed to be performed in peroxisomes, which is why cycling of the precursors of cho-

lesterol between ER and peroxisomes is the favored model of the location of cholesterol synthesis. The process of cholesterol synthesis is highly regulated. When cholesterol levels in the cells are low, it is sensed and a cascade is activated leading to the transcription of genes (i.e. encoding the HMG-CoA reductase) involved in cholesterol biosynthesis. When cholesterol levels are reaching a specific threshold again, the cascade is blocked and the transcription stops again (reviewed in [125]). While the phospholipids are the most abundant lipids in the ER membrane, the cholesterol content is only low (1 %) [126]. As the plasma membrane is the largest pool of cholesterol, the lipid needs to be transported to it efficiently. Although the transport is still not completely solved, it was reported that in mammalian cells the transport occurs rapidly with a half-time of 10-20 min [127]. Only about 20 % of the cholesterol is transported along the exocytic pathway [128], whereby cholesterol content increases along it, while the remaining 80 % are believed to be transported by non-vesicular lipid transfer [129]. Sphingolipid synthesis only starts at the ER by producing the backbone ceramide, but the lumen of the Golgi is the main location of the production of the head groups to produce sphingomyelin (SM) and glycerosphingolipids (GSL) like glucosylceramide (GluCer) [130–132], therefore reducing the phospholipid content. Likewise cholesterol, the sphingolipid content increases within the Golgi and in the plasma membrane.

Not only is there a gradient of cholesterol and sphingolipid content from ER to the plasma membrane, but also within a membrane of a compartment we can find a asymmetric lipid distribution between the two leaflets of a membrane that can be maintained by translocating specific lipids [124]. While the ER membrane exhibits equilibrium of membrane lipids, the Golgi and plasma membrane are using transporters to generate and maintain an asymmetry between the cytosolic and the luminal (extracellular) leaflet. This process is important for the functionality of the cell. For example, if PS is exposed on the cell surface it triggers phagocytosis and is a marker for apoptosis, as PS is actively transported by a scramblase to the outer leaflet upon activation by caspase 3 and 7 in the apoptotic process (reviewed in [133]). Additionally, active transport of lipids might be required for vesicle formation (reviewed in [134]). Already in the Golgi PS and PE are actively transported to the cytosolic side by a flippases called P4 ATPases (reviewed in [124,134]). That leads to an increased level of PE

and PS in the cytosolic leaflet and an increase of PC, GSL and SM in the extracellular leaflet of Golgi membranes. Due to the lack of an active transport from the luminal to the cytosolic side [135,136], only the precursor glucosylceramide (GlcCer) can be actively transported from the cytosolic side to the luminal side [137]. By increasing the amount of PE and PS having a small headgroup in the inner leaflet a negative curvature is induced, which is accompanied by the induction of a positive curvature on the outer leaflet by the increasing amount of lipids with a big headgroup like SM and cylindrical lipids like PC, thus facilitating vesicle formation. The same is true for the plasma membrane, where as well P4 ATPases transport PS and PE from the extracellular leaflet to the cytosolic leaflet [138]. This is accompanied by transport of ABC transporters, which are able to transport PC, PE, SM and GlcCer from the cytosolic side to the extracellular side (reviewed in [139]).

The plasma membrane itself can also exhibit differential lipid compositions depending on its function. Epithelial cells line cavities within the body and can be found for example in the lung or the gastrointestinal tract, where they polarize to form basal, lateral and apical membrane domains. Tight junctions separate basolateral and apical membrane domains from each other and limit the lipid exchange between them, but only in the cytoplasmic and not the extracellular leaflet [140]. Simons and Van Meer postulated the hypothesis of a lateral lipid asymmetry in 1988 withi the plasma membrane while investigating the sorting of lipids regarding their presence in apical or basolateral membranes of polarized epithelial cells (MDCK, Madin-Darby canine kidney cells) [140]. While basolateral membranes have a similar lipid composition as non-polarized cells, apical membranes are enriched in glycosphingolipids accompanied by a loss in PC (only 8 % of the phospholipids). The ratio of glycosphingolipids to phospholipids and cholesterol in apical membranes is 1:1:1, while basolateral membranes consist of 50 % phospholipids (of which 30 % is PC), 20 % glycosphingolipids but also 30 % of cholesterol. To explain this sorting of lipids Simons and van Meer hypothesized that glycosphingolipids form cluster within the extracellular leaflet already in the Golgi. These clusters can from vesicles that are transported to the apical membrane in which proteins can be sorted for directed transport from the Golgi to the apical side of the cell. As a reason for this lipid sorting, Simons and van Meer mention

that the high content of glycolipids might be beneficial for the stability of the apical membrane.

1.4 Lipid rafts

Based on the previous findings, Simons later on further defined these specialized clusters as lipid rafts, which are membrane patches in the outer leaflet that are enriched in sphingolipids and cholesterol [141]. The cholesterol is thereby filling in the voids between the sphingolipids that are caused by their bulky head groups. The inner leaflet is built by unsaturated phospholipids, whereby cholesterol is also filling in the space between interdigitating lipids. From studies with model membranes we learned that lipid membranes can exist in different physical states, which are defined by the lateral arrangement of the lipids and their mobility within the membrane, like rotation, lateral and transversal diffusion. The liquid disordered phase is thought to be equivalent to the physical state of biological membranes like the plasma membrane, where they are building the non-raft domains. In this state lipids exhibit a high range of dynamic and mobility of the fatty acids. By increasing the cholesterol content, liquid disordered phases are built.
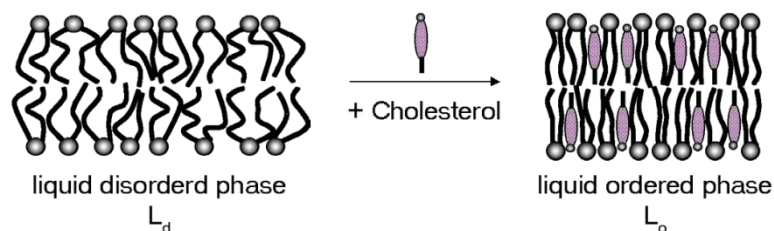
Figure 1-6: Phase transition from liquid disordered phase to liquid ordered phase. Incorporation of cholesterol and sphingolipids leads to a higher order of the saturated fatty acids and an overall increased thickness of the membrane (Adapted from [142]).

Additionally, phospholipids with unsaturated fatty acids are excluded and the amount of sphingolipids and phospholipids with saturated fatty acids increases (reviewed in [142]). The stabilizing effect of the cholesterol then in turn results in an elongated conformation of the saturated fatty acids, which leads to an increase in membrane thickness and consequently the formation of raft domains (Figure 1-6).

While in polarized cells the apical membrane is rich in lipid rafts, the basolateral membrane and non-polarized cells only exhibit a few raft clusters (see Fig. 2 in [141]), which supports the theory of Simons and van Meer from 1988, that lipid rafts are enriched in the apical membrane to increase stability. The official definition of rafts as "small (10–200 nm), heterogeneous, highly dynamic, sterol- and sphingolipid-enriched domains that compartmentalize cellular processes" was restated at a Keystone Symposium in 2006. They further defined that these "small rafts can sometimes be stabilized to form larger platforms through protein-protein and protein-lipid interactions" [143]. These platforms than can be used for cell signalling [144] or as sites for assembly and budding of many enveloped viruses (see 1.5 for detailed information).

1.4.1 Raft like structures in the exocytic pathway: Export domains

Simons and other researchers, proposed that membrane rafts already emerge in the TGN [145–147]. Their hypothesis relies on lipid sorting in the Golgi. The cholesterol content is increasing from *cis*- to *trans*-Golgi, which favours incorporation of proteins with longer TMDs that associate more easily into the thicker bilayer of rafts. This goes along with retrograde transport of COPI vesicles, having less sphingomyelin and cholesterol and therefore enriching these lipids on the trans side of the Golgi [148]. This theory is in line with the cisternal maturation model of Golgi transport, in which vesicles forming from the ER are coated with COPII proteins and are being transported to the Golgi, therefore transporting lipids along the secretory pathway, while vesicles being transported from the Golgi to the ER are coated with COPI, therefore transporting the lipids in a retrograde manner, restricting lipids to leave the Golgi compartment [149]. In addition, Simons assumes that clustering of rafts, by for example incorporated raft proteins, lead to further segregation of raft lipids and proteins in the TGN and finally budding of transport vesicles to the plasma membrane. Those vesicles were shown to be further enriched in raft lipids, but it needs to be stated that this sorting of lipids was only shown for polarized cells and in yeast [150].

Based on previous findings and new experiments Patterson et al. [151] proposed a model of intra-Golgi transport. In addition to an existing gradient of raft lipids from low content in the *cis*- to high content in the *trans*-Golgi they propose the existence of different domains already in each Golgi cisternae. They describe so-called processing

domains, in which raft lipids are less prominent and export domains, which are enriched in raft lipids. Proteins of all sorts can diffuse in and out of both domains, but with different probabilities. Golgi-resident proteins like the galactose transferase (GalT) have a higher probability to be in processing domains, while plasma membrane proteins are more likely to be found in export domain. These domains are believed to make up the transport vesicles to the plasma membrane. Nevertheless, this model has the drawback that it describes transport vesicles exiting the Golgi at every level and not only at the TGN, therefore contradicting the accepted idea of vesicular transport.

1.4.2 Raft targeting signals

Incorporation of proteins into lipid rafts can be mediated by different types of intrinsic raft targeting signals like hydrophobic modifications such as GPI anchors [152–154] and palmitoylation [155–157] or ill-defined signals in the transmembrane region (TMR).

While the mechanism of the integration of GPI anchors and palmitoylation are more discernable, due to their fatty acids being able to integrate between lipids into the membrane lipid bilayer, the mechanism or signal of TMRs is still elusive. So far only a few proteins with raft targeting signals in their TMR have been reported. For example, Benslimane et al. were able to show, that CD154 associates with lipid rafts, but it loses its raft targeting after exchanging the TMR by one of a non-raft protein [158]. Likewise, podoplanin no longer localizes to raft upon swapping TMRs [159]. Interestingly, podoplanin exhibit a GXXXG motif, which was recently described as having the ability to bind cholesterol [160,161]. In addition, some proteins exhibit more than one raft-targeting signal. The death receptor FAS is palmitoylated, but also needs a lysine-rich region for raft association and full functionality [162]. Binding of raft lipids like podoplanin might be one strategy to integrate into lipid rafts.

1.4.3 Sphingolipid- and cholesterol-binding motifs

Hitherto, only a few lipid-binding motifs have been identified. For instance the **sphingolipid-binding** motif recently found by Björkholm et al. The motif was originally described in the vesicular transport protein p24, comprises the amino acids VXXTLXXIY

[163] and can be located in single and in multiple spanning proteins like GPCRs (G-protein coupled receptors) [164].

In comparison, a variety of different **cholesterol-binding motifs** have been defined. Most of them share a similar pattern of amino acids, which consists of basic, aromatic and large hydrophobic residues. Positively charged, basic amino acids, like lysine (K) or arginine (R), usually flank the transmembrane region, to position it via their "snorkelling" effect at the interface of lipids and water [165]. This position allows the amino acids to form a hydrogen bond with the hydroxyl (OH) group of cholesterol, which is also located at the membrane-water interface. Aromatic amino acids bind to the sterane portion of cholesterol through CH-π stacking interactions. Finally, hydrophobic amino acids, like isoleucine (I), leucine (L) or valine (V) form van der Waals forces with the hydrocarbon side chain of cholesterol.

For example, the Cholesterol Recognition/interaction Amino acid Consensus sequence or CRAC domain, first described by Li and Papadopoulos [166], consists of the hydrophobic amino acids leucine or valine, followed by 1-5 undefined apolar amino acid residues, then a tryptophan, then again 1-5 undefined apolar amino acids and finally the basic amino acids lysine or arginine: $L/V-X_{1-5}-Y-X_{1-5}-K/R$. This motif can be found in many cellular and viral proteins like the GPCRs, which are located in lipid rafts and caveolae [167,168]. Moreover, in the viral context HIV gp41 [169] and more importantly influenza M2 protein [170] were reported to bind cholesterol via the CRAC domain. As the basic amino acid has to be located at the lipid-water interface, proteins exhibiting the CRAC motif must interact with the inner leaflet of the membrane.

The opposite orientated CARC motif, so far only described for the human nicotic acetylcholin receptor (nAChR), is located in proteins binding cholesterol in the outer leaflet of the membrane. Besides having the opposite direction, the CARC motif is distinguished from the CRAC motif by being less strict about the middle aromatic amino acid, which can be tryptophan as well as phenylalanine ($K/R-X_{1-5}-Y/F-X_{1-5}-L/V$) [171].

Additionally, Hanson et al. identified by crystallography and sequence comparison of 7-TMR-receptors the so-called CCM, a cholesterol consensus motif [172]. In this case the amino acids interacting with cholesterol are not a linear sequence motif but dis-

tributed between two helices. One helix contains the positively charged amino acid arginine (R) or lysine (K), the hydrophobic amino acid leucine (L), isoleucine (I) or valine (V) and the aromatic amino acid tryptophan (W) or tyrosine (Y), all facing the same side of the helix. In addition, another aromatic amino acid, either phenylalanine (F) or tyrosine (Y) is needed on a second helix of a multimer to bind the cholesterol from the other side. In short, the CCM for one helix can be described as W/Y-(X)$_{1-3}$-I/V/L-(X)$_{1-7}$-K/R. Likewise the CRAC and CARC motif, the CCM can be orientated in two ways. Either the charged amino acids K or R can face to the lipid-water interface of the inner or the outer leaflet.
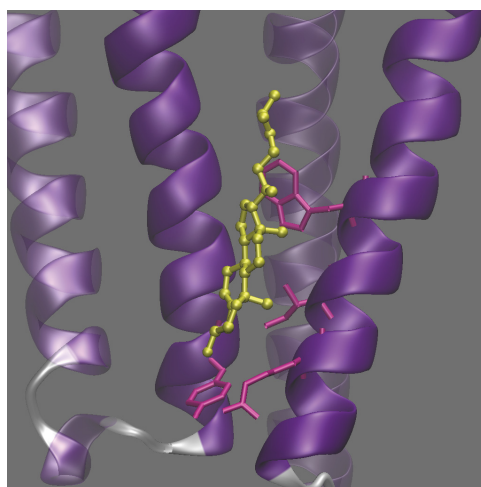
Figure 1-7: Partial crystal structure of the four transmembrane regions of the human ß-adrenergic receptor in purple. Non-interacting helices are translucent. Interacting amino acids of the cholesterol consensus motif are in magenta; Cholesterol in yellow. W, I and R are located on TMR IV and Y located on TMR II. Created with Visual molecular dynamics (VMD) 1.9.1 and POV-Ray 3.7.0 from PDB code 3D4S. Second binding cholesterol interacting with a protein-linked acyl chain was left out [172].

A different kind of cholesterol-binding motif was reported for the amyloid precursor protein (APP). Studies by the group of Charles Sanders revealed a double GXXXG motif to be involved in cholesterol binding (reviewed in [173]). By NMR studies of the 99 residues comprising the C-terminal domain incorporated in model membranes containing the cholesterol derivate CHOBIMALT, they could demonstrate cholesterol binding. The N-helix, N-loop and the N-terminal end of the TMR, form the structure involved in cholesterol binding, whereby the helix has a kink after the double GXXXG motif (see Figure 1-8). This structure forms a pocket in which cholesterol can be integrated. To further investigate the amino acids being involved in cholesterol binding, they per-

formed alanine scanning mutagenesis. Although they didn't publish a high resolution structure so far, they give information about the amino acids probably binding cholesterol. The GXXXGXXXG motif creates a flat surface that enables interaction with the flat surface of cholesterol, which is made by Van der Waals forces. In addition, they claim that after interaction of the cholesterol to the GXXXG motif the N-loop undergoes a conformational change that allows for interaction by the formation of a hydrogen bond of the hydroxyl group of cholesterol with an asparagine and a glutamic acid within the loop. Finally, a phenylalanine could form CH-π stacking interactions with the sterane portion, as also shown for the other cholesterol binding motifs mentioned above.
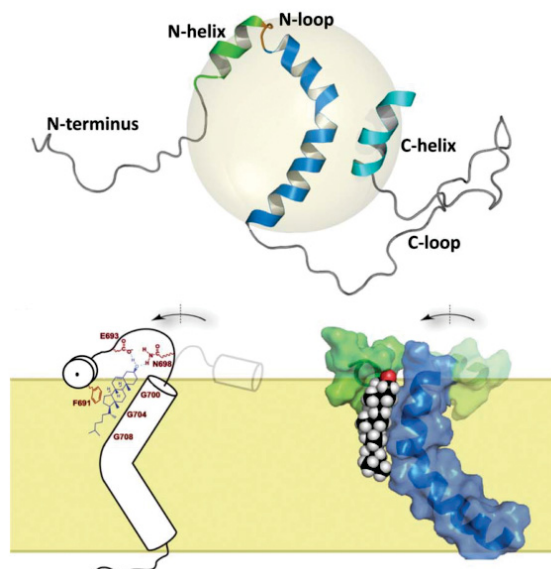
Figure 1-8: Structure of the C-terminal domain of APP in complex with cholesterol. **Upper panel:** Structure on model membrane micelles determined by NMR. **Lower panel:** Proposed model of interactions between APP and cholesterol [173]. Upper panel was adapted by the author from [161] with permission from American Association for the Advancement of Science. Lower panel was adapted from [161] with permission American Association for the Advancement of Science (left side) and from [174] with permission of American Chemical Society (right side).

1.5 Lipid rafts in the viral context

Lipid rafts are important for entry, fusion, replication, budding and assembly of a wide range of viruses. Hence, lipid rafts can be important in nearly every step of a virus' lifecycle. The filoviruses Ebola and Marburg use lipid rafts for assembly and budding as

well as for entry and fusion. Regarding fusion, lipid rafts probably cluster the receptor for efficient viral binding to induce the fusion process [175,176]. From the family *arenaviridae* representatives from the old world and new world viruses are reported to depend on cholesterol in their life cycle. Although Lassa virus (old world virus) does not bud from rafts, the extraction of cholesterol from the viral envelope does impair infectivity, presumably by a fusion defect [177]. In contrast to Lassa, Junín virus' glycoproteins associate with DRMs and cholesterol depletion by methyl-β-cyclodextrin led a decrease in budding and titer [178]. In case of Borna disease virus cholesterol is needed for the binding of the receptor, which probably is located in raft, but not for fusion [179]. Paramyxoviruses, for example, use lipid rafts as site of budding and assembly. The glycoproteins of measles, RSV (Respiratory syncytial virus), Sendai virus and New Castle disease virus (NDV) are located in lipid rafts at the plasma membrane [180–187]. Measles viral replication is impaired upon cholesterol synthesis inhibition [188] and cholesterol synthesis is downregulated in persistent infected neuronal cells [189]. Regarding Sendai virus, cholesterol depletion of infected cells, did not lead to a decreased virus production but to less infectivity [190], which hints to an entry defect as seen for NDV that uses rafts for its entry and fusion [191]. Even though not for all viruses assembly and budding are fully understood, literature data implicates a role of cholesterol and sphingolipids in the replication cycle of Hepatitis C virus, a member of the *flaviviridae*. Shi and colleagues reported that the RNA replication occurs on lipid raft structures [192]. Furthermore, the structural proteins associate with DRMs, mature virus particles are enriched in cholesterol and cholesterol as well as sphingolipids are needed for fusion of the virus with the host cell [193]. Hepatitis C virus even alters the sphingolipid synthesis to promote its own replication [194]. For *Hepadnaviridae* the hepatitis B virus is believed to bud from lipid rafts as the release of newly formed virus particles is impaired, when lipid rafts are depleted from cholesterol, and the phenotype is rescuable, when cholesterol is replenished [195]. Even herpesviruses, which bud into Golgi-derived vesicles, are linked to assembly in rafts. The glycoproteins of the human herpesvirus 6 (HHV6) can be found in DRMs and their lipid envelope contains GM1, a raft-located protein and general marker for rafts [196].

Several viruses are in need of functional lipid raft for their entry and/or their fusion. Dengue virus' fusion, for example, is inhibited upon cholesterol depletion from the viral envelope but not the cell membrane [197]. Therefore, most probably rafts are not important for receptor clustering but rather the lateral organization of the virus is crucial for fusion. In contrast, Coronaviruses are dependent on cholesterol in the cellular and viral membrane, but the detailed mechanism is still unknown [198]. Non-enveloped viruses also use lipid rafts as entry site. The bovine rotavirus is dependent on cholesterol and lipid rafts not for the attachment but rather the endocytosis. Surprisingly, treatment of cells with methyl-β-cyclodextrin after infection also reduces titer, which is why raft structures seam to play a role even in the assembly of non-enveloped viruses [199].

HIV, besides influenza virus, is one of the best-studied viruses regarding the role of lipid rafts in their replication cycle. As early as in the late 1980s, only five years after the discovery of the virus, it was already reported that the membrane of HIV has a high rigidity due to the high cholesterol/phospholipid ratio, which enables a long term stability at low temperatures [200]. In 2000 it was shown for the first time that HIV buds from lipid rafts [201], whereby subsequent publications demonstrated that the precursor Gag interacts with rafts, clusters them to build the assembly sites and recruits other viral components to the budding zone [202–204]. The origin of the viral envelope from lipid rafts is reflected in the lipid composition of the viral envelope. Raft lipids like cholesterol and sphingolipids are enriched in the virus membrane, revealed by investigations of the lipidome of HIV particles [205]. Furthermore, HIV upregulates the cholesterol and sphingolipid synthesis while reducing polyunsaturated PC levels depending on expression of the Nef protein [206–208]. HIV does not only use rafts as platform for assembly, but also transcytose trough the non-permissive epithelial cells in a raft dependent manner to cross the outer cells layer to finally reach the CD4-positive T-cells as their prime target [209]. The entry then occurs by endocytosis via CD4 containing lipid rafts [210]. For the subsequent fusion event again cholesterol in the host cell membrane is required, since viruses grown in cholesterol deprived cells only have minimal infectivity and extraction of cholesterol by methyl-β-cyclodextrin from virus particles leads to a loss in fusion activity [211]. Additionally, HIV is the first

virus reported to exhibit a CRAC motif in its gp41 protein that is crucial for fusion [212,213].

1.5.1 Influenza HA integration into lipid rafts: Molecular details

As mentioned before influenza A viruses bud from lipid rafts as well [75]. These findings made by extraction of detergent-resistant membranes (DRMs), a method that is prone to produce artefacts, were verified by various findings that HA is not randomly distributed in the plasma membrane but forms clusters of various sizes. Hess et al. were able to show by quantitative electron microscopy and FRET experiments after photobleaching that HA forms clusters on the cell surface. The pattern of these clustered changed after treatment with methyl-β-cyclodextrin or PDMP and PPMP (both structural analogues of ceramide that inhibit glycosphingolipid synthesis as well as sphingomyelin dependent on the concentration), thereby extracting cholesterol or reducing the amount of sphingomyelin, respectively, within the membrane [214]. In the same year Leser et al. verified these findings by using quantitative electron microscopy and also showed growing clusters of HA and NA on the surface of infected cells in dependence of time after infection and cholesterol content [215]. By using FPALM Hess et al. were able to prove the existence of HA clusters as well in living cells [216]. In addition to cholesterol and sphingolipid content, also the cytoskeleton influences the location and clustering of HA. The laboratory of Hess showed in a recent study, that HA cluster colocalize with actin-rich membrane regions, whose disruption led to a reduced size of the clusters and a reduced density of HA within these clusters [217]. Furthermore studies by Gerl et al. using quantitative mass spectrometry confirmed the hypothesis, that the cholesterol and sphingolipid content increases along the exocytic pathway and that raft lipids are even further enriched in the viral membrane [218].

To integrate into lipid rafts HA two raft targeting signals were proposed. On the one hand, three S-acylated cysteins, [61,104,219], on the other hand, hydrophobic amino acids (VIL) in the TMR facing the outer leaflet of the plasma membrane [74,220]. Interestingly, in the initial studies the TMR motif investigated by Scheiffele and Takeda was only loosely defined. Both studies applied alanine-scanning mutagenesis to identify VIL for incorporation into detergent-resistant-membranes (DRMs), the biochemical correlate of lipid rafts. However, biochemical extraction of DRMs might not reflect
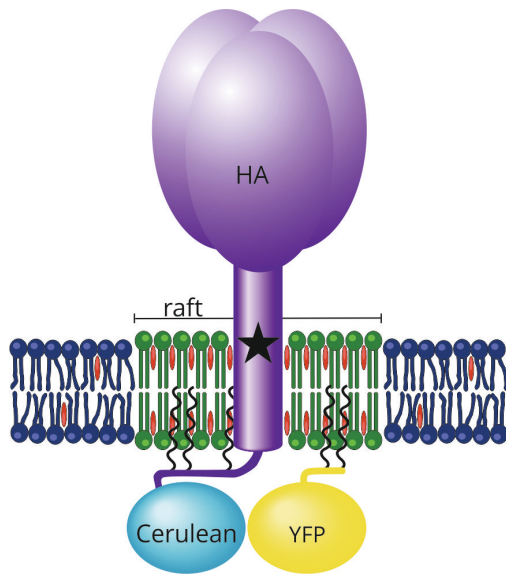
Figure 1-9: Schematic picture of the location of HA-Cerulean and Myr-Pal-YFP in the plasma membrane. Black star indicates the location of the TMR raft-targeting signal. Created with CorelDRAW

the status in living cells and is prone to artefacts [221]. This problem was overcome when Stephanie Engel (Veits group) and Silvia Scolari (Herrmanns group) used fluorescence resonance energy transfer measurements in living cells to analyse the association of HA with a known raft marker. They were able to demonstrate that HA indeed is dependent on the presence of both raft-targeting signals for incorporation into lipid rafts [222,223]. Stephanie Engel used the HA protein fused to Cerulean as donor fluorophore and as acceptor a myristoylated and palmitoylated peptide, an established lipid raft marker (Myr-Pal-YFP). This marker consists of the first 21 amino acids of the Lyn kinase and is fused to YFP.

1.6 Methods to study raft association of proteins and cholesterol interaction

The investigation of lipid raft association and in particular cholesterol binding is a complex field. So far several methods have been described, but mostly all of them have drawbacks. According to Gerald Gimpl several properties could hint towards an interaction of proteins with cholesterol: (1) the presence in cholesterol rich membranes (2) altered protein function after changing the cholesterol content in membranes (3) altered protein function upon substitution of cholesterol by sterol analogues (4) influence of cholesterol binding molecules as "competitors" (5) binding of radiolabeled cholesterol (6) spectroscopic binding assays with fluorescent sterol analogues (7) labeling of the protein with photoreactive cholesterol and (8) identification of cholesterol binding by structural studies [224].

The most common method to start with, when studying the association of proteins with lipid rafts, is the **extraction of cholesterol with methyl-β-cyclodextrin** to dis-

rupt lipid rafts. Cyclodextrins are a potent agent to specifically extract lipids from membranes. They posses a hydrophilic surface made up from seven glucose molecules building a ring, which encircles the highly hydrophobic cavity. Depending on the size and hydrophobicity, different lipids can be extracted from the membrane, whereby β-cyclodextrins were shown to have the highest affinity to cholesterol (reviewed in [225]). This method is highly dependent on the concentration of the compound and the incubation time. High concentrations incubated over a long time period are able to extract 80-90 % of the cellular cholesterol, but it leads to the loss of cell morphology and therefore, most probably, effect more cell functions than planned to be investigated. As mentioned in 1.3 the cholesterol content of the cell is highly regulated, depleting cholesterol in the plasma membrane by β-cyclodextrins therefore may lead to an altered distribution of cholesterol in the intracellular membranes due to induction of cholesterol synthesis. When β-cyclodextrins are used to study lipid rafts at the plasma membrane one need to take into account that not only the cholesterol from rafts can be extracted but also from non-raft phases, whereby this was reported to happen slower. Thus, again low concentrations (≤ 1 mM) should be used and incubated not longer than 10 min. Regarding the investigation of viruses, as summarized in 1.5, this method can give a first insight, even though not very specifically, if cholesterol is somehow involved in the replication cycle, leading to a decreased virus titer upon usage of β-cyclodextrins.

Another commonly used method is to test for the **solubility of proteins in non-ionic detergents** like Triton X-100, Brij 96 and Lubrol WX at 4°C and Brij 98 at 37°C. That allows drawing conclusions about the association of specific viral proteins with lipid rafts. While rafts and their associated proteins will stay insoluble and float up on a sucrose gradient, soluble membranes and proteins will be found at the bottom of the gradient. This method has the drawback that it relies on the effective solubilization of the membrane and its integrated proteins. At high detergent-to-lipid ratios even lipid rafts can be solubilized, which is why titration of the detergent is of great importance. Furthermore, proteins might be soluble in detergents but might still associate with lipid rafts *in vivo*. In addition, Triton X-100 resistant membranes tend to aggregate. New detergents used, like Brij and Lubrol WX have the advantage that solubilized raft

membranes no longer form aggregates, but they were chosen under the prerequisite that they are able to isolate proteins, which are soluble after Triton X-100 treatment. Insoluble membranes, extracted with these new detergents, are no longer highly enriched in cholesterol and sphingolipids, therefore they are maybe not reflecting the lipid composition of lipids rafts *in vivo* (reviewed in [226]).

Besides these two biochemical methods, fluorescent methods can be used to demonstrate association of proteins with lipid rafts. For example, **the increasing intrinsic fluorescence of fluorescent cholesterol derivatives** like dehydroergosterol or NBD-cholesterol in presence of a cholesterol binding protein can be used to study binding [227]. However, since this method relies on binding of purified protein, it does not resemble physiological conditions. The **coupling of FRET** (fluorescence resonance energy transfer) as a method to study energy transfer from one fluorophore to another, if in close contact (see 1.7.1), **with FLIM** (fluorescent lifetime imaging microscopy) allows for investigation of interactions of proteins in living cells. Even though in this system the direct interaction of a protein with cholesterol in not measured, but rather the energy transfer of a protein of interest to a marker protein for rafts, this system is one of the first being able to study protein-raft-association under physiological conditions in living cells, which is why I used this method in this study to investigate the association of HA with lipid rafts. The detailed methodology is described in 1.7.

A method used to study not only lipid raft interaction but rather the interaction of viral proteins with cholesterol is to **use enzymes with cholesterol as substrate** as a reporter for binding. The cholesterol oxidase converts cholesterol to H_2O_2 and the corresponding ketones. In turn, H_2O_2 is then, in presence of the horseradish peroxidase (HRP), detected by a reagent, which reacts with H_2O_2 to form a fluorophore that can be detected with a spectrometer [224]. For example, the terms and the extend of cholesterol binding of influenza M2 was studied using this kind of assay [119]. This reaction is highly sensitive, life technologies, one provider of a cholesterol assay kit (https://www.lifetechnologies.com/order/catalog/product/A12216), claims a detection level down to 200 nM and less, but in case of immunoprecipitated protein, the drawback is still in the choice of the right detergent to lyse the cells. In case the treatment is to harsh, the cholesterol can be removed as well, especially when the binding is not

very strong, as proteins often don't bind cholesterol covalently but rather interact with it. On the contrary, another detergent might be too mild and therefore not be able to remove cholesterol in the vicinity of the protein investigated. Hence, control samples must be chosen with great care.

Affinity chromatography with radiolabeled cholesterol can also be used to perform binding studies of cholesterol. Nickel agarose columns are loaded with a His-tagged protein upon which the radioactive labeled cholesterol ([3H]cholesterol) is incubated on the column. Unbound cholesterol is then washed off and bound protein/cholesterol complexes can be eluted from the column and measured in a scintillator [224]. **Non-radioactive labeled cholesteryl hemisuccinate agarose** was used to prove cholesterol binding of HIV env protein gp41 and influenza M2 [84,169]. Recombinant protein is incubated with the cholesteryl hemisuccinate agarose resin, unbound protein was washed off and the bound protein was eluted and analyzed by SDS-PAGE and Western Blot. Thaa and colleagues also used **radioactive labeled photocholesterol** to prove cholesterol binding of influenza M2. Thereby, M2 fused to GFP was purified from bacteria and incubated with [3H] photocholesterol and crosslinked by UV light upon which binding of cholesterol was detected [228]. A similar method was used to investigate the cholesterol binding properties of the Semliki Forest virus (SFV) E1 protein, which was incubated with [3H] photocholesterol in liposomes and crosslinked by UV light [229]. Nevertheless, as photocrosslinking can also occur, when the reactive compound and the target protein are only in close proximity, this method still lacks definite prove of binding. All three methods rely on recombinant protein, which might not exhibit the same features as the native protein within a membrane. In case of the M2 protein, the results from transient expressed protein described above in regard of the cholesterol oxidase assay, the transfected protein alone was not able to bind cholesterol and needed the other viral components expressed during infection, while the affinity chromatography and photocrosslinking revealed an intrinsic cholesterol binding ability. This demonstrates that often more than one method has to be applied to determine the binding properties of a protein.

The most direct prove of cholesterol binding is solving the structure of the membrane protein with the cholesterol still attached. Solving the structure of membrane proteins

itself is a complex methodology. Usually the protein of interest is expressed in a suitable cell system like *E.coli* or insect cells, whereupon it is solubilized in a detergent, purified and crystallized [230]. When studying the interaction of a membrane protein with lipids and in particular cholesterol the use of detergents is not optional, which is why new methods had to be developed. For example, the use of **lipidic cubic phase (LCP) technology in crystallography** allowed solving the structure of the human ß-adrenergic receptor (Figure 1-7). LCP is a membrane-mimetic matrix in which the recombinant protein of interest is integrated, which is then loaded to allow crystallization [231,232]. The biggest limitation of LCP is the extreme viscosity of the cubic phase, which makes it demanding to work with it. Another strategy is the usage of **solid state NMR** of recombinant protein in micelles or bicelles with the desired lipid composition [233]. This technique was used to determine the cholesterol-binding site of the C-terminal domain of APP in complex with cholesterol (Figure 1-8). Both of these methods need experts to perform the experiments, from choosing the right detergents to solubilize the recombinant protein and its purification to the performance of the actual experiments solving the structure, which is why these kinds of experiments should be performed in cooperation with groups already using these methods.

1.7 Fluorescence lifetime imaging microscopy by measuring fluorescence resonance energy transfer (FLIM-FRET)

1.7.1 Fluorescence resonance energy transfer (FRET)

Already in 1946 Theodor Förster described the non-radiative transfer of energy from one excited fluorophore (donor) to another (acceptor) via a dipole-dipole interaction [234]. The occurrence of energy transfer is thereby dependent on the following conditions: (1) an overlap of the donor's emission spectrum and the acceptor's excitation spectrum (2) the orientation of the dipoles, which must not be perpendicular (3) the quantum yield of the donor and (4) the distance between the donor and the acceptor.

The rate of the energy transfer can be described by the following formula:

$$k_T(r) = \frac{1}{\tau_D}\left(\frac{R_0}{r}\right)^6$$

where τ_D is the lifetime of the donor in absence of an acceptor, R_0 describing the Förster distance at which the energy transfer is 50 % efficient and r is the actual distance between donor and acceptor. In biological systems, R_0 usually ranges from 2-9nm, which is why FRET measurements can be used for interaction studies of proteins. The FRET efficiency is depending on the sixth power of R_0 (and therefore extremely dependent on the distance) and, in case of r being near R_0, can be described by the formula [235]:

$$E = \frac{R_0^6}{R_0^6 + r^6}$$

FRET can be used to study intra-molecule interactions, like folding processes of domains or structural refolding due to a trigger [236–239], to study direct protein-protein interactions [240], which can be assumed to exist in case of energy transfer at a distance of less than 10 nm, or to locate a protein in a specific surrounding by energy transfer with a specific marker for this location as has been applied in case of HA-Cer and Myr-Pal-YFP as a marker for lipid rafts.

To measure FRET there are mainly two different kinds of techniques, firstly, FRET by steady-state intensity. This method uses the fact that in case of energy transfer the intensity of the donor fluorescence drops, while the intensity of the acceptor fluorescence increases. Radiometric FRET measurements calculate the ratio of the intensity of the acceptor to the intensity of the donor. The disadvantage of this method are, that the molar ratio of acceptor and donor should be 1:1, which limits the method to intra-molecular energy transfer and the risk of bleed through of the donor signal into the acceptor signal. Several methods have been developed to correct for bleed through by including donor only and acceptor only controls [241]. The second technique is the determination of the FRET efficiency by fluorescent lifetime measurements like fluorescence lifetime imaging microscopy (FLIM). FLIM has the advantage of measuring the lifetime only in dependence on the environment of the donor but not on the ratio of donor and acceptor on a molecular level [242].

1.7.2 Fluorescence lifetime imaging microscopy (FLIM)

The lifetime of a fluorophore is the average time a fluorophore stays in its excited state before it again returns to its ground state. In case of biological experiments the time-dependent intensity *I(t)* is measured and can be described as following:

$$I(t) = I_0 \, e^{\left(\frac{-t}{\tau}\right)}$$

where I_0 is the intensity at time 0 [235].

FLIM uses time-correlated single-photon counting (TCSPC) for the determination of the lifetime. In TCSPC the fluorophore is excited with a short laser pulse in a way that less than one emitted photon will be detected. The time between the excitation and the emitted photon arriving at the instrument is then depicted as a histogram. Due to the different arrival times after the pulses the histogram will lead to an exponential function, the slope of which describes the lifetime of the fluorophore [235].
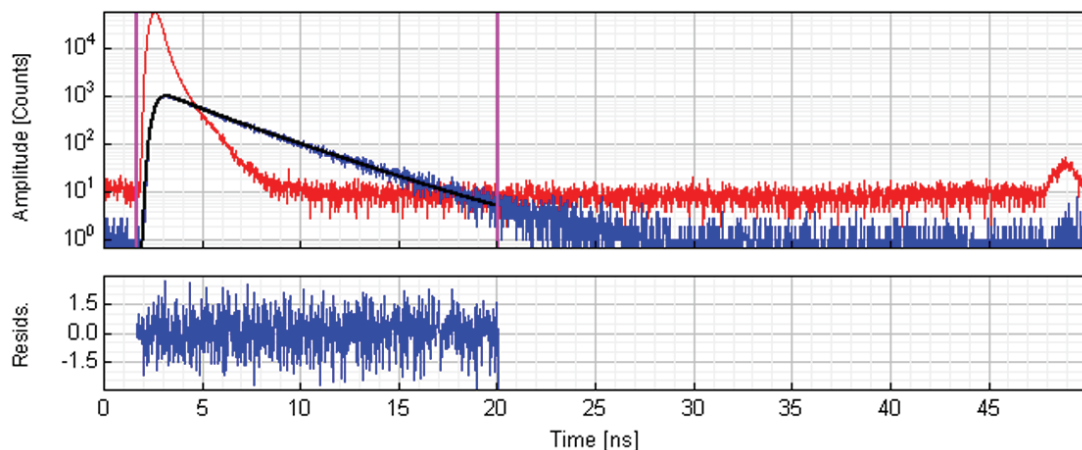
Figure 1-10: TCSPC histogram of FLIM-FRET measurement of HA. Histogram of selected region in blue, bi-exponential fit curve in black and recorded instrument response function in red; magenta vertical lines define the analyzed time frame

Using a single photon avalanche photodiode (SPAD) the emitted photons can be detected. While being very precise in their response, they also have the drawback of having a wavelength dependent timing response, which might interfere with the time-resolved measurement of the sample. Hence, the instrument response function (IRF) should be measured and included into the histogram [243] (see Figure 1-10 red curve). In the used setup the IRF can be measured by recording the Raman scattering of double distilled water.
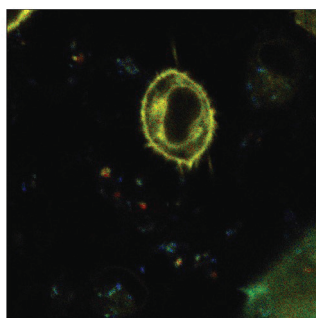
As the TCSPC recording not only recognizes the time until detection but also the position of the laser on the sample, it is also possible to reconstruct an image reflecting the according lifetimes to their location [242].

Figure 1-11: FLIM image of a transfected cell. Color resembles lifetime.

1.7.3 FLIM-FRET

FLIM-FRET is based on the acquisition of the lifetime of the donor in absence and presence of the acceptor. In case of FRET, the lifetime of the donor will be shortened in presence of the acceptor. Therefore, the FRET efficiency E can be calculated according to:

$$E = 1 - \left(\frac{\tau_{DA}}{\tau_D}\right)$$

where τ_{DA} and τ_D are the lifetimes of the donor in presence and absence of the acceptor, respectively.

The most significant advantage of FLIM-FRET is, that by bi-exponential fitting it is possible to account for interacting and non-interacting donor fractions. In case of using FLIM-FRET to study the incorporation of HA into lipid rafts one can assume that not all HA molecules (donor) are interacting with the lipid raft marker Myr-Pal (acceptor), which should be taken account for in the calculation of the FRET efficiency. The non-interacting donor fluorophores are decaying slower than the interacting ones. Out of the amplitudes and corresponding lifetimes for both donor populations it now possible to calculate an average lifetime, which than can further be used for the calculation of the corrected FRET-efficiency [242].

As FRET efficiency does not only reflect specific interaction but random interactions as well, measurements in membranes with limited space and diffusion are more complex. Due to over expression of the acceptor, false-positive FRET results could be measured. That means that under low expression levels of the acceptor, FRET would be absent and would increase upon higher levels of acceptor expression. In contrast, specific FRET already yields high FRET efficiencies at low acceptor concentrations and

is relatively independent of acceptor concentration. For the analysis of FRET efficiencies dependent on the acceptor concentration, cluster analysis proposed by Zacharias et al [244] can be applied. FRET efficiencies are plotted against the acceptor intensity, whereupon the data is fitted to the following hyperbolic function.

$$E(\%) = \frac{E_{max} * A}{K_D + A}$$

The respective equation yields K_D as a parameter to assess the associative properties (clustering) of donor and acceptor. Low K_D values compared to the average intensity indicate true clustering, which is independent on acceptor concentration, and would lead to a hyperbolic shape of the fitting curve. High K_D values, in contrast, indicate random interaction, which is dependent on increasing acceptor concentration and would lead to linear fitting.

1.8 Aim of the study

My thesis is a continuation of Stephanie Engel´s dissertation on the assembly of influenza viruses. She built up the basis of this thesis by performing experiments to confirm the integration of hemagglutinin into lipid rafts, the site of budding, in living cells using FLIM-FRET analysis. She was able to show that the integration of HA into lipid rafts at the plasma membrane indeed was dependent on the two proposed raft targeting signals, as clustering with an established raft was reduced. Beside the FLIM-FRET experiments, she carried out radioactive labeling of cells expressing the mutants to check for correct processing and thereby observed a different state of processed HA_0 in case of the VIL and double mutant, but not the palmitoylation mutant. For evaluation of the steps of processing being affected, she performed preliminary pulse-chase experiments to check for the kinetics of trimerization, glycosylation and proteolytical cleavage of the precursor HA_0 into its subunits HA_1 and HA_2. The kinetics obtained revealed a negative effect of the mutation of the hydrophobic raft-targeting signal, but not the palmitoylation on the transport of HA from the time of leaving the rER.

In the present study, the preliminary results on the delayed processing and therefore a delayed transport along the exocytic pathway of the VIL mutant were to be verified by repeating the pulse-chase experiments. Furthermore the underlying mechanism of the transport and the involvement of the VIL raft-targeting signal were to be analyzed. Colocalization studies of mutant and wild type HA with a cis-Golgi marker were to be performed to gain further inside of the location of the delay. As mentioned in the introduction, several investigators proposed an involvement of lipid raft like structures in the transport within the Golgi. As cholesterol content in context of HA transport was already published to have an effect on HA transport [245], the focus of was laid on the influence of sphingolipid content in cellular membranes on transport and studied by inhibiting sphingolipid synthesis and subsequent monitoring of the transport kinetics.

So far the VIL motif was only investigated by alanine scanning, but whether the motif is part of a larger signal for raft-targeting is still unknown. Since the isoleucine and

leucine of the VIL motif are highly conserved among all HA subtypes and are facing outwards of the trimeric complex [246], they are in a favourable position to interact with surrounding lipids. Therefore, the question arises, whether HA is able to bind cholesterol or sphingolipids via the VIL motif or an extended raft-targeting motif. This led to the aim of finding a putative lipid-binding motif within the sequence of the beginning of the transmembrane region of HA by using *in silico* methods. If a motif could be found, this motif was to be mutated, and constructs were to be investigated by the established methods to elucidate transport kinetics and raft association.

2 Material and Methods

2.1 Material

2.1.1 Chemicals

Table 1: Chemicals used in experiments directly and to prepare buffers and solutions

Compound	Manufacturer
2-[N-Morpholino] ethanesulfonic acid (MES) hydrate	Sigma-Aldrich, Taufkirchen
3-[N-Morpholino] propanesulfonic acid (MOPS)	Sigma-Aldrich, Taufkirchen
Agar	Gibco/Invitrogen, Karlsruhe
Agarose	Invitrogen, Karlsruhe
Acetic Acid 100 %	Carl Roth, Karlsruhe
Acrylamide/bisacryl (37.5:1), 30 %	Carl Roth, Karlsruhe
Ammonium persulfate (APS)	Sigma-Aldrich, Taufkirchen
Bacto ™ tryptone	BD Biosciences, Heidelberg
Bacto ™ yeast extract	BD Biosciences, Heidelberg
$CaCl_2$ dihydrate	Sigma-Aldrich, Taufkirchen
Cysteine	Sigma-Aldrich, Taufkirchen
DABCO (triethylendiamin)	Sigma-Aldrich, Taufkirchen
Dithiothreitol (DTT)	Sigma-Aldrich, Taufkirchen
Dimethylsulfoxid (DMSO)	Sigma-Aldrich, Taufkirchen
Dodecylsulafte sodium salt (SDS)	Biomol Feinchemikalien GmbH, Hamburg
Ethanol 100 %	AppliChem GmbH, Darmstadt
Ethylenediaminetetraacetic acid (EDTA)	Sigma-Aldrich, Taufkirchen
Ethidium bromide	Carl Roth, Karlsruhe
Fumonisin B_1	Sigma-Aldrich, Taufkirchen

Glutamine	Sigma-Aldrich, Taufkirchen
Glycerin	Carl Roth, Karlsruhe
Isopropyl alcohol	AppliChem GmbH, Darmstadt
Kanamycin	Carl Roth, Karlsruhe
KCl	Sigma-Aldrich, Taufkirchen
Kodak GBX developer/replenisher	Sigma-Aldrich, Taufkirchen
Methanol	AppliChem GmbH, Darmstadt
Methionine	Sigma-Aldrich, Taufkirchen
$MgSO_4$	Sigma-Aldrich, Taufkirchen
$MnCl_2$ tetrahydrate	Sigma-Aldrich, Taufkirchen
Mowiol 4-88	Sigma-Aldrich, Taufkirchen
NaCl	Sigma-Aldrich, Taufkirchen
Paraformaldehyde	Carl Roth, Karlsruhe
Protease Inhibitor "cOmplete Protease Inhibitor tablets"	Roche Diagnostics Deutschland GmbH, Mannheim
Protein-A sepharose	Sigma-Aldrich, Taufkirchen
Sodium salicylate	Carl Roth, Karlsruhe
Easy Tag Express Protein labeling Mix (> 70 % [^{35}S]-Methionin, 15 % [^{35}S]-Cystein)	Perkin Elmer, Rodgau
RbCl	Sigma-Aldrich, Taufkirchen
Tetramethylethylendiamin (TEMED)	Sigma-Aldrich, Taufkirchen
Tris	ICN Biomedicals Inc., Aurora
Triton X-100	Sigma-Aldrich, Taufkirchen
Trypsin	Sigma-Aldrich, Taufkirchen
Trypsin-Inhibitor Soybean T6522	Sigma-Aldrich, Taufkirchen

2.1.2 Consumables

Table 2: Consumable used in cell culture and fluorography experiments

Material	Manufacturer
Cell culture flasks T25, T75	Greiner Bio-One, Frickenhausen
Cell culture plates 6-, 12- and 24-well	Greiner Bio-One, Frickenhausen
Glass bottom dishes	MatTek , Ashland, Massachusetts
Cell scrapers	Greiner Bio-One, Frickenhausen
Cryo tubes	Sarstedt, Nümbrecht
Glass cover slips ⌀12mm	Carl Roth, Karlsruhe
Glass slides	Carl Roth, Karlsruhe
PVDF membrane	Amersham/GE Healthcare, Freiburg
Kodak Biomax XAR films (Fluorography)	Sigma-Aldrich, Taufkirchen

2.1.3 Enzymes and molecular biology reagents

Table 3: Enzymes and markers used in this study

Substance	Manufacturer
Phusion Polymerase	Thermo Scientific, Dreieich
One-Taq 2x Master Mix	New England BioLabs, Frankfurt
dNTP Mix 10 mM each	Thermo Scientific, Dreieich
Enzymes: EcoRI, BstZ17I	New England BioLabs, Frankfurt
CIP	New England BioLabs, Frankfurt
T4 DNA Ligase	New England BioLabs, Frankfurt
DNA Ladder "Smart Ladder"	Eurogentec, Köln
Protein Ladder „ColorPlus Prestained Protein Ladder, Broad Range"	New England BioLabs, Frankfurt

2.1.4 Kits

Table 4: Kits for molecular biology

Kit	Manufacturer
Miniprep Kit	Stratec Biomedical AG, Birkenfeld
"Invisorb Spin Plasmid Mini Two"	
Gelextraction Kit	Stratec Biomedical AG, Birkenfeld
"Invisorb Spin DNA Extraction Kit"	
PCR Cleanup Kit	Stratec Biomedical AG, Birkenfeld
"Invisorb Fragment Cleanup Kit"	
Maxiprep Kit	Promega, Mannheim
"PureYield™ Plasmid Maxiprep System"	

2.1.5 Antibodies

Table 5: Antibodies used for immuprecipitation and immunofluorescence

Antibody	Manufacturer
Primary antibodies:	
Rabbit anti-FPV (fowl plague virus)	Kindly provided by Hans-Dieter Klenk, Phillipps University Marburg, Institute of virology)
Mouse anti-membrine	Abcam, Cambridge
Secondary antibodies:	
Anti-IgG mouse Alexa 488	Life technologies GmbH, Darmstadt
Anti-IgG mouse Alexa 568	Molecular Probes/Invitrogen, Karlsruhe

2.1.6 Buffers and solutions

Table 6: Buffers and solutions prepared in this study and their composition

Buffer/Solution	Composition
PBS	0.8 % (w/v) NaCl, 0.02 % (w/v) KCl, 0.02 % (w/v) KH_2PO_4, 0.135 % (w/v) Na_2HPO_4 dihydrate
RIPA buffer	20 mM Tris·HCl, 150 mM NaCl, 10 mM EDTA, 10 mM Jodacetamid, 0.1 % (w/v) SDS, 1 % (v/v) Triton X-100, 1 % (w/v) Natrium-Desoxycholat, pH 7.4 (+ protease inhibitor)
MNT buffer	20 mM MES, 30 mM Tris, 100 mM NaCl, 1% Triton X-100 in H_2O pH 7.5
TAE buffer	40 mM Tris·HCl, 20 mM acetic acid, 1 mM EDTA, pH 8.0 (from 50x stock solution)
Loading dye agarose gels 5x	10 mM Tris-HCl, 100 mM EDTA, 50 % (v/v) glycerin, 0,1 % bromophenol blue pH 8,0
Loading dye (SDS-PAGE) 1x Reducing	62.5 mM Tris-HCl, 2 % (w/w) SDS, 10 % (v/v) glycerin, 0.01 % bromo-phenol blue pH 6.8, 5 % (v/v) β-Mercaptoethanol
SDS-PAGE running solution	25 mM Tris·HCl, 192 mM Glycin, 0.1 % (w/v) SDS (pH 8.3–8.5)
Stacking gel (SDS-PAGE)	5 % (w/v) Acrylamide/bisacrylamide (37.5:1; from 30-%-stock solution „Roti- phorese 30", Roth, Karlsruhe); 0.1 % SDS, 125 mM Tris·HCl pH 6.8 (from 4x stock solution), 0.075 % (w/v) APS, 0.15 % (v/v) TEMED
Resolving gel (SDS-PAGE)	Acrylamide/bisacrylamide (37.5:1) from 30-%-stock solution (Rotiphorese 30, Roth, Karls-ruhe); 0.1 % (w/v) SDS, 375 mM Tris·HCl pH 8.8 (from 4x stock solution); 0.05 % (w/v) APS, 0.1 % (v/v) TEMED

Fixing solution for SDS-PAGE	10 % ethanol, 10 % acetic acid in H_2O
Fixing solution for immunofluorescence (IF)	2 % PFA (paraformaldehyde, Carl Roth, Karlsruhe) in PBS w/o Ca^{2+} and Mg^{2+}
Blocking buffer for IF	3 % BSA in PBS w/o Ca^{2+} and Mg^{2+}
Permeabilization solution	0.5 % Triton X-100 in PBS w/o Ca^{2+} and Mg^{2+}
Washing buffer	PBS w/o Ca^{2+} and Mg^{2+} with 0.1 % Tween

2.1.7 Prokaryotic cells and media

Table 7: Bacteria used in this study and the prepared media with components

Cells / media	Manufacturer
Escherichia coli XL-1 blue Genotype *rec*A1 *end*A1 *gyr*A96 *thi*-1 *hsd*R17 *sup*E44 *rel*A1 *lac* [F′ *pro*AB *lac*I^{q}Z ΔM15 Tn*10* (Tet^r)]	Stratagene/Agilent, Waldbronn
YT medium	Powder stock (Invitrogen, Karlsruhe) (31 g/L in H_2O autoclaved); 50 µl/ml Kanamycin
YT agar plates	YT medium with 1.2 % (w/v) Agar; 50 µg/ml Kanamycin)
TYM medium (autoclaved)	2 % (w/v) Bacto™ tryptone, 0.5 % (w/v) Bacto™ yeast extract, 0.1 M NaCl, 10 mM $MgSO_4$ ad 1 l dest H_2O
TfB I (pH 6.2) (sterile filtered, 0.22 µm filter)	30 mM K-acetat, 10 mM CaCl2 dihydrate, 15 % (w/v) glycerine, 100 mM RbCl, 50 mM MnCl2 tetrahydrate ad 100 ml dest. H_2O
TfB II (pH 7.0) (sterile filtered, 0.22 µm filter)	10 mM MOPS, 75 mM CaCl2 dihydrate, 10 mM RbCl, 15 % (w/v) glycerine ad 40 ml dest H_2O

2.1.8 Eukaryotic cells and media

Table 8: Cell lines used in this study, composition of media and transfection reagents

Cells / media	Manufacturer
Chinese hamster ovary cells (CHO-K1)	ATCC CCL-61
DMEM (Dulbecco's Modified Eagle Medium) 10 % FBS, 1 % penicillin/streptomycin, 1 % L-glutamine	PAN Biotech GmbH, Aidenbach
DMEM without phenol red	PAN Biotech GmbH, Aidenbach
MEM (Minimal Essential Medium) with EBSS, without L-glutamine, L-cysteine and L-methionine	PAN Biotech GmbH, Aidenbach
Opti-MEM (reduced serum medium)	Gibcol/life technologies, Karlsruhe
Freezing medium	60 % DMEM, 30 % FBS, 10 % DMSO
FBS	Perbio, Bonn
PBS w and w/o calcium/magnesium	PAN Biotech GmbH, Aidenbach
TurboFect	Thermo Scientific..........

2.1.9 Equipment

Table 9: Equipments used in this study

Device	Manufacturer
Centrifuges	
Avanti J-25; Rotor JLA-16.250	Beckman Coulter, Krefeld
Sigma 3K12	Satorius, Göttingen
Tabletop centrifuge 5417R	Eppendorf, Hmaburg
Incubators	
Incubator for eukaryotic cells	Heraeus, Hanau

"Heracell"	
Incubator for prokaryotic cells	Satorius, Göttingen
"Certomat BS-1"	
Chemiluminescence detection system	PeqLab, Erlangen
"Fusion SL";	
Confocal microscope	Olympus, Hamburg
"FV1000", Objective UPLSAPO 60x,	
(numerical aperture 1.35);	
FACSCanto	BD Biosciences, Heidelberg
Fluorescence lifetime microscopy	PicoQuant, Berlin
"LSMupgrate Kit"	
Gel dryer	UniEquip, Martinsried
SDS-PAGE System	Biometra, Göttingen
Spectrometer "NanoDrop"	PeqLab, Erlangen
Thermo cycler	Eppendorf, Hamburg
"mastercycler gradient"	
UV hand lamp	Waldmann, Villingen-Schwenningen

2.1.10 Software

Table 10: Software used in this study, for analysis of data and creation of figures

Software	Company
Another plasmid editor (ApE) 2.0.47	http://biologylabs.utah.edu/jorgensen/wayned/ape/
Bio 1D	Vilber-Lourmat, Eberhardzell
CorelDRAW (Test version)	Corel GmbH, München
EMBOSS	http://www.ebi.ac.uk/tools/emboss/
FlowJO (test version)	http://www.flowjo.com/flowjo-free-trial/
Image J 1.47v	http://rsb.info.nih.gov/ij
Helical wheel plot	http://www.jci-bioinfo.cn/wenxiang2
NEBcutter 2.0	http://tools.neb.com/NEBcutter2/index.php

Photoshop CS6	Adobe Systems GmbH, München
POV Ray 3.7.0	http://www.povray.org/
Prism 5.01	GraphPad Software, Inc. La Jolla
SymPhoTime 4.7.3	PicoQuant, Berlin
Visual molecular dynamics	http://www.ks.uiuc.edu/Development/Download/
(VMD) 1.9.2 Open GL	download.cgi?PackageName=VMD

2.1.11 Plasmids and oligonucleotides

2.1.11.1 Plasmids

The plasmids used in this study, pYFP-N1 (Invitrogen) and pECerulean-N1 [247], were generated and kindly provided by Stephanie Engel. Both plasmids express a monomerric version of the yellow fluorescent protein (YFP) and Cerulean, which was achieved by mutating alanine in position 206 to lysine. pYFP-N1 was used to clone the raft marker Myr-Pal in front of the YFP (Myr-Pal-YFP). HA from influenza virus A/FPV/Rostock/34 (H7N1) was cloned in front of the cerulean spaced by a linker region consisting of the amino acids LRPEAPRARDPPVAT. All HA constructs exist in two versions, firstly the wild type version with a HA cleavable by furin and secondly a mutant version, which is not cleavable. The disruption of the cleavage site of furin was achieved by mutating arginine in position 339 to glycine.

Therefore 8 constructs were available for this thesis:

- Cleaved HA-mCer wt and uncleaved HA-mCer wt
- Cleaved HA-mCer VIL3A and uncleaved HA-mCer VIL3A
  (Carrying the mutation of valine, isoleucine and leucine (position 527-529) to alanine)
- Cleaved HA-mCer C3S and uncleaved HA-mCer C3S
  (Carrying the mutation of cysteine 551, 559 and 562 to serine)
- Cleaved HA-mCer VIL3A-C3S and uncleaved HA-mCer VIL3A-C3S
  (Carrying both before mentioned mutations)

2.1.11.2 Oligonucleotides

All oligonucleotides were used in the overlap-extension PCR (see 0). The oligonucleotides carry the mutated base pairs (solid underline, newly introduced mutations; dotted underline, mutations already existent in the template) in the middle of the sequence and are separately used to yield either part A or part B in the overlap-extension PCR. Dashed underline, recognition sequence of restriction enzyme (RE)

Table 11: Oligonucleotides for the creation of mutants

Name	Sequence 5' > 3'	RE
FPV-HA VAL fo (IA)	GGCTACAAAGATGTGGCACTTTGGTTTAGCTTCGGG	
FPV-HA VAL re (IA)	CCCGAAGCTAAACCAAAGTGCCACATCTTTGTAGCC	
FPV-HA VIA fo (LA)	GGCTACAAAGATGTGATAGCATGGTTTAGCTTCGGG	
FPV-HA VIA re (LA)	CCCGAAGCTAAACCATGCTATCACATCTTTGTAGCC	
FPV-HA W530A fo (WA)	GGCTACAAAGATGTGATACTTGCTTTTAGCTTCGGGGC	
FPV-HA W530A re (WA)	GCCCCGAAGCTAAAAGCAAGTATCACATCTTTGTAGCC	
FPV-HA VIAA fo (LW2A)	GGCTACAAAGATGTGATAGCAGCTTTTAGCTTCGGGGC	
FPV-HA VIAA re (LW2A)	GCCCCGAAGCTAAAAGCTGCTATCACATCTTTGTAGCC	
FPV-HA YK2A fo	CCAGTCAAATTGAGTAGTGGCGCTGCAGATGTGATACTTTGG	
FPV-HA YK2A re	CCAAAGTATCACATCTGCAGCGCCACTACTCAATTTGACTGG	
FPV-HA KLW3A fo	GGCTACGCAGATGTGATAGCAGCTTTTAGCTTCGGG	
FPV-HA KLW3A re	CCCGAAGCTAAAAGCTGCTATCACATCTGCGTAGCC	

FPV-HA ΔCCM fo (YKLW4A)	CCAGTCAAATTGAGTAGTGGC<u>GCTGCA</u>GATGTGATA<u>GCAGC</u>	
FPV-HA ΔCCM re (YKLW4A)	<u>GCTGC</u>TATCACATC<u>TGCAGC</u>GCCACTACTCAATTTGACTGG	
Bastian 71F	GATAAT<u>GAATTC</u>ACTGAGGTGG	EcoRI
Bastian 72R	GTCTCA<u>GTATAC</u>AAATAGTGCACCGCATG	Bstz17I

2.2 Methods

2.2.1 Molecular Biology

To insert mutations in the provided plasmids overlap-extension PCR was used. The amplified mutated gene segments and the vector were cut with the according restriction enzymes, seperated by agarose gel electrophoresis and cleaned up by using the "Invisorb Fragment CleanUp" Kit. The cut and dephosphorylated vector and the cut DNA fragments were ligated and transformed into competent bacteria. After plating the bacteria on YT-agar plates containing the according antibiotic, single colonies were picked and submitted to colony PCR or cultured in liquid YT-medium. To check for correct insertion of the mutated gene segment into the plasmid, either the colony PCR was checked for presence of the insert and further used for inocultation of liquid culture or plasmid DNA was isolated from directly inoculated liquid culture and checked by restriction digest and further verified by sequencing.
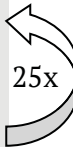
2.2.1.1 PCR

The polymerase chain reaction (PCR) is a method used to amplify DNA in an exponential manner. A basic PCR requires a template DNA, a nucleotide mixture (dNTPs), two primers, a forward primer binding in 5'>3' direction and a revers primer binding in 3'>5' direction and a suitable DNA polymerase. The PCR is carried out in a thermo cycler, which allows fast heating and cooling throughout the different steps of the reaction. A conventional PCR includes an initial denaturation at 98°C for 2min followed by three main steps, which are repeated in 25 cycles. After denaturation (98°C) of the DNA, the primers anneal (50-55°C) to the separated single strands and therefore allow the elongation (72°C) of the DNA fragment. Finally, the elongation is extended to

10min and the reaction is stopped by cooling down to 12°C for storage. A typical PCR is reported in Table 12.

Table 12: Protocol for a regular PCR

Component	Amount		PCR step	Temp	Time	
Template DNA	10 ng		Initial Denaturation	98°C	2 min	
5' primer	0.5 µM		Denaturation	98°C	10 sec	
3' primer	0.5 µM		Annealing	55°C	30 sec	25x
Phusion pol.	2 U		Extension	72°C	40 sec per kb	
dNTPS	200 µM		Final Extension	72°C	10 min	
Buffer (5x HF)	5 µl		Cooling	12°C	∞	
DMSO	1.5 µl					
ddH$_2$0	Ad 50 µl					
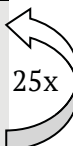
2.2.1.2 Colony PCR

The Colony PCR can be used to check for the insertion of a mutated gene segment into a vector without inoculation of a liquid culture followed by plasmid preparation and restriction digest. For this purpose a part of a single colony is picked with a sterile 10 µl tip and resuspended in the PCR mix. In case the PCR result confirms the insertion of the mutated gene segment, the remaining <u>positive</u> colony can be picked and used for inoculation of a liquid culture followed by plasmid preparation and direct sequencing.

Table 13: Protocol for the colony PCR

Component	Amount		PCR step	Temp	Time	
Single colony	1x		Initial Denaturation	94°C	3 min	
5' primer	0.5 µl		Denaturation	98°C	30 sec	
3' primer	0.5 µl		Annealing	55°C	30 sec	25x
One Taq	12.5 µl		Extension	68°C	1 min per kb	
2x Master Mix			Final Extension	68°C	10 min	
dd H$_2$0	11.25 µl		Cooling	12°C	∞	

2.2.1.3 Overlap-extension PCR

All the mutations in the HA gene described in this thesis were produced by using the overlap-extension PCR [248]. This method allows introducing site-directed mutations into a gene of interest. Insertion or mutation of sequences by a regular PCR has the disadvantage that only mutations near a restriction site, which is needed for cloning the PCR product into the vector, are permitted. By using overlap-extension PCR it is possible to introduce a mutation in a region, that is located between two restriction sites, therefore extending the possible insertion sites.
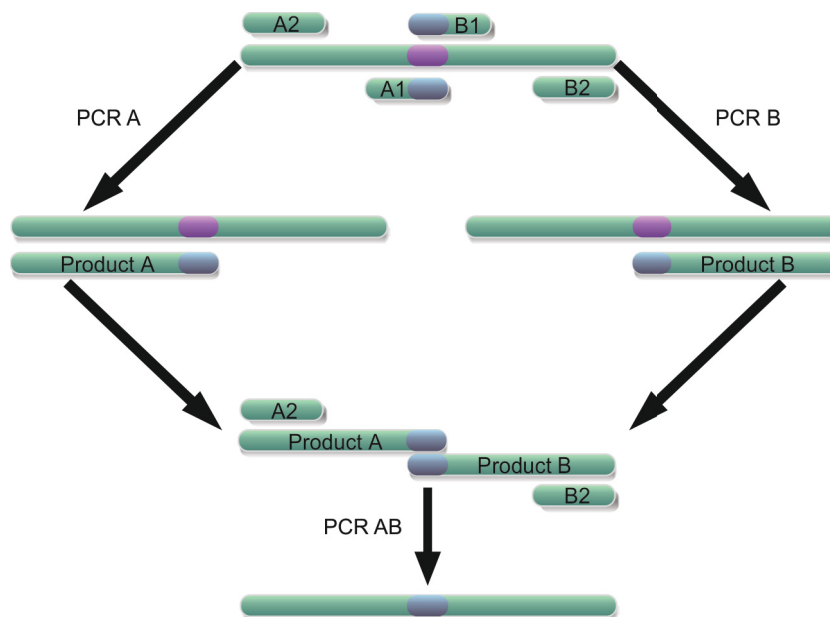
Figure 2-1: Overlap-extension PCR. Template DNA (green) is carrying original target sequence (purple) in between two restriction sites. Primers A1 and B1 carry mutated target sequence (blue), Primers A2 and B2 bind to end of selected fragment and carry the chosen restriction sites. PCR A uses primers A1 and 2 to create product A, while PCR B yields product B using primers B1 and 2. Product A and B are used as templates for AB PCR in which primers A2 and B2 are used to amplify the complete sequence carrying the wanted mutation. Created with CorelDRAW

The overlap-extension PCR requires the design of four individual primers. Two overlapping primers (A1 and B1) are complementary to the target site containing the desired mutation in the middle of the sequence and two primers (A2 and B2) complementary to the ends of the fragment carrying the chosen restriction sites. The procedure consists of two PCR steps. First, two PCRs are performed side by side using the primers A1 and A2, respectively B1 and B2, yielding two overlapping PCR products

carrying the mutation at the ends of the fragments. In the second PCR step, the two PCR products of the first step are used as templates for the creation of the final mutated gene segment. Thereby, primers A2 and B2 are used to create a fusion product that contains both restriction sites at the ends and the mutated gene sequence in the middle of the fragment.

2.2.1.4 Agarose gel electrophoresis

In order to determine the size of DNA fragments, loading dye was added to the samples and the mixture was loaded on a 1 % (w/v) agarose gel and run in TAE buffer (0.5 µg/ml Ethidiumbromid). Electrophoresis was run at 100 V to separate the DNA fragments according to their size. 5 µl Smart Ladder was used as marker to determine the size of the separated fragments. For further purposes, DNA bands were visualized using a UV hand lamp (320 nm) and if needed cut out with a scalpel to extract the DNA from the gel by using the „Invisorb Spin DNA Extraction" or „Invisorb Fragment CleanUp" Kit. Clean up was performed according to the manufacture's protocol. Elution was always performed in H_2O.

This clean up is needed either to yield pure PCR products for further cloning or for cleaning restriction digests from enzymes, which may hinder following steps of the cloning process.

2.2.1.5 Restriction digest

Restriction enzymes are endonucleases, which cut a specific DNA sequence with recognition sequences often containing 4-8 palindromic nucleotides. Restriction enzymes yield either blunt or sticky ends. If the vector and the insert (PCR product) are cut with the same two restriction enzymes yielding two different sticky ends, directed insertion of the insert is possible and religation of the vector is prevented. Typically 1-5 µg of DNA is digested with 20 U of enzyme under according buffer conditions. An example for a typical restriction digest for cloning HA mutant gene segments in the Cerulean vector is reported in Table 14.

Table 14: Protocol for a typical restriction digest

Component	Amount
DNA	1 µg
EcoRI-HF	20 U
BstZ17I	20 U
Buffer 4	3 µl
dd H$_2$0	Ad 30µl

The reaction mix was incubated for 2 hrs at 37°C and loaded on an agarose gel to purify the cut DNA. The vector was additionally treated with an alkaline phosphatase, which dephosphorylates the 5'-end of the cut vector, to further prevent religation.

2.2.1.6 Ligation

After the restriction digest insert and vector have complementary sticky ends, which will anneal spontaneously and can be joined by using T4 ligase. The ligase is an enzyme that forms the phosphodiester bond between the 5'- and 3'-end of insert and vector.

The ratio of vector to insert is crucial during the process and can be calculated by

$$mass_{insert}[ng] = \frac{5 \; x \; mass_{vector}\,[ng]\; x \; lengthfof\; fragment\,[bp]}{length\; of\; vector\,[bp]}$$

2.2.1.7 Preparation of competent bacteria

TYM medium, TfB I and TfB II solutions were prepared before starting the preparation of the competent bacteria. For the TYM medium all the components listed in Table 7 were mixed and autoclaved. For the TfB I solution first potassium acetate, calcium chloride dihydrate and glycerin were dissolved in 70 ml dest H$_2$O and pH was adjusted with diluted acetic acid to 6.2. Then rubidium chloride and manganese chloride were added, dissolved and filled up to 100 ml with dest H$_2$O. The solution was then filter sterilized with a 0.22 µm filter. For the TfB II solution MOPS, calcium chloride dehydrate, rubidium chloride and glycerin were dissolved in 40 ml dest H$_2$O, adjusted with 1N KOH to a pH of 7.0 and filter sterilized before being filled up with dest H$_2$O to the

final volume of 50 ml. TfB I and II should be stored at room temperature (RT) and pre-cooled to 4°C before use.

For the preparation of the competent cells, a single colony of bacteria was used to inoculate 10 ml TYM medium (starter culture) and incubated overnight in a 37°C shaker. Then, 50 ml growth culture was inoculated with 0.5 ml of the starter culture and incubated in a 37°C shaker until the OD reached 0.2-0.6. Subsequently, the 50 ml growth culture was used to inoculate 500 ml final culture and shaken at 37°C until the OD reached 0.4, not more. The culture was cooled down in ice-cold water for 10 min while shaking. The cells were collected by centrifugation for 10 min at 1000 x g. All centrifugation steps should be performed at 4°C. The supernatant was discarded and the cells were resuspended in 100 ml ice-cold TfB I solution and incubated on ice for 10 min. After transfer of the cells to 50 ml falcon tubes they were centrifuged for 8min at 1500 x g. Cells were resuspended in 10 ml ice-cold TfB II solution per falcon tube and stored in ice water. Finally, the cells were aliquoted à 250 µl in precooled microtubes and snap-frozen in liquid nitrogen before storage at -80°C.

2.2.1.8 Transformation

For amplification of plasmid DNA *E.-coli* bacteria were transformed either with existing plasmid DNA or freshly ligated new constructs. 1 µg of DNA was mixed with 100 µl competent cells and incubated on ice for 30 minutes. After a 45 sec "heat shock" at 42°C cells were directly transferred on ice to incubate for 2 min. 600 µl of pre-warmed YT-Medium (37°C) was added and shaken (200 rpm) for 45 min at 37°C to enable expression of the according antibiotic resistance gene. 200 µl of the bacterial culture were subsequently plated on antibiotic containing agar plates and incubated over night at 37°C.

2.2.1.9 Plasmid purification

For the purification of plasmids two Kits were used. For the preparation of newly made constructs, single colonies of transformed and plated bacteria was picked to inoculate 3 ml of YT-medium plus antibiotic and shaken (200 rpm) at 37°C over night. Bacteria were pelleted, and by using the "Invisorb Spin Plasmid Mini Two" Kit plasmid DNA was isolated according to the manufacturer's manual. For preparation of large

amounts of plasmid DNA 100 ml of YT-Medium was inoculated and DNA was isolated by using the "Pure yield" Kit by Promega. Both Kits are based on alkaline lysis followed by binding of the plasmid DNA by either matrix material and elution under low-salt conditions (Invisorb) or anion exchange (Promega). Concentration of eluted DNA was determined by measuring the absorbance at 260 nm using a NanoDrop spectrometer.

2.2.2 Cell culture

2.2.2.1 Cell culture maintenance

To maintain an adherent CHO-K_1 cell culture, cells were passaged 1:20 every 3-4 days when a confluence of 90-100 % in a 75cm^2 cell culture flask (T75) was reached. To that end, adherent cells were washed once with 10 ml PBS without Calcium and Magnesium followed by an incubation with 2 ml trypsin/EDTA for 5 min at 37°C. Trypsin was inactivated by adding 8 ml complete DMEM containing 10 % FBS, 1 % L-glutamine and 1 % penicillin/streptomycin. Finally, 0.5 ml suspension was transferred to a new T75 cell culture flask containing 10-15 ml fresh complete DMEM. All steps were performed under sterile conditions under a lamina flow. Cells were incubated at 37°C, 5 % CO_2 and 80 % humidity.

2.2.2.2 Cell freezing and thawing

For longtime storage cells were detached with trypsin/EDTA as described above and resuspended in 8 ml complete DMEM. Cells were pelleted by centrifugation for 10 min at 100-200 x g at RT. The supernatant was discarded and cells were washed once with cold PBS w/o Ca^{2+} and Mg^{2+}. After resuspension in 6 ml freezing medium (60 % DMEM, 30 % FBS and 10 % DMSO), 4 aliquots of each 1.5 ml were distributed in suitable cryo tubes and frozen in an isopropanol tank at -80°C over night to assure a slow freezing of approximately 1°C per minute. Longtime storage was performed at -196°C in a liquid nitrogen tank.

For thawing, complete DMEM was preheated to 37°C. Frozen cells were directly transferred to a preheated water bath to ensure fast defrosting and mixed with 10 ml of the preheated complete DMEM to dilute the DMSO. After centrifugation at 200 x g, cells were resuspended in 5 ml complete DMSO and transferred in a 25cm^2 (T25) cell culture flask, which allows the cells to reach a confluence of 90 % already after 1 day. Fast

splitting after thawing helps to remove residual DMSO and optimizes the recovery. Cells of a T25 flask can be transferred to a T75 flask and will reach 90 % confluence within 3 days and should be passaged a couple of times before usage in further experiments.

2.2.2.3 Transfection

Transfection was performed using TurboFect (Thermo Scientific) according to the manufacturer's protocol. For transfections of 6-well cell culture plates or 35-mm glass bottom dishes (MatTek) 4 µg of DNA was mixed with 6 µl of TurboFect reagent and 400 µl of Opti-Mem and incubated for 15-20min at RT. Meanwhile, 70 % confluent cells were washed once with PBS with Ca^{2+} and Mg^{2+} to avoid detachment of cells and 1.5 ml of fresh, warm Opti-Mem was added per well. After 15-20 mins the mixture was added drop wise to the cells. 5hrs post transfection the medium was replaced by fresh Opti-MEM and protein expression was allowed for 16-24 hrs.

2.2.2.4 Usage of inhibitors

Fumonisin B_1 was used to inhibit sphingolipid synthesis. Sphingolipids are synthesized in a stepwise manner. First, serine and palmityl-CoA are condensed to form sphinganine, which is further acylated to dihydroceramide by the ceramide synthase and finally modified to ceramide. In addition, ceramide can be transformed to sphingosine by removing the 2nd acylation and reformed by acylation of sphingosine again by the ceramide synthase. Sphingomyelin and glycerophospholipids are then formed out of the ceramide backbone in the Golgi.

Fumonisin B_1 is a potent inhibitor of the ceramide synthase and therefore inhibits sphingolipid synthesis at a precursor stage already in the ER [249]. The inhibitor (Sigma, 20 µM end concentration out of a 7 mM DMSO stock solution) was added 16 hrs prior to transfection of CHO-K1 cells for metabolic labeling and was present throughout the experiment except during the transfection time of 5 hrs.
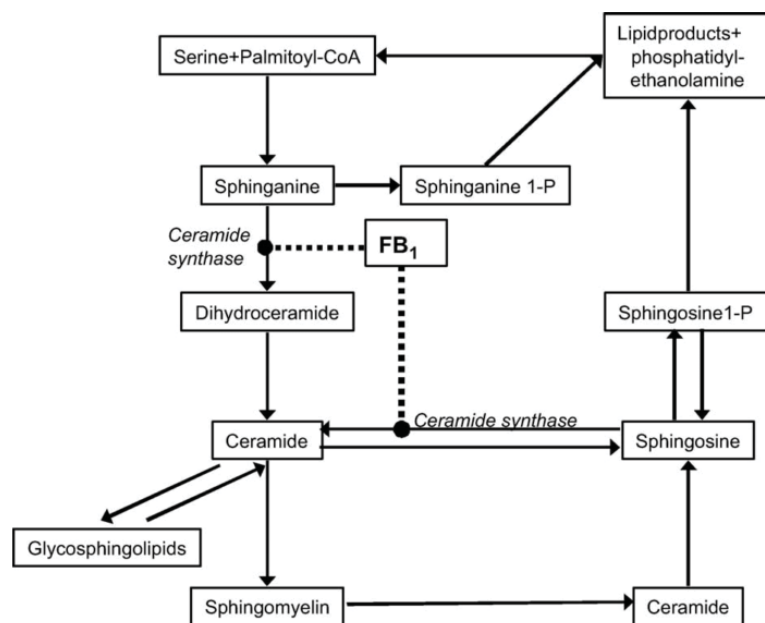
Figure 2-2: Scheme of sphingolipid synthesis. Inhibition of Fumonisin B₁ shown as dashed line. Reprinted rom [249] with permission by the CC-BY license by SAGE Publications

2.2.3 Biochemistry

2.2.3.1 Metabolic labeling

For the metabolic labeling of CHO-K_1 cells expressing variants of the HA protein, cells were seeded 1:3 into 6-well plates one day prior to transfection. Constructs of choice were transfected (see 2.2.2.3) into the CHO-K_1 cells and expression was allowed for 24 hrs. For prestarving the cells, they were first washed twice with PBS with Ca^{2+} and Mg^{2+} and further incubated for 2 hrs at 37°C in MEM without L-methionine and L-cysteine. Labeling for pulse-chase experiments was performed by adding 3 µCi/ml [^{35}S]-methionine/cysteine (EasyTag™ EXPRESS ^{35}S Protein Labeling Mix, Perkin Elmer) for 3 or 30 min according to which further analysis was performed (see 3.2.3.1.1-3). Labeling (pulse) was followed by varying chasing periods with DMEM containing 100x surplus unlabeled L-methionine and L-cysteine.

For the analysis of the labeled proteins, cells were washed once with PBS with Ca^{2+} and Mg^{2+} before adding 500 µl ice-cold RIPA buffer for 15 min for lysis. Cell debris was pelleted by centrifugation for 20 min at 20.000 x g and 4°C, and supernatant was subtracted to immunoprecipitation. Therefore, supernatant was transferred to a new tube, 0.5 µl of goat anti-FPV primary antibody was added and incubated over night at 4°C under shaking conditions to allow binding of HA. To precipitate the protein 40-50 µl of

Protein-A-Sepharose was added and further incubated for 2.5 hrs at 4°C under shaking conditions. After the binding, samples were washed 4x by centrifugation of the target complex at 3000 rpm for 3 min and adding of 500 µl ice-cold RIPA buffer containing cOmplete Protease inhibitor (Roche, 1 tablet dissolved in 50 ml buffer). Finally, the pelleted complexes were solubilized either directly in SDS-buffer or according buffers for further analysis.

Trimerization-test

To analyze the trimerization status of a protein one can use proteolytic digestion. Influenza HA monomers are not resistant to digestion with trypsin, but upon trimerization will gain resistance. That means, in case of a short pulse-chase experiment HA monomers will be digested completely, while HA trimers will be cut into HA_1 and HA_2.

Transfected cells were labeled for only 3 min to ensure labeling of only ER located protein. Samples were chased for 0, 7.5, 15 and 30 min. For 0 min chase samples, the 6-well plate was directly put on ice to avoid further transport and processing of the HA molecules. All other samples were washed once with 100x surplus DMEM to avoid further uptake of residual ^{35}S label before chase incubation with 100x surplus DMEM. In this case lysis was performed by using 700 µl MNT buffer, which doesn't affect the tertiary and quaternary structure of proteins, instead of RIPA buffer as described above. After centrifugation samples were divided in two, one sample was mock treated (1.5 µl PBS) while 1.5 µl of trypsin was added to the other. After 2 min of incubation at RT, 3 µl of Soybean-protease inhibitor was added to stop the process and immunoprecipitation was performed as described above. Washed samples were solubilized in SDS-buffer.

Endo-glycosidase H digest

To test whether a protein has already reached the medial Golgi one can investigate the acquisition of Endo-H resistant carbohydrates. Upon passing of the *cis*-Golgi mannose-rich carbohydrates get further trimmed and modified to yield complex sugars, which are no longer Endo-H susceptible.

In this case non-cleavable (uncleaved HA-mCer X) variants of the HA protein were used for easier detection. Transfected cells were labeled with ^{35}S for 30 min and chased for 0, 1, 2, 4, 6 or 14 hrs. After lysis with RIPA buffer and immunoprecipitation, washed complex samples were divided in two. The mock sample was mixed with 8µl H_2O, while the other was mixed with 8 µl denaturation buffer (delivered with Endo-H, Sigma-Aldrich) and heated to 100°C for 10 min. After centrifugation the supernatant, which contained the detached proteins, was transferred to a new reaction tube. Either 4 µl H_2O (mock) or 1 µl of G5 buffer and 1 µl of Endo-H (1:10 pre-diluted) was added to the sample and incubated for 1 h at 37°C before adding of SDS-buffer.

<u>Intra cellular cleavage of HA</u>

To test for passing of the *trans*-Golgi cleavage of the precursor HA_0 into its subunit HA_1 and HA_2 was investigated.

Transfected cells were labeled with ^{35}S for 30 min and chased for 0, 1, 2, 4, or 6 hrs. After lysis with RIPA buffer and immunoprecipitation, samples were solubilized in SDS-buffer. All SDS-buffer solubilized samples from all types of experiments were heated for 5 min to 95°C, centrifuged and subjected to SDS-PAGE and fluorography.

2.2.3.2 SDS-PAGE

Denatured proteins were separated according to their differences in mass by using the discontinuously sodium dodecyl sulfate polyacrylamide gel electrophoreses (SDS-PAGE) [250]. This method relies on the principle that each SDS anion binds to two amino acid residues and therefore applies a negative charge, which is approximately proportional to the mass of the protein.

Gels were prepared as resolving gel with 12 % acryl amid and a stacking gel on top with 5 % acryl amid. Samples were centrifuged after heating to 95°C and loaded onto the stacking gel. The electrophoresis was run at constant voltage of 100 V for the stacking gel and of 180 V for the resolving gel. Radioactive protein bands were visualized by fluorography.

2.2.3.3 Fluorography

Fluorography is used to visualize radioactive proteins separated by SDS-PAGE. Radioactive material can be visualized by exposing X-ray films to the radiation. To enhance the signal, gels can be treated with sodium salicylate, which converts the radioactive energy in fluorescence. Therefore, gels were fixed in fixing solution for a minimum time of 1 h, washed 2x for 15 min in H_2O and treated with a 1 M sodium salicylate solution for 30 min. Subsequently, gels were dried and incubated in a film cassette with X-Ray films at -80°C for 3 days or up to a month in case of short pulse-chase experiments. Films were developed in a darkroom, dried and bands were analyzed using the Bio1D software (peqlab).

2.2.4 Flow cytometry

CHO-K_1 cells were seeded into 24-well plates (Greiner) and transfected 24 hrs prior to the experiment. For 24-well plates 1 µg of DNA was mixed with 2 µl of TurboFect and 200 µl Opti-MEM per well. All other steps were performed as described in 2.2.2.3. For detection of surface expression cells were detached by using Trypsin/EDTA and recovered in DMEM/FCS at 37°C for 10 min. After fixation with 2 % PFA cells were blocked with a 3 % BSA solution and stained with an anti-FPV antiserum (1:1000) followed by goat anti-rabbit Alexa 488 antibody (1:1000). Overall and surface protein expression was analyzed using FACSCanto and FlowJo software.

2.2.5 Microscopy

2.2.5.1 Confocal laser scanning microscopy (CLSM)

The confocal laser scanning microscopy is of great advantage to the classical epifluorescence microscopy. Instead of light sources like xenon arc lamps or LEDs, CLSM uses lasers to excite the fluorophores and scans the sample point by point, whereby the emitted light passes a pinhole to block out the out-of-focus light. The light signal is then detected by a photomultiplier tube (PMT) and recorded by the computer. The full image is recorded by scanning the sample horizontally line by line. This allows for a higher resolution of the picture taken.

In all microscopic experiments an Olympus FluoView 1000 microscope was used. Pictures were obtained by using the UplanSApo oil immersion objective with a 60x mag-

nification and a numerical aperture of 1.35. The temperature was kept constant at 25°C. While Cerulean was excited with a laser diode with a wavelength of 440 nm and YFP with an argon laser with a wavelength of 515 nm, emission was detected between 460 and 490 nm, respectively 535 and 575 nm. Alexa 568 conjugated secondary antibody was excited with a 559 nm Helium-Neon-Laser and detected between 580-664 nm. Signal of double transfected or double-labeled cells was recorded sequentially.

2.2.5.2 Immunofluorescence

For Colocalization studies of HA raft and non-raft variants with the *cis*-Golgi marker membrin, CHO-K$_1$ cells were seeded into 24-well plates equipped with $\varnothing$12mm cover slips. 24 hrs after transfection of 1μg DNA, cells were fixed with 2 % PFA for 15 min at RT, washed 2x with PBS 0.1 % Tween and one time with PBS 0.1 M glycine to inactivate the PFA, permebealized (0.5 % Triton X-100 in PBS) and blocked for 1h with 3 % BSA. Membrin was detected by incubation of the cells with a mouse anti-membrin primary antibody (1:500) for 1 h at RT. Followed by 3x washing with PBS 0.1 % Tween cells were incubated with an anti-mouse Alexa 568 secondary antibody (1:1000) for another 45 min. Cover slips were washed 3x with PBS 0.1 % Tween and 2x with dest. H$_2$0 to remove residual Tween before mounting on glass slides with Mowiol mounting solution and drying over night. Confocal images were sequentially obtained and used for further analysis and quantification of colocalization.

2.2.5.3 Quantitative analysis of colocalization – Calculation of pearson's correlation coefficient R

By using Image J's colocalization analysis plugin the Pearson's correlation coefficient (R) can be determined. Therefore the perinuclear region was selected as region of interest (ROI) and analyzed according to:

$$R = \frac{\sum(R_i - \overline{R})x(G_i - \overline{G})}{\sqrt{\sum(R_i - \overline{R})^2 \, x \sum(G_i - \overline{G})^2}}$$

where R_i and G_i are the intensity values of the red and green channels of pixel i, and $\overline{R}$ and $\overline{G}$ are the mean intensities of the red and green channels across the entire image. Values for R can range from 1 to -1, with fluorescence intensities for the green and red channel being perfectly linear related or inversely perfectly related, respec-

tively. Values around zero can be interpreted as uncorrelating samples [251]. Defining the region of interest is of great importance, because incorporation of unlabeled pixels into the analysis can lead to higher values for R. Values from 0.1 to 0.3 can be interpreted as small association, while values from 0.3 to 0.5 and from 0.5 to 1.0 can be interpreted as medium and high association, respectively.

2.2.5.4 Fluorescence lifetime imaging microscopy by measuring fluorescence resonance energy transfer (FLIM-FRET)

FLIM-FRET was carried out as in [118,222,223]. CHO-K_1 cells were seeded into 35mm glass bottom dishes (MatTek Corporation) and co-transfected 24 hrs prior to the experiment with the appropriate uncl. HA-mCer variants as FRET donor and Myr-Pal-YFP as FRET acceptor. For calculation of the donor lifetime in absence of the acceptor, additionally, uncl. HA-mCer alone was transfected. Confocal images were obtained sequentially for Cerulean and YFP using a FluoView 1000 microscope (Olympus) as describes in 2.2.5.2 (see Figure 2-3 A-C). Using the PicoQuant LSMupgrate kit FLIM measurements were performed. Excitation of Cerulean was executed using a 440 nm pulsed laser diode with a 20MHz pulse frequency. Emission was detected with a single photon avalanche photodiode (SPAD) with a 470/30 bandpass filter, and a TimeHarp 300 photo counting board processed the signal. For later analysis of the obtained data the instrument response function (IRF) was recorded by measuring the scattered light of a double distilled water drop with the same excitation but emission detection with a 440/10 bandpass filter. All signals were accumulated over 90 seconds and 60 pictures with a count rate of 2-4 x 10^4 counts per second.

Using the SymPhoTime software FLIM analysis was performed. A TCSPC histogram was generated after manual selection of the plasma membrane of at least 25 cells co-expressing HA−Cer and Myr-Pal-YFP (see Figure 2-3 D-F).

To calculate the lifetime of the donor fluorophore in the absence of acceptor, ten cells expressing only the donor were analyzed on each day an experiment was performed. The amplitude-weighted lifetimes where calculated according to:

$$\overline{\tau} = \left(\frac{\alpha_1}{\alpha_1 + \alpha_2} * \tau_1 \right) + \left(\frac{\alpha_2}{\alpha_1 + \alpha_2} * \tau_2 \right)$$

The optained lifetimes were judged by the χ^2 values and the residues of the fit. χ^2 values between 0,85 and 1,0 were considered valid for further analysis, while values of χ^2 less than 0,85 were excluded. The FRET efficiency (E in %) was calculated using the equation:

$$E = \left(1 - \frac{\overline{\tau}_{DA}}{\overline{\tau}_D}\right) * 100$$

where τ_{DA} is the lifetime of a single cell co-expressing donor and acceptor and τ_D is the average lifetime of the ten cells expressing only the donor.

In an enclosed system like the plasma membrane, energy transfer between the donor and acceptor can occur due to specific interaction or random collision in case of high acceptor concentrations. To account for the two possible interactions the amount of acceptor Myr-Pal-YFP at the plasma membrane measured and displayed as the mean intensity of the fluorescence was determined and plotted against the FRET efficiency (E). Therefore, the region of interest of the FLIM analysis (Figure 2-3 F) was exported as a picture and used as matrix for the selection of the according area in Image J, which was further used for the analysis of the fluorescence intensity. The obtained values were corrected for background and laser intensities.

The data were fitted with GraphPad Prism 5 to the hyperbolic function resembling a binding kinetic model:

$$E(\%) = \frac{E_{max} * A}{K_D + A}$$

whereby E_{max} is the maximal FRET efficiency calculated from the fitting, A is the acceptor intensity and K_D is a measure of clustering (detailed information in Zacharias et al. [244]). Low K_D values compared to the average intensity indicate true clustering, which is independent on acceptor concentration while high K_D values indicate random interaction, which is dependent on increasing acceptor concentration.
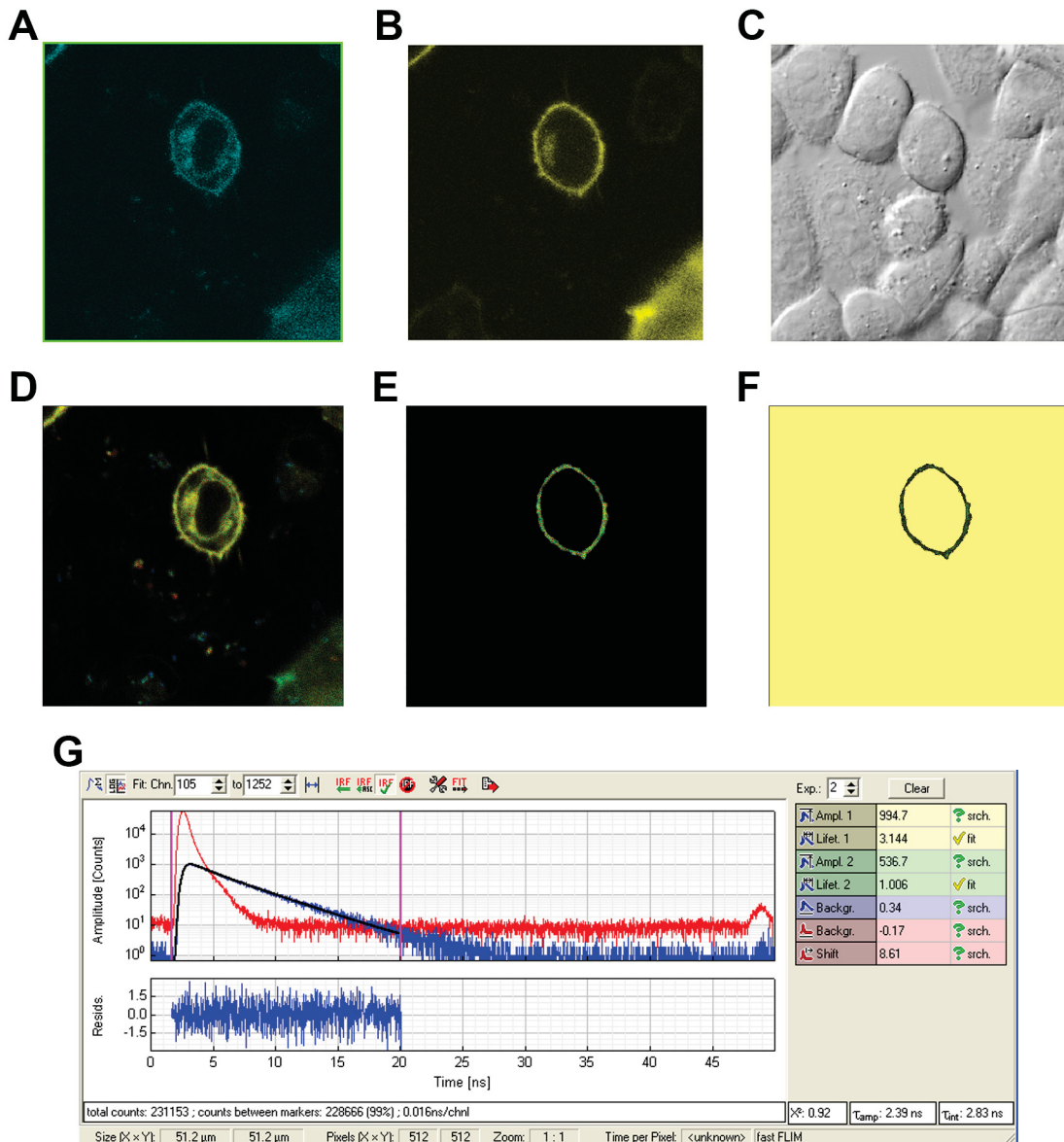
Figure 2-3: Analysis of FLIM-FRET. (A, B) Fluorescence image of HA-Cer and Myr-Pal-YFP **(C)** DIC image for evaluation of the cell vitality **(D)** FLIM pseudocolor image **(E)** selected plasma membrane as ROI **(F)** background color exchange to exclude weak signals in the vicinity of the ROI and for export as TIFF as matrix for intensity analysis **(G)** histogram of the selected ROI (blue), fitted decay curve (black) and IRF (red), lifetimes and amplitudes are shown in the adjacent box on the left, χ^2 and amplitude-weighted lifetimes are given in the lower right panel

3 Results

3.1 Effect of mutations in the raft-targeting signals of HA on the transport along the exocytic pathway

3.1.1 Verification and replication of Stephanie Engels data on the transport of raft targeting mutant HA

The first part of the results will focus on the verification and partial replication of previous experiments performed by Stephanie Engel. The description of previous and recent data is needed for understanding the hypothesis being made in this thesis and for the interpretation of the acquired data. The origin of the data will always be indicated to clarify the ownership.

3.1.1.1 Trimerization kinetics of raft-targeting HA mutants

The first determinant for an efficient transport is trimerization after the expression, folding and start of glycosylation of the HA monomers. Non-trimerized or misfolded protein will be retained in the ER and subsequently degraded. Differences in trimerization of wild type and mutant protein therefore can hint towards an aberrant protein due to the mutations made. As Stephanie Engel only performed this experiment once in the previous work, the findings made before, were to be verified.

CHO-K_1 cells expressing HA-Cer wt, VIL3A or VIL3A-C3S were shortly labeled (3 min) to only label protein within the ER and chased for 7.5, 15 and 30 min. After digestion of immunoprecipitated HA with or without trypsin and SDS-PAGE, the kinetic of trimerization was analyzed. In this time setting cleavage should only be performed by trypsin, as intracellular cleavage by furin takes place at later stages of the transport along the exocytic pathway. Trypsin digestion will still lead to the cleavage of HA_0 into its subunits HA_1 and HA_2, but with varying subunit sizes due to the multibasic cleavage site. Since HA is fused to the fluorophore Cerulean in this experiment, trypsin digestion should only lead to one band representing HA_1 and HA_2-Cer.

When analyzing the fluorography of any given HA construct the appearance of two to three distinct bands in the trypsin treated sample can be observed. This is in contrast to the prediction of two subunit bands after cleavage. The uppermost band is representing most probably HA_1 with a mass of approximately 50kDa. Cleavage sites within the Cerulean can explain the two lower bands with a mass of approximately 45kDa even after trimerization of the fusion protein, whereby the small shift in mass between the two bands can be explained by differential cleavage within the multibasic cleavage site.
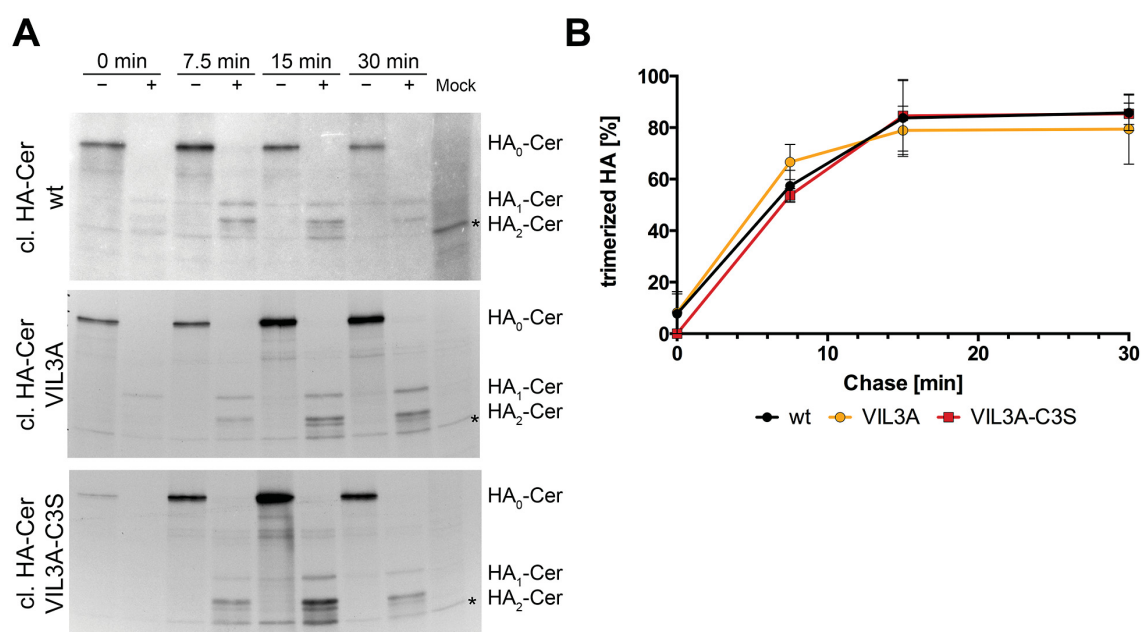

Figure 3–1: Trimerization of raft-targeting mutant HA. (A) CHO-K_1 cells expressing cl. HA-Cer wt, VIL3A or VIL3A-C3S were labeled with [^{35}S]-methionine for 3 min and chased for 0, 7.5, 15 or 30 min. Cell extracts were left untreated (−) or were digested with trypsin (+) prior to immunoprecipitation with anti-FPV antibodies and reducing SDS–PAGE. * Indicates an unspecific band. All fluorography pictures are from experiments performed by me. **(B)** Densitometric quantification of bands from three experiments. Stephanie Engel performed one experiment, while I performed the other two. The intensity of HA-Cer, HA_1 and HA_2-Cer bands was determined and the value for HA-Cer was set to 100 %. Trimerization was calculated [rel. intensity HA-Cer/(rel. intensity HA_1 + rel. intensity HA_2-Cer)] for each time point and is plotted against time of chase. Error bars indicate the standard deviation. Non-parametric Friedman test for grouped (repeated) measurements with Dunn's multiple comparison test of all time points shows no significant difference between wt and VIL3A or VIL3A-C3S, respectively. Reprinted from [252] with permission from Elsevier [OR APPLICABLE SOCIETY COPYRIGHT OWNER].

The analysis of the reproduced experiment verifies the findings of Stephanie Engel by showing an almost complete digestion of HA by trypsin after 0 min of chase. Already

after 7.5 min the band pattern of HA_1 and HA_2-Cer variants can be observed (Figure 3–1 A). Analysis of the kinetics shows that the trimerization is complete after 15 min, since the amount of trimerized HA does not increase after 30 min of chase (Figure 3–1 B).

As wild type HA-Cer, HA-Cer VIL3A and HA-Cer VIL3A all show the same kinetics, a folding or trimerization defect of the mutated protein can be excluded and the constructs can be used for further experiments.

3.1.1.2 Transport from ER to Golgi of raft-targeting mutants

The following experiment and data is not part of this thesis, but was included for a better understanding of the modification kinetics of the raft-targeting mutants. All data shown here belong to Stephanie Engel and were first published in her thesis [253].

As described in 1.2.2 acquisition of Endo-H resistant carbohydrates takes place in the medial-Golgi. Analysing the status of glycosylation therefore is a valid tool to check the effect of the mutations on the transport of HA from the ER to the medial Golgi. Pulse-chase experiments were performed by Stephanie Engel to measure the amounts of Endo-H resistant HA after various times. CHO-K_1 cells expressing HA-Cer wt, VIL3A, C3S or VIL3A-C3S were labelled with [^{35}S]-methionine and chased for 0, 1, 2 and 4 hrs. Transport affecting mutants VIL3A and double mutant VIL3A-C3S were additionally chased for 6 and 21 hrs to show that the acquisition of Endo-H resistant carbohydrates is delayed but still completed. The by furin uncleavable (uncl.) version of HA was used for easier quantification. After immunoprecipitation, digestion with (+) or without (−) Endo-H and SDS-PAGE band intensities for Endo-H resistant and non-resistant HA were calculated. It needs to be stated that only 5 of the 7 glycosylation sites are fully processed, which is why even after 4 hrs an Endo-H sensitive band is still detectable. Additionally, data was normalized to wt in the densitometric quantification.

Stephanie Engel was able to show that $t_{1/2}$ of 40 min for wt and palmitoylation mutant C3S was doubled to ~80 min in case of the transmembrane mutant VIL3A and the double mutant VIL3A-C3S. Acquisition of Endo-H resistant carbohydrates was completed after 4 hrs for wt and C3S, while VIL3A and VIL3A-C3S acquire full modification only

after more than 6 hrs. Thus, only the mutation of the raft-targeting signal in the transmembrane region is of importance for transport from ER to the medial Golgi.
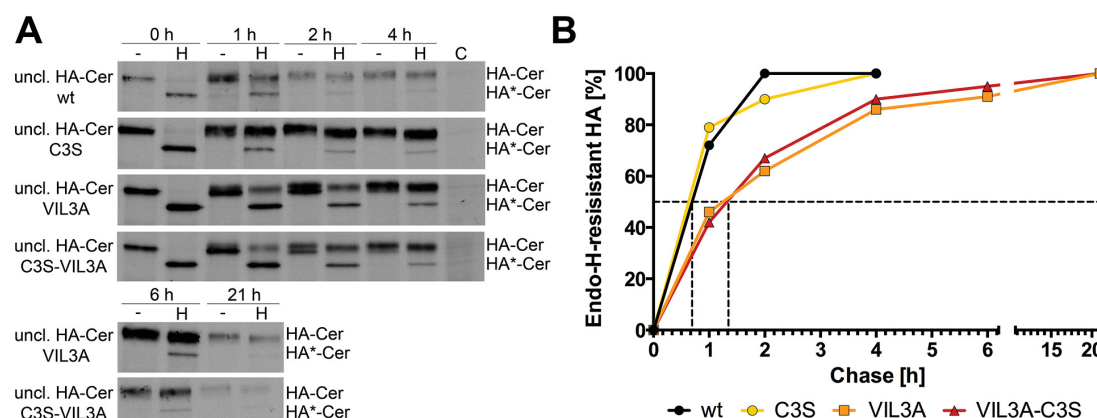

Figure 3–2: Acquisition of Endo-H resistant carbohydrates of raft-targeting mutant HA. **(A)** CHO-K1 cells expressing the indicated HA constructs were with [35S]-methionine for 30 min and chased for 0, 1, 2, 4, 6 or 21 hrs. HA was immunoprecipitated with anti-GFP antibodies and digested with Endo-H (H) or was left undigested (−) prior to reducing SDS–PAGE. *: Endo-H-sensitive. **(B)** Densitometric quantification of bands. Endo-H-resistant HA in % was calculated [(HA-Cer/(HA-Cer + HA⁄-Cer) x 100] and is plotted against time of chase. Data is normalized to wt. The horizontal broken line indicates 50% Endo H-resistance and the vertical broken line the corresponding chase time. Error bars indicate standard deviation. Reprinted from [252] with permission from Elsevier [OR APPLICABLE SOCIETY COPYRIGHT OWNER].

3.1.1.3 Transport within the *trans*-Golgi network of raft-targeting mutants

The precursor HA_0 is cleaved into its subunits HA_1 and HA_2 in the TGN by furin, therefore investigation of cleavage kinetics allows us to monitor the transport speed in between Golgi cisternae. Cleavable versions of the HA-Cerulean fusion constructs were transfected into CHO-K_1 cells and cleavage was assayed via radioactive pulse-chase after 0, 1, 2 and 4 hrs.

The following data shown is combined from experiments performed by Stephanie Engel and me. Data for wt and TMR mutant VIL3A were acquired by me, while the data for the palmitoylation (C3S) and double mutant (VIL3A-C3S) was acquired by Stephanie Engel during her PhD [253]. Since HA-Cer wt and C3S as well as HA-Cer VIL3A and VIL3A-C3S didn't display a difference in their cleavage kinetics during the studies of Stephanie Engel, only HA-Cer wt and VIL3A were used to reproduce and verify the data.

The wild type HA-Cer has a $t_{1/2}$ of ~50 min, which is the same for the palmitoylation mutant C3S. In contrast, mutation of the raft-targeting signal in the TMR alone and as double mutation, likewise acquisition of Endo-H resistant carbohydrates, retards the transport of HA-Cer as $t_{1/2}$ is 140 min (see Figure 3–3 B). Cleavage for wild type HA is nearly completed after 4 hrs as can be seen in Figure 3–3 A, right lane, which is why the obtained data was normalized to the highest value for the wt. Therefore, I was able to confirm the data obtained by Stephanie Engel.

Compared to the transport from ER to medial Golgi the delay in transport increases within the Golgi from doubling the time needed to nearly tripling it.
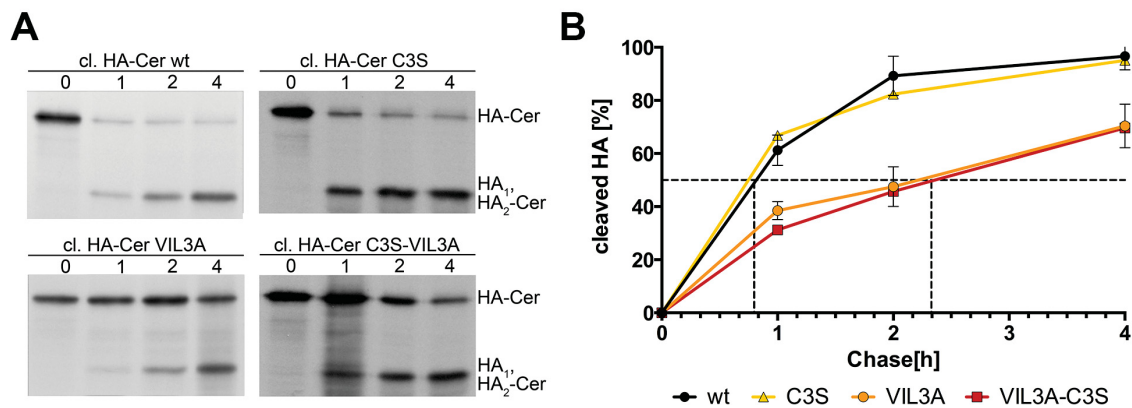
Figure 3–3: Cleavage of raft-targeting mutant HA. (A) CHO-K$_1$ cells expressing the indicated HA constructs were labeled with [35S]- methionine for 30 min and chased for 0, 1, 2 or 4 hrs . HA was immunoprecipitated with anti-FPV antibodies prior to reducing SDS–PAGE. **(B)** Densitometric quantification of bands from A and for cl. HA-Cer wt and cl. HA-Cer VIL3A from three to five other experiments. Cleaved HA in % was calculated [(HA$_1$ + HA$_2$-Cer)/(HA$_1$ + HA$_2$-Cer + HA-Cer) x 100] and is plotted against chase time. The horizontal broken line indicates 50% cleavage and the vertical broken line the corresponding chase time. Error bars indicate standard deviation. Reprinted from [252] with permission from Elsevier [OR APPLICABLE SOCIETY COPYRIGHT OWNER].

From here on, all experiments were performed by me alone.

3.1.1.4 Colocalization of HA-Cer wt and VIL3A with the *cis*-Golgi marker membrin

According to Patterson et al. [151] so-called export and processing domains exist in the Golgi in which the proteins part according to their function. While Golgi resident proteins will mainly be localized in the processing domains due to exclusion from the export domains, cargo protein, which is transported to the plasma membrane, will be enriched in the export domains.

In case this hypothesis is valid, it might be possible to visualize this state by co-localization studies with the HA-Cer wt as an example for a raft protein and membrin, an endogenous t-SNARE, as an example of a resident protein, which is located in the ER-Golgi intermediate compartment (ERGIC) and the first two cisternae of the Golgi [254,255]. Transport delayed VIL3A protein should more likely be localized within the processing domains like membrin, whereas wild type proteins would favor the export domains.

To test for localization of HA proteins in comparison with the *cis*-Golgi marker membrin, CHO-K$_1$ cells were transfected with the according variant of HA, wt and VIL3A mutant, respectively. After 24 hrs of transfection cells were stained with an anti-membrin antibody and confocal images were taken. Using Image J's colocalization analysis plugin pictures were pseudocolored and Pearson's correlation coefficient (R) was calculated. The R value determines the linear correlation of two fluorescence intensities in two channels, preferably red and green. Values between 0 and 0.3 can be interpreted as small correlation or colocalization, while values ranging from 0.3 to 0.5 as medium association. Values from 0.5 to 1.0 are indicating high correlation. In combination with a scatter plot of the intensities against each other, the colocalization can be determined quantitatively.

As a positive control for colocalization HA fused to Cerulean and fused to YFP were used (Figure 3−4 left panel). CHO-K$_1$ cells transfected with both constructs should express mixed trimers of the HA protein, therefore showing the highest colocalization that is possible is this set up.

A
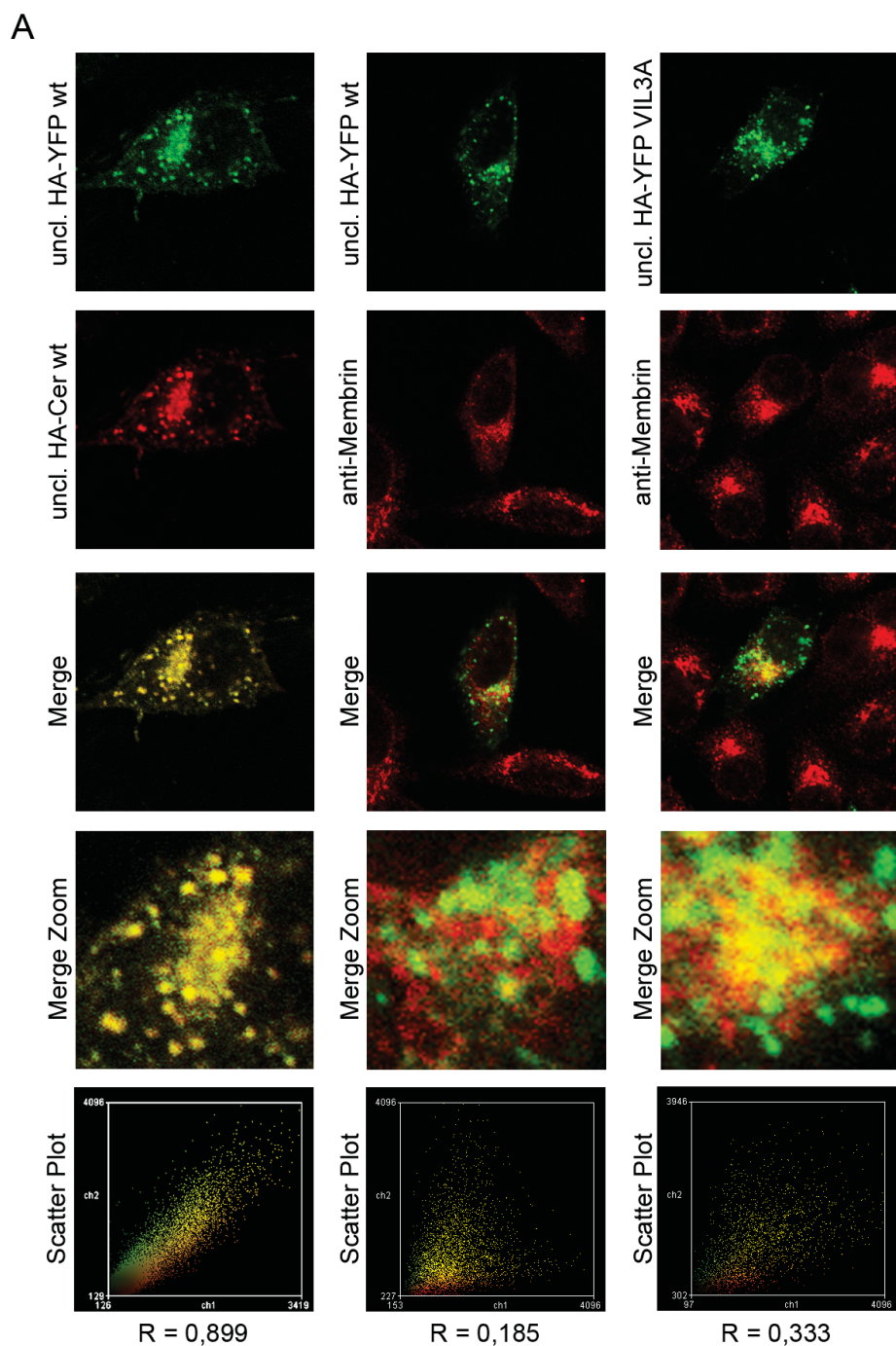
Figure 3–4: Colocalization of HA with membrin. Pseudocolored confocal images of CHO-K$_1$ cells expressing the indicated constructs. Anti-membrin and Alexa568-coupled secondary antibodies were used to stain the *cis*-Golgi. Third and fourth row: merge of the whole visual field or the zoomed perinu-clear region. Fifth row: Scatter plot showing the fluorescence intensities for each pixel in the two channels (x-axis: YFP, y-axis: Cer/Alexa568). R: Pearson's coefficient, calculated from the perinuclear region of n cells (mean ± SEM): HA wt YFP/CFP: 0.899 ± 0.009, n = 9; HA VIL3A YFP/CFP: 0.862 ± 0.021, n = 7 (flu-ourescence pictures not shown); HA wt/membrin: 0.185 ± 0.036, n = 23; HA VIL3A/membrin: 0.333 ± 0.047, n = 16. Results for HA wt/membrin are statistically significantly different (p = 0.0154, p < 0.05) from HA VIL3A/membrin as calculated using a two-tailed unpaired Student's t test. Reprinted from [252] with permission from Elsevier [OR APPLICABLE SOCIETY COPYRIGHT OWNER].

The confocal images in Figure 3–4 are false color-coded, HA-YFP to red and HA-Cer to green, respectively, to allow easy classical merge. After 24 hrs of expression an almost complete overlap of the two signals was observed. For further analysis the Golgi was chosen as ROI (Figure 3–4 merge zoom). When analyzing the Pearson's correlation coefficient a value of 0.899 was calculated, which indicates high correlation of the two signals. Also the scatter plot shows a high linear dependence of the two fluorescence intensities. The same was true for heterotrimers of HA-Cer and HA-YFP of the VIL3A mutant (R= 0.862, data not shown). These results show that the Pearsons's R can be used to determine colocalization.

Expression of wt and VIL mutant HA-YFP and subsequent staining of membrin leads to a partial colocalization in both cases (see merge Figure 3–4 middle and right panel), however, in case of HA-YFP VIL3A to a higher degree. Calculation of R supports this finding as values of 0.333 for mutant HA and 0.185 for wt HA were determined. Additionally, the scatter plot of HA-YFP VIL3A and membrin signal shows a more quasi-linear form than HA-YFP wt.

3.1.1.5 Intra-Golgi transport with Fumonisin B_1 as inhibitor of sphingolipid synthesis

In order to elucidate the role of raft lipids in transport of HA within the Golgi, synthesis of cholesterol and sphingolipids was to be analysed. The effect of cholesterol on the transport of HA was already published by Keller and Simons [245], where they stated that inhibition of cholesterol synthesis by Lovastatin in combination with extraction by methyl-β-cyclodextrin does not effect the transport from ER to Golgi, but the transport from the Golgi to plasma membrane. Not only the arrival on the surface was delayed, but also a missorting of HA from the apical to the basolateral membrane in differentiated MDCK cells was observed. Therefore, we focussed on the influence of sphingolipid on the transport of HA within the Golgi.

Sphingolipid synthesis was inhibited using Fumonisin B_1, which inhibits the ceramide synthase being localized in the ER membrane, therefore inhibiting sphingolipid synthesis at an early time point. This allows for studying the intra-Golgi transport under conditions, where raft like structure can't be built.

CHO-K_1 cells treated with 20 µM Fumonisin B_1 for 16 hrs were transfected with HA-Cer wt and VIL3A, whereby the inhibitor was also present throughout all of the following procedures. 24 hrs post transfection, cells were radioactively labelled for 30 min and chased for 0, 1, 2 and 4 hrs.
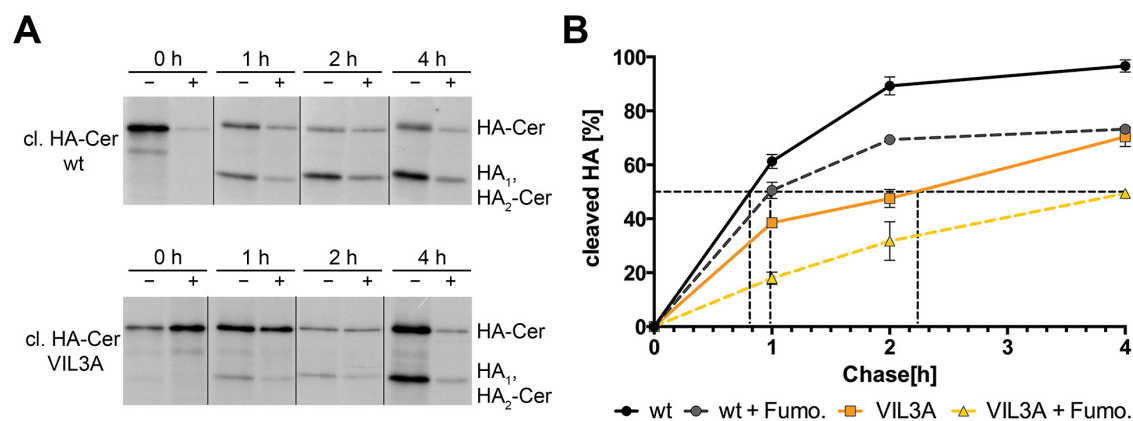

Figure 3–5: Cleavage of HA with sphingolipid synthesis blocker Fumonisin B_1. (A) CHO-K_1 cells expressing the indicated HA constructs were labeled with [^{35}S]- methionine for 30 min and chased for 0, 1, 2 or 4 hrs. Cells were left untreated (–) or incubated with 20 µM Fumonisin B_1 (+) prior to immuno-precipitation of HA with anti-FPV antibodies and reducing SDS–PAGE. **(B)** Densitometric quantification of bands from A and from three to five other experiments. Data points connected by dotted line: Cells expressing cl-HA-Cer wt or cl-HA-Cer VIL3A were treated with Fumonisin B_1 (Fumo). Cleaved HA in % was calculated [(HA$_1$ + HA$_2$-Cer)/(HA$_1$ + HA$_2$-Cer + HA-Cer) x 100] and is plotted against chase time. The horizontal broken line indicates 50% cleavage and the vertical broken line the corresponding chase time. Error bars indicate standard deviation. Reprinted from [252] with permission from Elsevier [OR APPLICABLE SOCIETY COPYRIGHT OWNER].

HA cleavage was delayed for both HA variants. The overall amount of cleaved protein after 4 hrs was reduced by 20 % for both variants. However, if $t_{1/2}$ is compared a difference can be observed. While HA-Cer wt has a $t_{1/2}$ of 50 min without and 60 min with the inhibitor, HA-Cer VIL3A has a $t_{1/2}$ of 2 hrs and 15 min without and 4 hrs with the inhibitor (Figure 3–5 B). Therefore, transport of HA-Cer VIL3A is impaired to a higher degree than HA-Cer wt.

Additionally, it can be noted that Fumonisin B_1 blocks transport at an earlier stage, as expected, as the shape of the curves do not vary significantly from the untreated samples. Untreated HA-Cer wt shows a sharp increase of cleavage until 2 hrs of chase until it turns to a slow rise. The same can be observed for Fumonisin B_1 treated cells, but to

a lesser overall extent. For HA-Cer VIL3A an overall slower increase can be observed, whereby in Fumonisin B$_1$ treated cells exhibit a similar curve shape from 1 h chase time on.

3.2 Effect of a putative cholesterol-binding motif on the transport and raft association of HA

From the data obtained in the first part of the thesis one can conclude, that the hydrophobic amino acids at the beginning of the TMR not only function as raft-targeting signal at the plasma membrane, but also further the transport along the exocytic pathway. As both, cholesterol and sphingolipid synthesis, are needed for a successful transport of HA, the amino acids within the VIL motif might be able to interact with lipids in their surrounding. The isoleucine and leucine are highly conserved among HA subtypes and are facing outwards of the trimer [246], thus, they are in a position allowing them interaction with lipids. Therefore, the next part will first focus on identification of possible lipid interaction motifs in the vicinity of the VIL motif.

3.2.1 Sequence analysis to identify putative cholesterol-binding motifs

To test the hypothesis, further sequence analysis was performed. The VIL motif is located in the outer leaflet of the plasma membrane following the connecting linker region of the ectodomain and therefore is prone to interact with lipids in their surrounding. So far, in the literature one motif for sphingolipid binding and several motifs for cholesterol binding are described. Starting with the sphingolipid-binding motif, which was defined as followed VXXTLXXIY, no sequence could be found in HA.

As described in 1.4.3 cholesterol-binding motifs are more diverse and in principle need basic, aromatic and large hydrophobic amino acids to interact. The VIL stretch and its vicinity matches these requirements: (1) one can find positively charged basic residues (K) to position the TMR inside the membrane, prior to (2) the hydrophobic VIL stretch which is followed by (3) the aromatic tryptophan (W) (see Figure 3–6 A).

Neither a CRAC (L/V-X_{1-5}-Y-X_{1-5}-K/R) nor a CARC motif (K/R-X_{1-5}-Y/F-X_{1-5}-L/V) is present in the HA sequence. In order to identify a putative cholesterol consensus motif (CCM) the sequence W/Y-I/V/L-K/R defined for 7-TM- receptors (see Figure 3–6 B for structure of the human β-adrenergic receptor) has to be inverted, since the relevant region in HA contacts the outer leaflet of the membrane bilayer (Figure 3–6 D). The HA sequence contains the amino acids K, I/L and W and thus corresponds to the in-

verted CCM motif K/R-I/V/L-W/Y. The required helical structure and the position of the involved amino acids on this helix are present as well. The membrane-anchoring region of HA (including the linker) has a α-helical structure [256,257] and by using the Wenxiang diagram, which shows the angle of the amino acid around the centre of a helix, the desired location of the amino acids K, L and W (but not I) on the helix (Figure 3–6 C) was confirmed. The second requirement for a CCM is the presence of an aromatic residue, either Y or F, located at the end of another transmembrane helix, binding the hydroxyl group of cholesterol together with the charged amino acid (R, K) (Figure 3–6 A). Although HA contains only one TMR that, however, forms a trimer, it exhibits a tyrosine preceding the lysine in the sequence that in principle could bind the hydroxyl group from the other side.
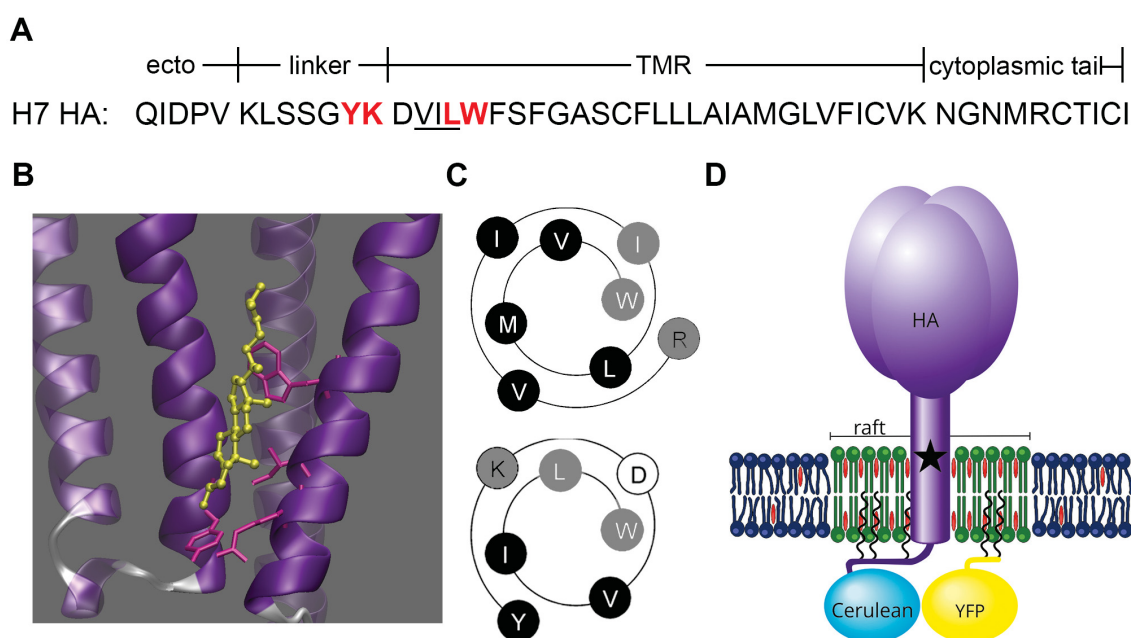
Figure 3–6: Comparison of putative CCM of HA with CCM of β-adrenergic receptor (A) Amino acid sequence of H7 HA from FPV (A/FPV/Rostock/34). VIL (underlined) is the TMR raft-targeting motif [22,23]. Amino acids of the CCM are in red. 'Ecto' denotes the beginning of the crystalized ectodomain of HA [51]. **(B)** see **Figure 1-7 (C)** Wenxiang diagram (http://www.jci-bioinfo.cn/wenxiang2) from the inner half of TMR IV of the β-adrenergic receptor (upper part) and part of the linker and outer part of the TMR of H7 subtype HA. The amino acids RIW (upper part) and KLW (lower part) known or supposed to contact cholesterol are in grey. **(D)** see **Figure 1-9**. The black star denotes the location of the putative CCM in HA. This figure was originally published in [258].

Even though HA proteins are very variable, motifs being important for the viral life cycle should be conserved among the subtypes. Phylogenetically, HA subtypes are di-

vided into two groups that have ~ 45% amino acid identity, but sequences considerably vary also within one subtype [259]. A comparison of the consensus sequences determined for each HA subtype reveals that the amino acids Y, K, L and W are completely conserved through all group 2 HAs, but this motif is not present at all in group 1 HAs (Table 3-1).

Table 3-1: Sequence analysis of all HA subtypes. Conserved IL is underlined, CCM in red.

Group	Subtype	Sequence
1	A_H1	LESTR–IYQILAIYSTV
1	A_H2	LSNMG–VYQILAIYATV
1	A_H5	LESIG–TYQILSIYSTV
1	A_H6	LENLG–VYQILAIYSTV
1	A_H8	LEENT–TYKILSIYSTV
1	A_H9	LESEG–TYKILTIYSTV
1	A_H11	LDSNGNVYKILSIYSCI
1	A_H12	LEENS–TYKILSIYSSV
1	A_H13	LKSEDNVYKALSIYSCI
1	A_H16	LKTEDNVYKVLSIYSCI
2	A_H3	LKSGY––KDWILWISFA
2	A_H4	LTQGY––KDIILWISFS
2	A_H7	LSSGY––KDVILWFSFG
2	A_H10	LSSGY––KDVILWSFSG
2	A_H14	LTMGY––KDIILWISFS
2	A_H15	LSSGY––KDVILWFSFG

3.2.2 Creation of HA-Cerulean constructs with mutations in the putative CCM

For the investigation of the influence of mutations in the CCM on transport, surface expression and raft association, seven mutant constructs with single to quadruple ex-

change of the triplets coding for the identified amino acids were created (Table 3-2). The different HA mutants were created as N-terminal fusion constructs with Cerulean as a fluorophore according to Engel et al. [222]. In the transmembrane raft-targeting signal VIL the highly conserved isoleucine and leucine were both exchanged individually against alanine (mutants IA and LA), while the poorly conserved valine was left unmutated. In case the assumption of a CCM is right, the mutation of the isoleucine shouldn't show an effect, as it is located on the other side of the helix according to Figure 3–6 C. To further exchange amino acids in the CCM located on one helix, additionally the tryptophan was mutated either individually (WA) or in combination with the leucine (LW2A). Subsequently, the whole sequence on one helix was mutated to alanines (KLW3A). To elucidate the role of the tyrosine on the other helix two mutants were constructed, firstly a double mutant with exchanged Y and K, as both of the amino acids are thought to bind the hydroxyl group of the cholesterol and secondly a quadruple mutant, where the Y on one helix and all amino acids on the other helix are mutated, therefore destroying the CCM completely.

Table 3-2: Mutations of the cholesterol consensus motif

Constructs	Amino Acid Sequence
Cholesterol consensus motif	−−−−−YK−−−LW
wt	KLSSGYKDVILW
IA	−−−−−−−−−A−−
LA	−−−−−−−−−−A−
WA	−−−−−−−−−−−A
LW2A	−−−−−−−−−−AA
YK2A	−−−−−AA−−−−−
KLW3A	−−−−−−A−−−AA
YKLW4A	−−−−−AA−−−AA

3.2.2.1 Characterization of the transmembrane features of the newly con-structed CCM mutants

In order to exclude that the mutations made have an influence on the overall helical structure of the beginning of the transmembrane region, *in silico* analysis of the TMR was performed. Two prediction programs of transmembrane regions were used to determine the length of the transmembrane region. The programs were run entering the sequence of the wild type and in comparison the quadruple mutant YKLW4A, which would exhibit the most drastic change in case of an influence of the mutations.

Firstly, TMpred (http://www.ch.embnet.org/software/TMPRED_form.html) predicted type two transmembrane regions for the wild, one reaching from amino acid 1 to 18 resembling the signal peptide sequence of the FPV influenza strain (see Figure 2 in [260]) and another reaching from amino acid 527 to 552 resembling the anchoring transmembrane region. Thus, the sequence of the TMR is defined as VILWFSF-GASCFLLLAIAMGLVFICV (Figure 3–7) being delimited by the helix breakers Y and D in the beginning and K at the end (Figure 3–6 A). This result does not change in case of entering the mutated sequence (Figure 3–8).
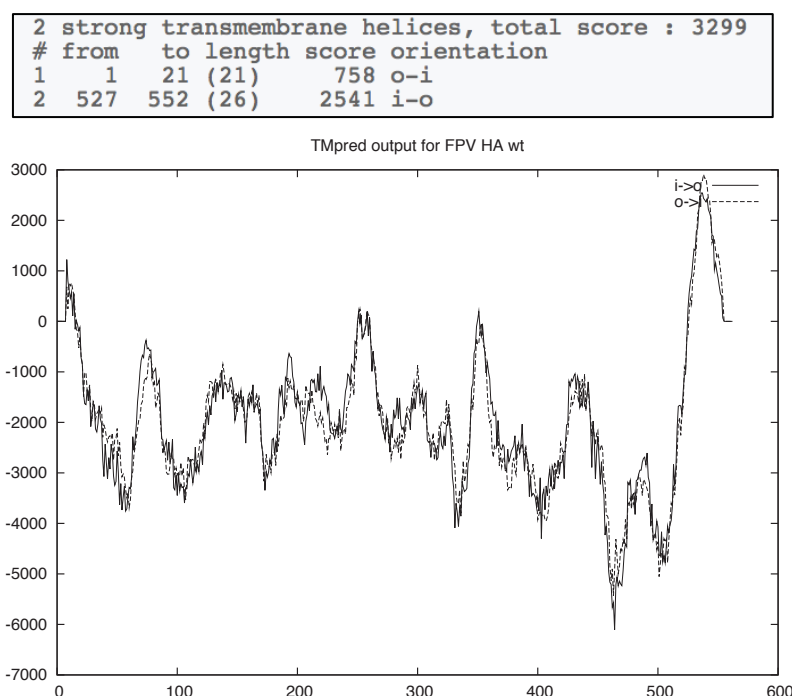

Figure 3–7: Output of TMR prediction using TMpred for HA wild type. Suggested model for transmembrane location and topology and hydrophobicity plot.

```
2 strong transmembrane helices, total score : 3130
# from   to length score orientation
1    1   21 (21)      758 o-i
2  527  552 (26)     2372 i-o
```
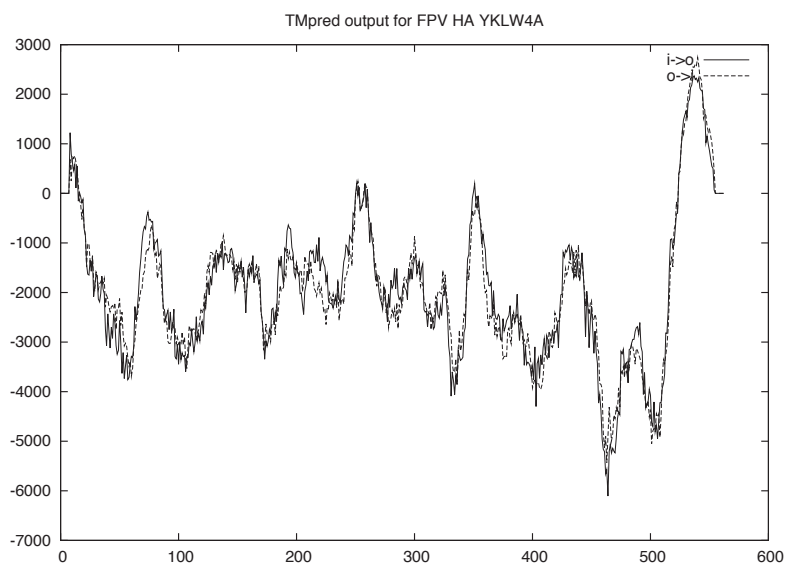

TMpred output for FPV HA YKLW4A

Figure 3–8: Output of TMR prediction using TMpred for HA YKLW4A. Suggested model for transmembrane location and topology and hydrophobicity plot.

However, prediction softwares sometimes give contradicting results, therefore, the open software HMMTOP (http://www.enzim.hu/hmmtop/) was used for a second run of predictions. In contrast to TMpred HMMTOP predicts only the anchoring TMR with a slightly shorter helix for wild type HA ranging from amino acid 528 to 552, therefore starting at the isoleucine of the VIL motif (Figure 3–9).

```
Protein: noname
Length:  563
N-terminus: OUT
Number of transmembrane helices: 1
Transmembrane helices: 528-552

Total entropy of the model:  17.0254
Entropy of the best path:  17.0259

    seq  TNQQFELIDN EFTEVEKQIG NLINWTKDSI TEVWSYNAEL IVAMENQHTI   450
    pred 0000000000 0000000000 0000000000 0000000000 0000000000

    seq  DLADSEMNRL YERVRKQLRE NAEEDGTGCF EIFHKCDDDC MASIRNNTYD   500
    pred 0000000000 0000000000 0000000000 0000000000 0000000000

    seq  HSKYREEAMQ NRIQIDPVKL SSGYKDVILW FSFGASCFLL LAIAMGLVFI   550
    pred 0000000000 0Oooooooooo oooooooHHH HHHHHHHHHH HHHHHHHHHH

    seq  CVKNGNMRCT ICI   563
    pred HHiiiiiiii iii
```

Figure 3–9: Output of TMR prediction using HMMTOP for wild type HA. Sequence shown from amino acid 400 on. Topology displayed in alignment O= outside, H= helix, i= inside

Likewise, HMMTOP does not predict a change in the length of location of the transmembrane helix in case of HA YKLW4A (Figure 3–10).

```
Protein: noname
Length:  563
N-terminus: OUT
Number of transmembrane helices: 1
Transmembrane helices: 528-552

Total entropy of the model:  17.0248
Entropy of the best path:  17.0253

    seq   TNQQFELIDN EFTEVEKQIG NLINWTKDSI TEVWSYNAEL IVAMENQHTI   450
    pred  0000000000 0000000000 0000000000 0000000000 0000000000

    seq   DLADSEMNRL YERVRKQLRE NAEEDGTGCF EIFHKCDDDC MASIRNNTYD   500
    pred  0000000000 0000000000 0000000000 0000000000 0000000000

    seq   HSKYREEAMQ NRIQIDPVKL SSGAADVIAA FSFGASCFLL LAIAMGLVFI   550
    pred  0000000000 000oooooooo ooooooooHHH HHHHHHHHHH HHHHHHHHHH

    seq   CVKNGNMRCT ICI   563
    pred  HHiiiiiiii iii
```

Figure 3–10: Output of TMR prediction using HMMTOP for HA YKLW4A. Sequence shown from amino acid 400 on. Topology displayed in alignment O= outside, H= helix, i= inside

Consequently, the mutant constructs with mutation in the putative CCM of HA do not interfere with helix forming of the transmembrane region and therefore can be used for further experiments.

3.2.2.2 Cellular localization of the CCM mutants

CHO-K$_1$ cells were transfected with the according HA constructs 24 hrs before imaging the localization in living cells.

As expected HA-Cer wild type is localized mainly at the plasma membrane and is enriched in the Golgi. Likewise, mutants HA-Cer IA, WA and YK2A show clear plasma membrane staining and delimited Golgi localization. In contrast to the wild type, mutants HA-Cer LA, LW2A, KLW3A and YKLW4A are less delimited in their Golgi localization, although their plasma membrane localization is still present even though less distinct.

Despite their differences in the expression pattern, all mutants show expression and location at the plasma membrane, but to different extent. For detailed analyses of the surface expression see 3.2.4.
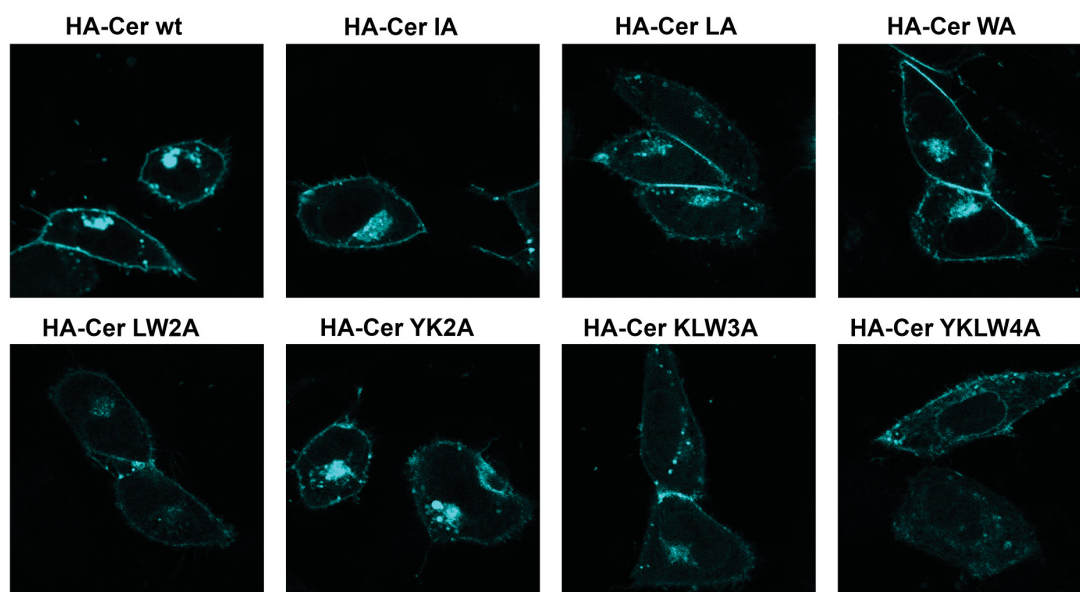
Figure 3–11: Characterization of the CCM mutants. Expression of CCM mutants in CHO-K$_1$ cells 24 hrs after transfection. Two representative cells each.

3.2.3 Investigation of the transport along the exocytic pathway of the CCM mutants

As shown previously in 3.1.1.1 the trimerization is not affected by mutations in the HA. The same was true for all CCM mutants, which is why the data is not shown here.

3.2.3.1 Transport from ER to the medial Golgi

CHO-K$_1$ cells expressing an uncleaved version of the HA mutants were labelled with [^{35}S]-methionine and chased for 0, 1, 2, 4, 6 and 16 hours. After immunoprecipitation, digestion with (+) or without (−) Endo-H and SDS-PAGE band intensities for Endo-H resistant and non-resistant HA were calculated. The results obtained for the different mutants can be grouped according to their delay in transport. The first group consist of HA-Cer IA, WA (Figure 3–12 A, B) and YK2A (Figure 3–12 C, D), all showing the same behaviour in transport as the wild type with a $t_{1/2}$ of ~40 minutes. The second group comprises HA-Cer LA (Figure 3–12 A, B) and HA-Cer LW2A (Figure 3–12 C, D), with already a delay of 50 min compared to the wild type as they exhibit a $t_{1/2}$ of ~90 minutes. The third group (HA-Cer KLW3A and HA-Cer YKLW4A; Figure 3–12 C, D) has an increased delay up to more than 3 hrs with a $t_{1/2}$ of ~4 hrs. Processing of the mutants is still not completed after 6 hrs, an additional time point after 16 hrs was included to

exclude a general transport defect. With ~80% of Endo H-resistant carbohydrates all mutants showed the same processing level as the wild type (Figure 3–12 D).
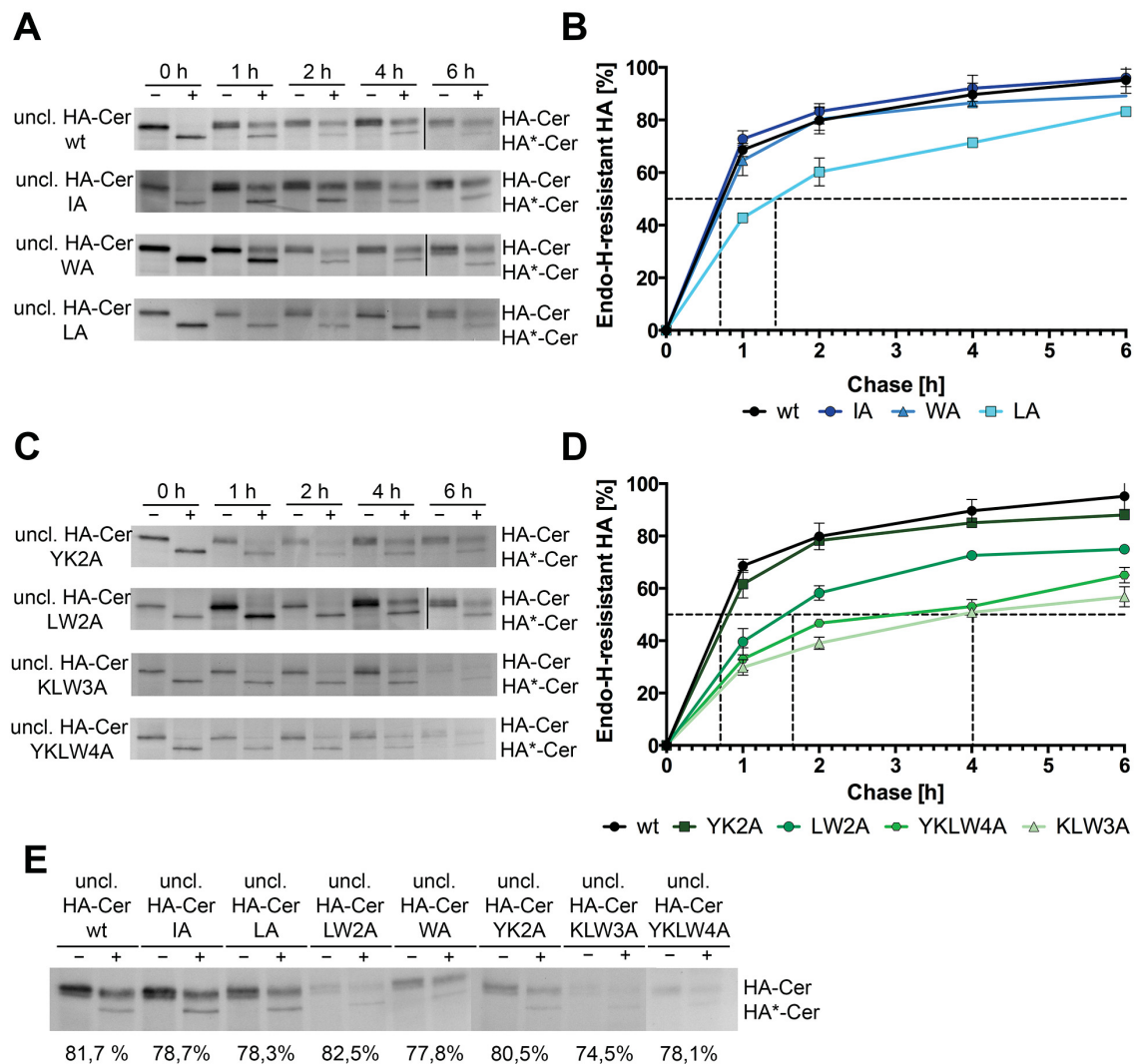
Figure 3–12: Transport from ER to medial Golgi. (A and C) CHO-K$_1$ cells expressing the indicated HA constructs were labeled with [^{35}S]methionine for 30 min and chased for 0, 1, 2, 4 or 6 hrs. HA was immunoprecipitated with FPV antiserum and digested with Endo H (+) or was left undigested (−) before reducing SDS-PAGE and fluorography. Endo H-sensitive HA−Cer is denoted by an asterisk. Black lines between lanes indicate that the lanes are from different fluorograms. **(B and D)** Densitometric quantification of bands from three to six independent experiments. The percentage Endo H-resistant HA was calculated [(HA−Cer/(HA−Cer+HA* − Cer)×100], normalized to HA−Cer wt and plotted against time of chase. The horizontal broken line indicates 50 % Endo H-resistant carbohydrates and the vertical broken line the corresponding chase time. Results are means ± S. D. **(E)** CHO-K$_1$ cells expressing the indicated HA constructs chased for 16 hrs. The percentage of Endo H-sensitive HA (not normalized) is specified below the lanes. This figure was modified and originally published in [258].

HA-Cer LW2A, HA-Cer KLW3A and HA-Cer YKLW4A are less stable than the wild type, as can be seen by the more faint bands after 16 hrs of chase (Figure 3−12 E). This means that besides the transport defect, they are more often degraded. As trimerization is not affected (data not shown), this is not due to folding or trimerization defects. Therefore, degradation must take place in later stages of expression.

3.2.3.2 Transport within the trans-Golgi-network

CHO-K_1 cells expressing cleavable versions of the HA-Cerulean fusion constructs were labeled with [^{35}S]-methionine chased for 0, 1, 2, 4 and 6 hrs.

The analysis of the cleavage of HA_0 into HA_1 and HA_2 reveals a different evaluation of the results obtain for the various mutants from the analysis of the acquisition of Endo-H resistant carbohydrates. Despite Ha-Cer IA, all other six mutations show a negative effect on the kinetics of cleavage (Figure 3−13 B, D). The increase of $t_{1/2}$ for HA-Cer IA compared to HA-Cer wt from a $t_{1/2}$ of 55 min to 70 min is only subordinate, since a grouped analysis of the percentages of cleaved HA at the different time points with a two-way ANOVA and Dunnet's multiple comparison didn't show a significant difference. Whereas the single exchange of W against A (HA-Cer WA; Figure 3−13 A, B) and the double mutation HA-Cer YK2A (Figure 3−13 C, D) had no influence on the acquisition of Endo-H resistant carbohydrates, $t_{1/2}$ for cleavage of both mutants was only reached after ~2 hrs, which means a delay of 1 h compared to wild type. For HA-Cer LA an even higher delay was determined with a $t_{1/2}$ of 190 min and a delay of over 2 hrs (Figure 3−13 A, B). The highest impact on transport to the TGN was determined for HA-Cer LW2A, HA-Cer KLW3A and HA-Cer YKLW4A with a $t_{1/2}$ of roughly 5 hrs and a delay of ~4 hrs (Figure 3−13 A, B). The drastic increase in transport delay for HA-Cer LW2A can be explained by the additive effect of the mutation of the tryptophan and the leucine. The 2 hrs of transport time of HA-Cer WA and the 3 hrs of HA-Cer LA add up to an overall delay of 5 hrs for HA-Cer LW2A. Additional mutations of the lysine and tyrosine (YKLW4A) in comparison do not further retard the protein.
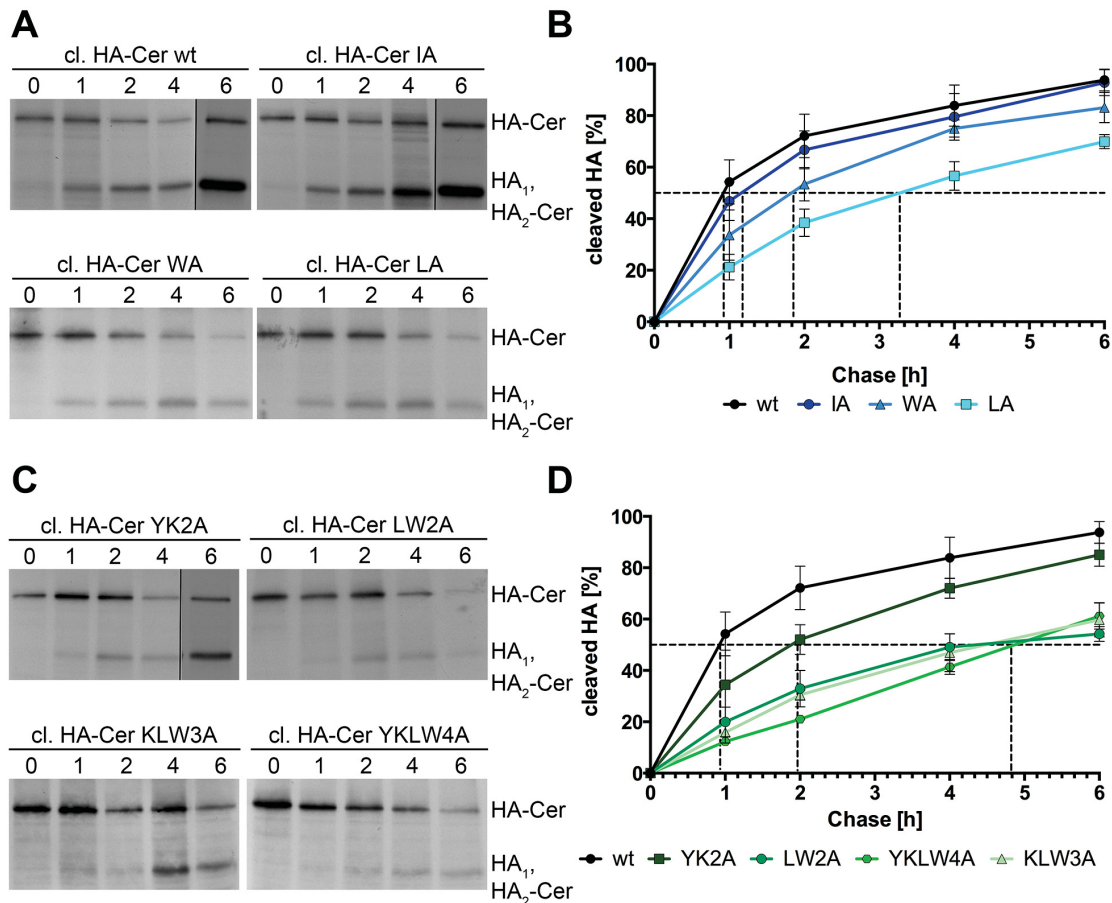
Figure 3–13: Intra-Golgi transport. (A and C) CHO-K$_1$ cells expressing the indicated HA constructs were labeled with [^{35}S]methionine for 30 min and chased for 0, 1, 2, 4 or 6 hrs. HA was immunoprecipitated with FPV antiserum before reducing SDS-PAGE and fluorography. Owing to fusion of Cer to HA$_2$, both HA subunits HA$_1$ and HA$_2$–Cer have an identical molecular mass. Black lines between lanes indicate that the lanes are from different fluorograms. **(B and D)** Densitometric quantification of bands from three to six independent experiments. The percentage cleaved HA was calculated [(HA$_1$+HA$_2$ –Cer)/(HA$_1$+HA$_2$ –Cer+HA–Cer)×100], normalized to HA–Cer wt and plotted against the chase time. The horizontal broken line indicates 50 % cleavage and the vertical broken line the corresponding chase time. Results are means ± S. D. This figure was modified and originally published in [258].

From the data on acquisition of Endo H-resistant carbohydrates and cleavage of HA$_0$ we can calculate the time the proteins need to be transported from the medial Golgi to the TGN (see Table 4–1 "transport Golgi to TGN"). Likewise the cleavage, the leucine and tryptophan act in an additive manner. While HA-Cer LA again showed the strongest effect on transport with a $t_{1/2}$ of 100 min and HA-Cer WA showed a milder effect with a $t_{1/2}$ of 70 min, while the combination of both mutations leads to a $t_{1/2}$ of 190 min. On the contrary, the additional mutation of Y and K only resulted in a $t_{1/2}$ of 50 min.

This either suggest that mutations of the outer amino acids can compensate for the mutation made in the hydrophobic and aromatic amino acids or the triple and quadruple mutation, respectively, already lead to a strong defect in transport from the ER to the medial Golgi, which is not further enhanced in the transport to the TGN.

3.2.4 Surface expression of CCM mutants

For quantification of the expression level of the mutant proteins at the plasma membrane, we conducted flow cytometry experiments. Imaging, even if applied confocally, only allows for a qualitative but not quantitative analysis of the expression levels of the different mutants at the plasma membrane. Especially for mutants with high degree in transport delay (i.e. Figure 3–11 HA-Cer YKLW4A) it becomes difficult to distinguish between cytoplasm and membrane. Therefore, flow cytometric analysis was used due to its ability to quantify reliably the levels of protein at the plasma membrane, and in addition it is able to separate the signals from cytoplasm and plasma membrane. Anti-FPV polyclonal serum was used on non-permeabilized cells to specifically label HA on the surface of expressing cells. To evaluate the amount of surface expression compared to overall expression, the signal of the Cerulean tag was measured as well. Additionally, this allows the comparison of the results in respect to the overall expression level of the different mutants, which might be different due to lower stability.

Cells transfected with the HA-Cer variants were fixed after 24 hrs of transfection to prevent re-endocytosis of the protein and subsequently stained with a rabbit anti-FPV antiserum followed by an anti-rabbit Alexa 488 secondary antibody.

First, the number of cells showing surface localization relative to the number of total transfected cells was analyzed (Figure 3–14 A). The results show that all HA variants are transported to the cell surface, but to a different extent. Again, it can be discerned between 3 groups. The first group consists of wild type HA-Cer and HA-Cer IA, both with approximately 90 % of cells with signal at the surface. The second group comprises HA-Cer LA, WA and YK2A, all having ~80 % surface expressing cells. The last group, HA-Cer LW2A, KLW3A and YKLW4A, has an even lower amount of surface expressing cells with only ~60 %.

Secondly, by measuring the mean fluorescence intensity the amount of HA at the plasma membrane relative to the overall expression was determined (Figure 3–14 B). The results are normalized against the surface expression of the wild type. The results confirm the previous grouping of the mutants. Group 1 contains HA-Cer wt and IA with a non-significant change (100 %, 95 %, respectively) in surface expression. Group 2 consists of HA-Cer LA, HA-Cer WA and HA-Cer YK2A, where the amount of HA is significantly reduced to ~80 %, whereas in group 3, containing HA-Cer LW2A, KLW3A and YKLW4A, the amount is decreased to 50 % relative to HA-Cer wt.

A   **B**
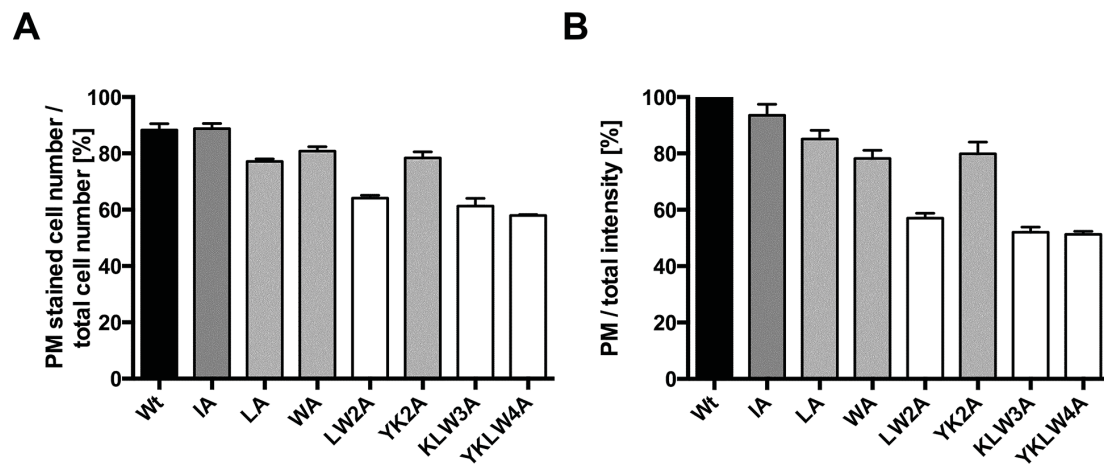
Figure 3–14: Surface expression of indicated HA constructs. Flow cytometric analysis of CHO-K_1 cells expressing the indicated HA constructs. Cells were stained with FPV antiserum. The fluorescence from Cerulean was also recorded to include only cells that express HA in the analysis. **(A)** Percentage of HA-expressing cells with HA at the cell surface. **(B)** Median fluorescence intensity (equivalent to the HA amount) at the plasma membrane normalized to HA wt. Black to white nuances indicate statistically significantly different groups. Black and dark grey are significantly different from light grey and white, while light grey is significantly different from white. P<0,001 between all groups by Ordinary one-way ANOVA followed by Tukey's multiple comparison test. This figure originally published in [258].

In summary, these results resemble the amount of cleaved HA after 6 hrs of chase (see Figure 3–13 B and D), despite of HA-Cer LA, which had only 70 % cleaved HA but 77 % of surface expressing cells.

3.2.5 Lipid raft association of CCM mutants

Finally, we asked the question, if raft association at the plasma membrane is dependent on the presence of the CCM. Thus, FLIM-FRET experiments were performed. CHO-K_1 cells were transfected with suitable FLIM-FRET donor and acceptor pairs; in this case HA fused to Cerulean as donor and the established inner leaflet raft marker Myr-Pal fused to YFP as acceptor.

24 hrs post transfection the lifetime of the donor in presence and absence of the acceptor was measured at the plasma membrane of living cells and used for further calculation of the FRET efficiency according to:

$$E = \left(1 - \frac{\overline{\tau}_{DA}}{\overline{\tau}_{D}} \right) * 100$$

As mentioned in the introduction, the possibility of false-positive FRET efficiency arises due to the limited space within a membrane. There the FRET efficiencies were plotted against the acceptor concentration and the data was fitted according to this hyperbolic function:

$$E(\%) = \frac{E_{max} * A}{K_D + A}$$

whereby low K_D values compared to the average intensity indicate true clustering, which is independent on acceptor concentration, and would lead to a hyperbolic shape of the fitting curve and high K_D values, in contrast, indicate random interaction, which is dependent on increasing acceptor concentration and would lead to linear fitting (see Figure 3–15).
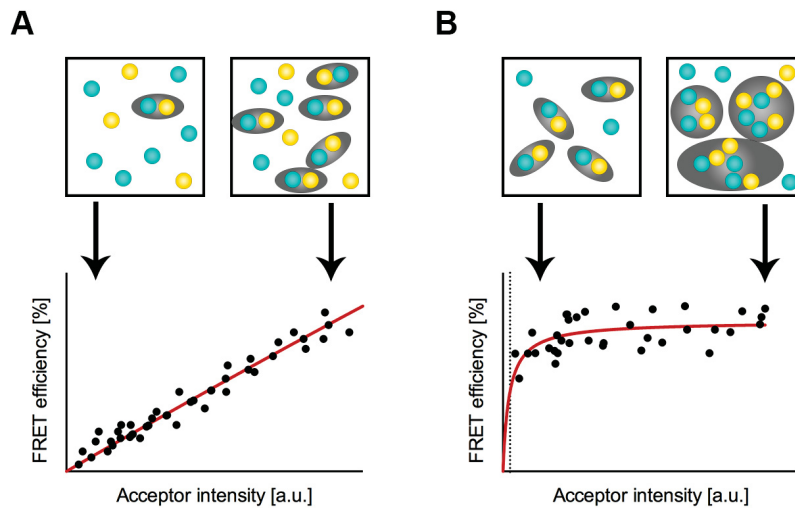
Figure 3–15: Principle of FRET cluster analysis. Schematic representation of donor and acceptor clustering. **(A)** FRET efficiency increases linearly according to availability of acceptor. **(B)** FRET efficiency increases following a hyperbolic function due to high clustering already at low acceptor concentrations. Created with CorelDraw.

Note, however, that the values should not be interpreted in a strict quantitative fashion, but rather qualitatively to consider different conditions of comparable FRET pairs.

First, the results for HA wild type and the VIL mutant from Engel et al. [222] were reproduced to validate the methodology and to use them as controls for clustering and impaired clustering. Figure 3–16 A shows the expected high median FRET efficiency of 17,6%, which is decreased to ~7% in case of mutating the transmembrane raft-targeting signal VIL. Likewise, clustering between wild type HA-Cer and the raft marker yielded a low K_D of ~1,31x10^{-6} (Figure 3–16 B) and a high K_D of 7488 in case of HA-Cer VIL (Figure 3–16 C). Additionally, the shape of the fitting curve changes from levelling off at low acceptor concentrations to a quasi-linear shape (Figure 3–16 B and C).

For analyzing the CCM mutants, we chose to use a suitable set, which is visibly expressed at the plasma membrane and reflects the different transport defects. HA-Cer WA is a mutant, which was only mildly affected in transport and also shows just a slight impact on plasma membrane expression, while HA-Cer LW2A is highly impaired in transport and one of the mutants expressing only to 50 % of HA on the plasma membrane (like HA-Cer KLW3A and YKLW4A). As both mutants only reflect mutations on one helix, which are both located within the TMR, HA-Cer YK2A was also in-

cluded to elucidate the role of the combined binding of both helices and the role of mutations in the linker region.
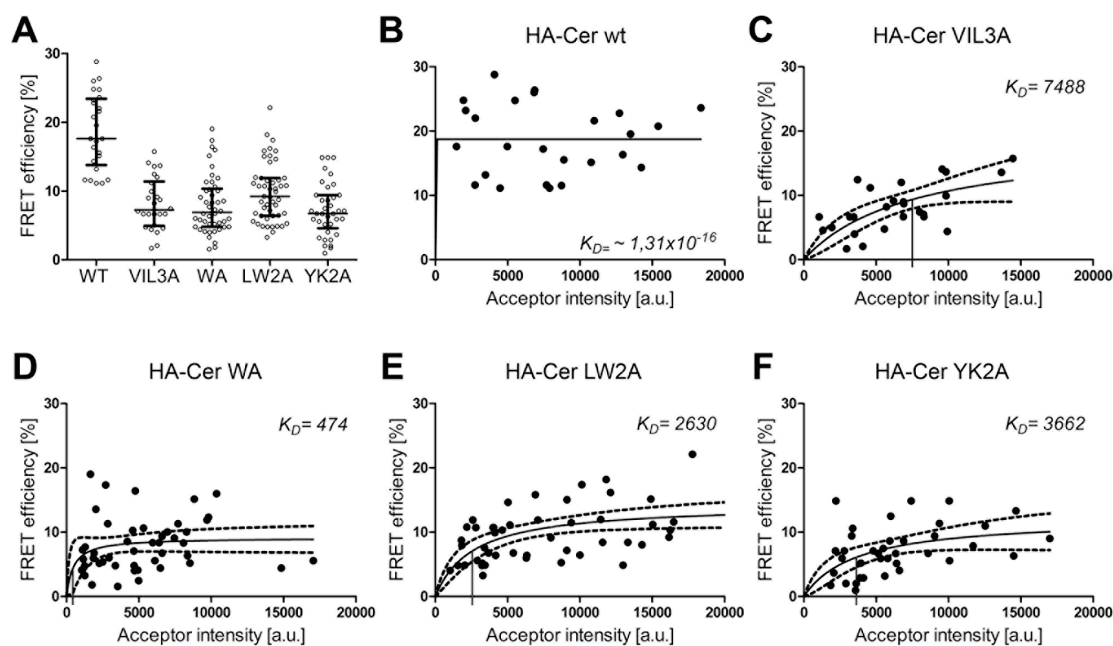
Figure 3–16: Cluster analysis of HA-Cer mutants with the raft marker Myr-Pal. (A) FRET efficiencies calculated for association of the raft-marker with the indicated HA mutants. FRET efficiency (E) measured for each cell is indicated as a dot. E is indicated as the median with interquartile range. P<0,0001 between wild type and mutants by Ordinary one-way ANOVA followed by Tukey's multiple comparison test. **(B–F)** FRET efficiency (E) for each cell plotted against the relative acceptor intensity in that cell; hyperbolic fit (unbroken line, broken line: 95 % confidence interval) provides K_D to assess clustering. The K_D is displayed as a vertical line. **(B)** Co-expression of HA–Cer wt and Myr-Pal–YFP; n (number of analyzed cells) = 25. **(C)** Co-expression of HA–Cer VIL3A and Myr-Pal–YFP; n = 26. **(D)** Co-expression of HA–Cer WA and Myr-Pal–YFP; n = 46. **(E)** Co-expression of HA–Cer LW2A and Myr-Pal–YFP; n = 49. **(F)** Co-expression of HA–Cer YK2A and Myr-Pal–YFP; n = 37. This figure was originally published in [258].

When co-expressed in CHO-K_1 cells with the raft marker Myr-Pal, all mutants reveal a strong reduction in FRET efficiency similar to HA-Cer VIL3A of ~7% for HA-Cer WA and YK2A and non-significantly different 9% for HA-Cer LW2A (Figure 3–16 A). The cluster analysis, in contrast, enables to perform a more detailed analysis. While HA-Cer LW2A (Figure 3–16 E) and YK2A (Figure 3–16 F) both are in the same range than HA-VIL3A with a K_D of 2630 and 3662, respectively, for HA-Cer WA (Figure 3–16 D), compared to the other mutants, only a K_D of 474 was calculated. As the result is about

one order of magnitude lower, one can suggest that the clustering with the raft marker is also reduced, but to a lesser extent than the other two mutants. Therefore, the signal that determines association of HA with rafts encompasses not only hydrophobic, but also aromatic and positively charged, residues located at the interface between the lipophilic core of a bilayer and the hydrophilic extracellular region.

4 Discussion

4.1 Transport of HA along the exocytic pathway

The hemagglutinin protein of influenza A viruses not only performs functions in the entry of the virus into its host cell, but also is the main determinant of the budding zone of the virus. By incorporation into lipid rafts, specialized cholesterol- and sphingolipid-rich plasma membrane domains, it builds the foundation of the assembly site [110]. Two raft-targeting signals of HA have been proposed so far. Firstly, the S-acylation of the three cysteines being located at the edge of the transmembrane region and in the cytoplasmic tail and secondly the hydrophobic amino acids valine, isoleucine and leucine (VIL) being located in the transmembrane region facing the outer leaflet of the plasma membrane. During the studies of the former PhD student Stephanie Engel exploring the raft integration of HA at the plasma membrane in living cells, the observation was made that the raft-targeting signals, in particular the hydrophobic stretch, could also be crucial for the correct processing of HA and therefore the proper transport of the protein along the exocytic pathway.

The first aim of this thesis was to validate the observations made regarding the transport, which was feasible, and showed that the mutation of the VIL motif but not the three S-acylation sites led to a delay in transport compared to the wild type. In addition, inhibition of cholesterol [245] and sphingolipid synthesis, as investigated here, also influence the transport kinetics of HA in a negative manner (all transport data will be discussed collectively in detail in 4.1.2). These observations on the importance of both, the VIL raft targeting signal and the presence of raft enriched lipids, for the correct processing and transport of HA in combination with the published data on raft-like structures already emerging in the Golgi (see 1.4.1) led to the *hypothesis, that cholesterol and sphingolipid rich membrane domains are not only important for the localization of HA at the plasma membrane, but also already early during the transport along the secretory pathway.*

4.1.1 Influenza A group 2, but not group 1, hemagglutinin possess a putative cholesterol consensus motif

How can the hydrophobic raft-signal facilitate the interaction with lipid rafts either in the Golgi or at the plasma membrane?

Raft interaction of influenza HA has not been studied in detail so far. The data available, especially on the hydrophobic beginning of the transmembrane region, is based only on alanine scanning mutagenesis [220,261]. The underlying mechanism of raft association by this motif was not studied further, which is why we were trying to elucidate the possibility of interaction with lipid rafts. As the amino acids isoleucine and leucine of the motif are facing outwards of the trimer [246], an *in silicio* analysis was performed to find possible binding motifs for raft lipids. The analysis revealed no sphingolipid-binding motif being present in the sequence of FPV HA, but a putative cholesterol consensus motif (CCM; K/R-I/V/L-W/Y) (Figure 3−6), which encompasses at least the leucine of the VIL motif. *This is the first time this particular motif is described for a viral protein.* So far only the CRAC motif was found to be present in virus proteins like gp41 of HIV [169] and M2 of influenza virus [84], where they facilitate raft integration [262] or localization to the edge of lipid rafts [84], respectively. The CCM was only described for human class A G protein-coupled receptors (GPCRs) and the structural details of binding were defined for the human β-adrenergic receptor [172]. HAs of influenza A viruses are very diverse and can be divided phylogenetically into group 1 and group 2, whereby the here used H7 HA of FPV, in which the CCM motif was found, is member of group 2 HAs. Analysis of the consensus sequence of all classical 16 subtypes revealed that *the CCM motif is highly conserved among group 2 HA but not group 1* (Table 3-1). No cholesterol-binding motif could be found in the sequence of group 1 HAs, only the isoleucine and leucine are highly conserved.

As the CCM is involved in the transport of HA, the question arises, whether the phylogenetic conservation pattern is reflected in already published transport data. When the isoleucine and leucine were mutated in a protein expression system using a group 1 H2 HA of an influenza A/Japan /305/1957 isolate, despite loosing raft association, neither an effect on the arrival at the Golgi nor at the cell surface could be detected [261], which would support our hypothesis of a putative CCM being involved in

transport only of group 2 HAs. *This indicates that in group 1 HAs a different mechanism of transport might be used, as integration into raft structures does not influence transport kinetics.* The fact that the mutation in the IL motif still leads to the loss of raft integration at the plasma membrane further hints to a different way of raft association within the Golgi and at the plasma membrane, which could be explained by the altered lipid composition of the compartments. In contrast, when in a group 2 H3 HA (A/Udorn/72) the conserved IL motif in combination with the preceding tryptophan was mutated, the transport to the Golgi was delayed in a comparable manner as for the VIL mutant we analyzed [220]. Combination experiments investigating Endo-H resistance and Triton-X 100 solubility also confirmed that integration into raft-like structures occurs within the Golgi, as full processing of the carbohydrates correlates with insolubility of the proteins being expressed, therefore supporting the before mentioned theory of emerging raft-like structures within the Golgi. Takeda and colleagues not only investigated the influence of the mutation on protein level, but also studied the phenotype of viruses expressing the altered HA protein produced by using a recombinant rescue system. The subsequent characterization of the virus mutants confirmed the result of the loss of raft integration of the WIL mutant, which led to a decrease in virus titer of 3 logs that was accompanied with the loss of clustering of HA on the surface of infected cells and 50 % less incorporation of HA into virus particles. Therefore, the data on the H3 HA confirms our data on the transport delay, when mutating the conserved IL and additionally elucidate the role of the WIL motif in the viral replication cycle. *These results support our theory of a putative cholesterol-binding motif being involved in transport and raft integration in group 2 HAs.*

To study the influence of the putative CCM, first, mutations were introduced into the sequence of HA by exchanging the triplets coding for single to quadruple amino acids of the motif by triplets coding for alanines in the according expression plasmids. This enabled studying single and synergistic effects of the assumed cholesterol binding factors, thereby elucidating if all amino acids are needed for interaction with raft-like structures and correct transport.

In the following chapter the role of the VIL motif and the putative CCM in transport of HA will be discussed collectively and in relation to each other.

4.1.2 The hydrophobic raft-targeting signal VIL and the CCM are crucial for the correct transport of HA along the secretory pathway, especially through the Golgi

Table 4–1: Summary of the transport kinetics results

Mutant	Transport to medial Golgi ($t_{1/2}$)	Transport to TGN ($t_{1/2}$)	Transport Golgi to TGN	Surface expression
wt	40 min	55 min	15 min	100%
C3S	40 min	55 min	15 min	ND
VIL3A	80 min	150 min	70 min	ND
IA	40 min	70 min	30 min	95%
LA	90 min	190 min	100 min	85%
WA	40 min	110 min	70 min	80%
YK2A	40 min	120 min	80 min	80%
LW2A	100 min	290 min	190 min	50%
KLW3A	240 min	290 min	50 min	50%
YKLW4A	240 min	290 min	50 min	50%

Half times for transport to the medial Golgi and to the TGN were compiled from Figures 3-2, 3-12 and 3-13. The time for transport between Golgi and TGN was calculated as the difference between the $t_{1/2}$ for transport to the TGN minus the $t_{1/2}$ for transport to the medial Golgi. Data for surface expression are from Figure 3-14. Results are divided into three classes: Mutants with the strongest effect on the respective process are highlighted in dark gray, with an intermediate effect are highlighted in light gray and with no (or very little) effect are not highlighted.

For the interpretation of the data obtained regarding the transport and localization of the HA variants, firstly the kinetic data will be analyzed followed by the data on the steady-state localization within the cell.

To investigate the effect of mutations in the raft-targeting signals of HA and in the cholesterol consensus sequence on the kinetics of the transport from the ER to the plasma membrane, different radioactive pulse-chase experiments and differential post-treatments were conducted as explained in the results. The processing of HA

along the exocytic pathway can be divided into three steps, which are possible to examine with metabolic labeling of newly produced protein.

When interpreting the data obtained, the results for the trimerization are very prominent. Most of the HA mutants described so far, which are defective in transport, have a defect in folding and/or trimerization [263,264]. For example, Garten and colleagues created temperature sensitive mutants and found two groups of mutation abolishing the exit from the ER. Either the proteins were unable to trimerize and stayed monomeric or the proteins were forming aggregates [263]. Formation of correct trimers is the limiting step for the efficient export of the protein from the ER, as aberrant trimers are retained in the ER [99,100]. Surprisingly, all the mutants analyzed in this study showed times until trimerization (see Figure 3–1 for VIL3A and C3S, data for the CCM mutants are not shown) that are in with the previous observations by Stephanie Engel [253] and with the kinetics of previous published transport data for FPV H7 HA and other HA subtypes [263–265], *therefore, a folding defect is very unlikely. Furthermore this study is the first one describing a transport defect of HA protein occurring not before the Golgi.*

Analyzing the arrival of the protein at the medial-Golgi, the data shows that only the mutation of the VIL motif but not the S-acylation leads to a doubled time of transport from the ER to the medial Golgi (Figure 3–2). When interpreting the results obtained for the CCM mutants (Figure 3–12 B, D), we can make several assumptions. First of all, *even though the cholesterol content in the ER is low, mutations in the cholesterol consensus motif still have an impact on the transport from the ER to the medial Golgi.* But cholesterol binding is not absolutely required for the transport, as all mutants reach the medial Golgi, even though after different times (Figure 3–12 E). Under the assumption that the putative CCM in HA is able to interact with cholesterol, we can additionally draw conclusions about the importance of the different amino acids in the motif. In the following part, I will interpret the importance of the different amino acids of the CCM for the correct transport by starting with the quadruple mutant, as the mutant with the most drastic effect on transport kinetics and analyze the improvement of transport by reintroduction of the amino acids into the motif (Figure 4-1).
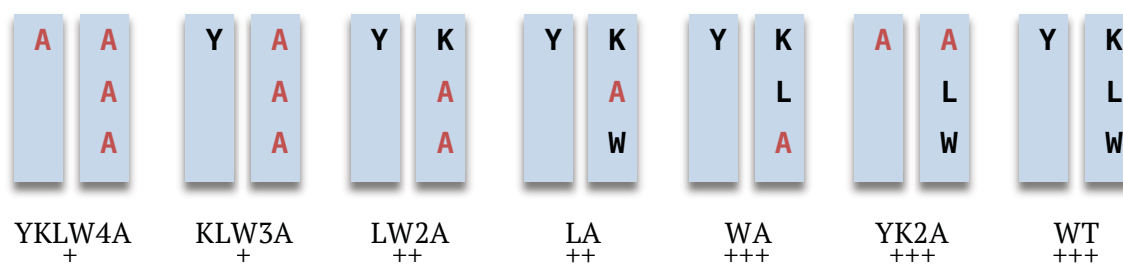
Figure 4-1: Schematic depiction of the location of the CCM mutations on the helices of two HA TMRs and their corresponding effect on transport to the medial Golgi.

Since the most prominent delay in transport was observed in case of mutating all four amino acids (YKLW4A), but introduction of the tyrosine on one helix (KLW3A) did not improve the transport kinetics, we can conclude that *the tyrosine is not able to rescue the phenotype induced by the loss of the main interaction made by the three amino acids binding from the other helix.* Binding the hydroxyl group of cholesterol from both sides (via Y and K), as still possible in the LW2A mutant, seems to rescue the phenotype at least partially, as the delay is less prominent compared to the triple mutant. Additional introduction of the tryptophan (LA mutant) does not improve transport, while introduction of leucine (WA mutant) rescues the phenotype. Moreover, the presence of L and W (YK2A mutant) is also sufficient to rescue the phenotype, which is why we can assume that *leucine is the crucial amino acid binding the cholesterol in the middle of the molecule.* The finding that neither the mutation of the tryptophan, the innermost amino acid in the motif, nor the double mutation of the outermost lysine and tyrosine affected the transport further supports this theory.

How do the results for the mutation of the VIL motif fit to the results for mutations in the CCM? As mentioned in 3.2 only the isoleucine and leucine of the VIL motif are highly conserved and their location on the helix facing outwards of the trimer would enable them to interact with lipids. However, only the leucine is part of the CCM facing to the right direction for interaction with cholesterol, as seen in the Wenxiang diagram (Figure 3–6 C). Therefore, only the mutation of the leucine but not the isoleucine should affect the transport. This is indeed reflected in the results obtained for the single mutants. While the mutation of the conserved isoleucine (IA) led to the same transport speed as the wild type, the single mutant HA-Cer LA shows a similar delay as the VIL mutant (see Table 4–1, first column). *Thus, the results clearly show that the delay of the VIL mutant is indeed due to the mutation of the leucine within the CCM.*

Mostly the same coherence can be found, when analyzing the cleavage kinetics of the HA variants. Both mutants, VIL3A and LA, respectively, show a medium effect on transport, when compared to the other mutants (Table 4–1, second column), while HA-Cer IA shows a non-significant difference. Hence, in the following analysis only HA-Cer LA will be discussed, as it represents the VIL3A mutant as well.
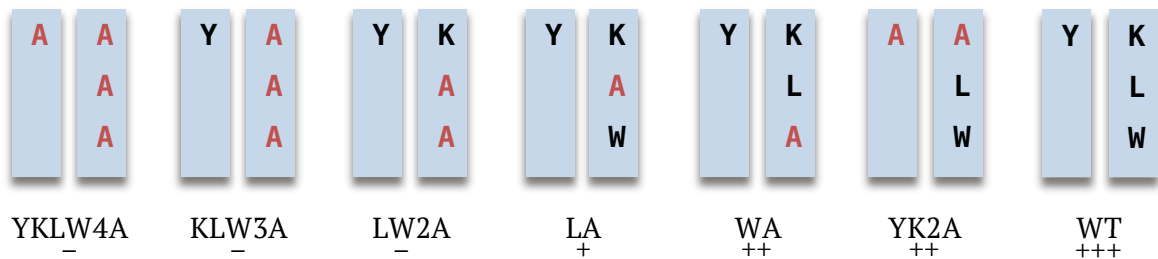

Figure 4-2: Schematic depiction of the location of the CCM mutations on the helices of two HA TMRs and their corresponding effect on transport to the TGN.

Like the previous results concerning the transport to the medial Golgi, the quadruple exchange of tyrosine, lysine, leucine and tryptophan (YKLW4A) has the most prominent delay in transport to the TGN (Figure 3–13). On the contrary, neither the introduction of Y (KLW3A) alone nor the additional introduction of K (LW2A) was able to rescue the phenotype. While for the transport from the ER to the medial Golgi the binding of the hydroxyl group of cholesterol by the outer Y and K was at least partially able to accelerate the transport (LW2A), for the transport within the Golgi either the additional introduction of the tryptophan (LA mutant) or the leucine (WA mutant) is needed. The aforementioned importance of the leucine is reflected in the results as well. The additional introduction of W (HA-Cer LA) accelerates the protein only half as much as the introduction of L (HA-Cer WA). In the case of the YK2A mutant, where both leucine and tryptophan are still present, the transport shows the same kinetic as in the case, where leucine is present together with aromatic Y and charged K (WA). *Therefore, we can conclude that for partial rescue of the phenotype two features in combination are needed, either the middle hydrophobic amino acid leucine with the outer two amino acids, the aromatic tyrosine and the charged lysine or with the inner aromatic amino acid tryptophan. Nevertheless, for recovery of wild type kinetics in cleavage all three components of the CCM are needed, whereby the leucine is the crucial amino acid.*

When studying the involvement of raft lipids in the transport of HA by blocking the synthesis of sphingolipids with Fumonisin B_1, we were able to demonstrate that the transport is affected by the treatment in case of wild type protein and the mutated variant (VIL3A) in the same manner (Figure 3–3). *Hence, we conclude that sphingolipids are involved in the transport through the Golgi independent from cholesterol binding.* It was already published that inhibition of cholesterol synthesis interferes with the transport of HA [245] and we showed that inhibition of sphingolipids interferes as well with the transport. Our findings on transiently expressed protein were supported in an infection model by a study published by Tafesse et al. [266] a year later than our publication. They used a sphingomyelin (SM) synthase deficient cell line, which is incapable of transferring the phosphocholine moiety from phosphatidylcholine (PC) to ceramide [267,268], thus interrupting the sphingolipid synthesis within the Golgi and reducing SM levels to 20 %. Kinetic studies of intracellular transport of HA expressed after an infection with a A/WSN/33 virus revealed, that ER to Golgi transport was not affected, but transport from the Golgi to the cell surface was significantly delayed yet not abolished, which is in line with our observations regarding Fumonisin B_1 treatment. Tafesse et al. confirmed their data, by using myriocin in MDCK cells, an inhibitor of the serine palmitoyltransferase (SPT) that blocks the initial step of sphingolipid synthesis even before the point of application of Fumonisin B_1 leading to a near complete inhibition of the synthesis. *As they were performing the experiments in infected cells, their virus results confirm our observations in transfected cells, showing that our results are not just an artifact of an over-expression system.* Since WSN is a group 1 virus expressing a H1 HA, their findings also support our result that sphingolipids are generally important for the transport of HA, independent from the ability to bind cholesterol, as group 1 HAs do not contain a CCM. *The findings of us and other groups indicate that sphingolipids and cholesterol play a key role in transport of viral hemagglutinin in an additive way, as inhibition of synthesis of either one or the other lipid does not abolish transport but slows it down.*

In addition to the kinetic studies, the steady-state intracellular and plasma membrane localization of HA after 24 hrs of expression was studied. The co-expression and subsequent immunostaining of the HA variants and the ERGIC or *cis*-Golgi resident t-

SNARE membrin revealed HA-Cer VIL3A being more co-localized with membrin than the wild type HA (Figure 3–4). *This supports our conclusion, that the VIL mutant, as a representative of a cholesterol-binding mutant, is transported slower than the wild type protein, as it is more associated with the cis-Golgi, while the wild type HA is probably already transported to further Golgi compartments.* As a complementary method FACS was used to observe the plasma membrane located amounts of the HA variants. Furin cycles between the TGN and the plasma membrane [109], and cleavage of HA by Furin takes place in the TGN or even in transport vesicles to the plasma membrane. Therefore, we would expect the amount of surface localized HA to resemble the amount of cleaved HA. The data obtained for surface expression is in accordance with this assumption, as the percentages calculated for surface amount (see Figure 3–14 B) do reflect the amount of cleaved HA. The same grouping of the different mutants as for the kinetics can be applied, with HA-Cer IA showing no effect, HA-Cer LA, WA and YK2A having a mild effect and HA-Cer LW2A, KLW3A and YKLW4A with the strongest effect on surface expression. *Therefore, we can conclude that transport to the surface is not further delayed or even halted. All HA variant with mutations in the CCM are transported to the surface only with different efficiency.*

4.1.2.1 Cholesterol binding might be already important for transport from the ER to the Golgi

Mutations in the cholesterol consensus motif already influence the transport of HA to the medial-Golgi. As the trimerization in the ER is not affected, a different mechanism must lead to the delayed arrival at the medial-Golgi. Although the cholesterol content is low, a lipid dependent sorting might already take place at the ER. GPI-anchored raft proteins for example are exported from the ER in cholesterol containing vesicles that are differently coated than vesicles transporting non-raft proteins [269]. Nevertheless, our assay of acquisition of Endo-H resistant carbohydrates can only monitor the arrival at the medial Golgi, where the N-actyl glucosamine transferase is located and therefore is not able to distinguish between an export from the ER in different vesicles or a transport delay from the *cis-* to the medial Golgi due to mechanisms within the Golgi, which will be discussed in the following subchapter.

4.1.2.2 Cholesterol and sphingolipid enriched raft-like structures might be involved in transport of HA through the Golgi

What could be the underlying mechanism explaining the retarded transport through the Golgi of HA protein with alterations in the CCM motif?

Munro and his group established the theory, that the different compositions of cellular membranes, with increasing amounts of cholesterol and sphingolipids from the ER to the plasma membrane, should be reflected in the physical properties of proteins, which reside in the respective membrane. By analyzing the sequences of the TMR of integral proteins, they found that the physical properties are organelle-specific, whereby the *length of the TMR correlates with the thickness of the membrane* it is incorporated in. Plasma membrane proteins usually have transmembrane regions with a length of more than 23 amino acids, while ER and *cis*-Golgi localized protein TMRs only have a length of not more than 17 amino acids [270,271]. Therefore, proteins will only be transported as far as they can integrate into a membrane with the appropriate thickness and will be retained there. *One possible explanation for the delayed transport kinetics might be that the length of the transmembrane is shortened in case of the exchange of hydrophobic amino acids by alanines.* Regarding this, we have to make a difference between the HA with exchanged VIL or CCM. The VIL is highly hydrophobic comprising three hydrophobic amino acids, while the CCM only comprises one, the leucine. Exchanges by alanines might have a different effect on the length of the TMR. If one includes the polar amino acids as delimiting anchors, the TMR of HA is even 27 amino acids long. *In silico* analysis of the amino acid sequence of HA wild type and the VIL mutant resulted in contradicting results depending on the program used. HMMTOP (http://www.enzim.hu/hmmtop/index.php) and Phobius (http://phobius.sbc.su.se) predict a TMR having a length of 24 amino acids, as they are not including the polar amino acids. No change in the location or length could be detected, when the sequence of the VIL mutant was entered into these programs. In contrast, TMHMM (http://www.cbs.dtu.dk/services/TMHMM/) and TMpred (http://www.ch.embnet.org/software/TMPRED_form.html) give a TMR with a length of 22 and 19 amino acids, respectively, in the mutant case. *Therefore, it is not possible to define the TMR in the mutant case immaculately.* The first two predictions contradict the theory of length of

TMRs being important for incorporation into raft-like structures in the Golgi as wild type and mutant HA exhibit the same length of the TMR, whereas the last two predictions, even with different outcome, support the theory since the mutation of the VIL motif leads to a decreased length of the TMR. *However, it needs to be stated that even if the predictions calculate shorter TMRs, the length is in between the described length of more than 24 AA for plasma membrane proteins and less than 17 AA for ER and cis-Golgi resident proteins.* This length is already sufficient to be transported to the plasma membrane as this has been shown in polarized MDCK cells by our group [252]. *Thus, we could conclude from two of the four predictions that the possible reduction in TMR length in the VIL mutant could lead to slower transport of the protein.* If we compare this result with the result for the CCM, HMMTOP and TMpred, as examples for the two program types giving contradicting results for the TMR lengths after mutation of the VIL motif, we can see that both programs do not predict a change in the TMR length (see Figure 3–7 to Figure 3–10), when exchanging all four amino acids of the CCM. *Since the delay in transport in the VIL motif is due to only the mutation of the leucine, the first two predictions with no change in TMR length should be considered and therefore, we can conclude that a reduction in the length of the TMR is not the reason for the slow transport of the CCM mutants along the secretory pathway.*

Intra Golgi transport is a process still under debate, and different lipid based theories have been put forward. According to Glick and Luini, so far five models have been proposed trying to explain the experimental data gained on the traffic kinetics of various proteins: "(1) the anterograde vesicular transport between stable compartments, (2) cisternal progression/maturation, (3) cisternal progression/maturation with heterotypic tubular transport, (4) rapid partitioning in a mixed Golgi, and (5) stable compartments as cisternal progenitors" (reviewed in [149]).

In chapter 1.4.1 two models of intra-Golgi transport involving raft-like structures were introduced and are part of the upper five general models. Except the rapid partitioning model of Patterson and Simons' model none of the other models include raft-like domains or more general lipids in their assumptions. When we compare the model of Simons with the existing ones, the cisternal maturation model is the one most compati-

ble; as both theories take retrograde COPI vesicle transport into account regarding the formation of the different Golgi stacks (see Figure 4-3).
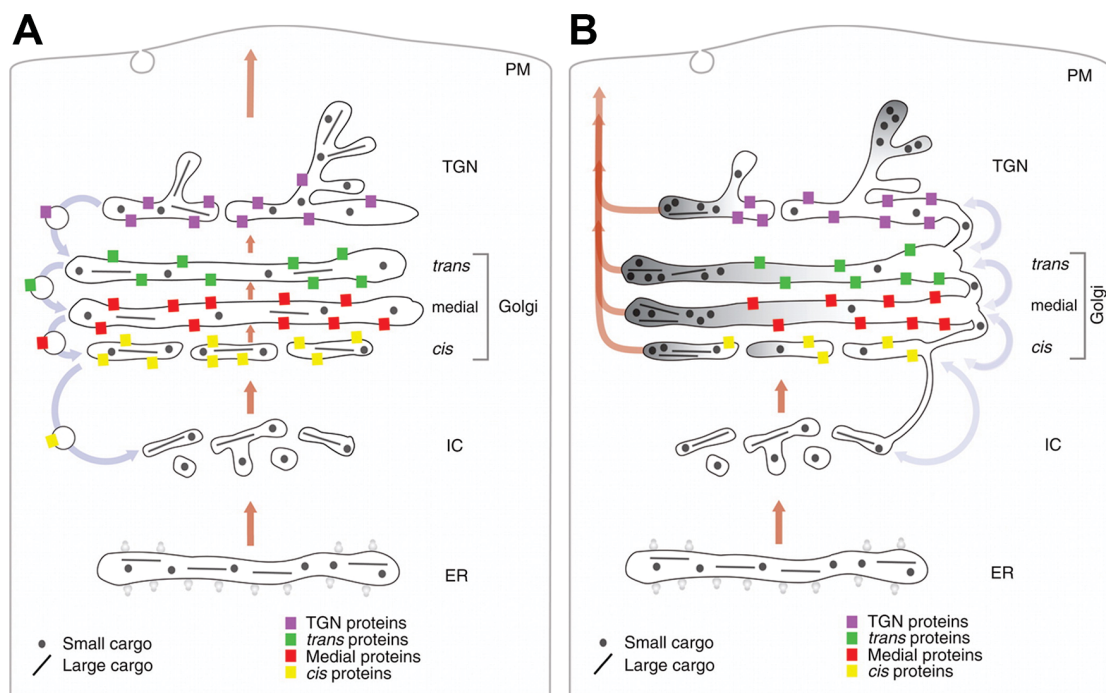

Figure 4-3: Models of Golgi transport: (A) Cisternal maturation model: The different cisternae of the Golgi mature by coalescence of previous compartments with retrograde transported COPI vesicles from the older cisternae. **(B)** Rapid partitioning model: Plasma membrane proteins and Golgi resident proteins partition in processing (white) and export domains (grey), whereby proteins can exit the Golgi at every cisternae. Reprinted by permission of Cold Spring Harbor Laboratory Press [149].

Simons' theory of lipid rafts being involved in proteins transport along the secretory pathway of polarized cells (reviewed in [145,146]) includes the findings of Munro and adds investigations of the lipid composition of the different compartments and carrier vesicles. It is based mainly on two observations: (1) the cholesterol and sphingolipid content increases form ER over *cis-* to *trans*-Golgi and is enhanced due to retrograde transport of COPI vesicles, which exclude both lipids and therefore leads to a thicker bilayer of the membrane [148] and (2) the existence of raft-carriers originating from the TGN being further enriched in raft lipids, transporting cargo to the apical membrane [150,272]. The hypothesis includes that the line tension that builds up between ordered, in raft lipids enriched domains and non-ordered membrane domains results in budding of vesicles, which then transport the included proteins. The budding out of the membrane thereby reduces the line tension and induces further lipid and protein sorting (reviewed in [145]). Proteins with raft-targeting signals will help to further

cluster already enriched raft lipids leading to a higher line tension resulting in vesicle formation. HA itself can form clusters at least at the plasma membrane [215,216], which is why a clustering within raft-like structures already in the Golgi cannot be excluded and could explain the difference of wild type and mutant protein regarding transport kinetics. Interestingly, VIP17/MAL, also a raft protein localized in transport vesicles from the Golgi to the plasma membrane of MDCK cells, seems to be involved in HA apical transport [273]. When overexpressed it enhances the transport of HA to the apical membrane, while down regulation by RNAi led to an inhibition of transport of HA [274]. VIP17/MAL is thought to have the ability to cluster small rafts within the Golgi to larger platforms. These large raft platforms increase the line tension between the ordered and disordered domains of the membrane and might then finally lead to budding out of the membrane forming transport vesicles [275]. The additional clustering by HA clusters in raft-like structures might even increase the effect, leading to more efficient transport from the Golgi to the surface. *As CCM motif mutants might not be able to localize in the cholesterol and sphingolipid enriched environment, they might be no longer able to cluster as much within the Golgi, as already seen on the plasma membrane for the H3 WIL mutant by Takeda et al. [220]. This in turn would lead to a slower vesicle formation for transport along the secretory pathway.* But it needs to be stated, that the theory of Simons and colleagues was established to explain the special lipid composition of apical membranes of polarized cells. The experiments of this study were performed in non-polarized CHO cells, which is why we cannot translate all the observations and conclusions of the theory. To find out if our findings also apply in polarized cells, the experiments need to be repeated in the according system.

Patterson's theory was created using a simulation of the secretory pathway on the one hand based on published lipid distribution data for ER, Golgi and plasma membrane, to ensure the right gradient of raft lipids and on the other hand based on the length of TMRs of proteins and their according location. This simulation led to the *hypothesis of two different domains existing within the Golgi cisternae, so-called "export" domains, from which cargo will exit the cisternae and stable "processing" domains, which are enriched in Golgi enzymes and in which modification of proteins is located* [151]. All proteins can enter and exit both domains, but exhibit a specific partitioning or equilib-

rium. *Golgi resident proteins like enzymes would be more likely to be found in the processing domains, while plasma membrane proteins like HA would be more likely to be found in the export domains.* The results obtained by the simulation were then further validated experimentally by following the transport dynamics of VSV-G protein as plasma membrane protein and GalT (galactosyltransferase) as a Golgi resident protein. The main difference between the model of Simons and Patterson is, that in the partitioning model proteins can exit the Golgi towards the plasma membrane at every cisterna since every level already has both domains (see arrows in Figure 4-3 B), while the theory of Simons like any other model of intra-Golgi transport includes protein first being transported from one cisternae to the next in *cis* to *trans* direction, with cargo leaving at the TGN in vesicles, which are then transported to the plasma membrane (see arrows in Figure 4-3 B). *As wild type HA and the mutant protein gets fully processed before leaving the Golgi including cleavage in the TGN, albeit in case of the mutant after a longer time period, our findings object the part of Patterson's theory of cargo leaving the Golgi at every level.* However, the existence of two domains within the Golgi and consequently the differential partitioning of proteins could still explain the difference in transport of wild type HA and the mutants. The data obtained for the intracellular localization of the wild type and mutant HA in comparison with the t-SNARE membrin could hint to different domains being responsible for the different transport kinetics. As it is known, that membrin as a Golgi-resident protein should be found in the processing domains, the higher colocalization of the VIL mutant compared to the wild type HA can be interpreted as a slower transport, as it still colocalizes with earlier cisternae of the Golgi. Similar observations were made investigating the transport properties of HA as a raft protein in comparison with YFP-p75 (75-kDa neurotrophin receptor) as a non-raft protein. Immunofluorescence studies within the Golgi revealed [276] segregation into different subdomains of the Golgi, whereby YFP-p75 located mostly in the same domains as Furin, while HA was found in different subcompartments. *These data might allow the assumption that the delay in transport within the Golgi could be due to longer length of stay in the processing domains indicated by the higher colocalization with Golgi resident proteins, while the wild type protein is already transported into the export domains and subsequently to the plasma membrane.* Additionally, Schwarzer and colleagues investigated the association of the HIV gp41 protein with raft-like domains

within the Golgi by FLIM-FRET. The glycoprotein gp41 of HIV does not exhibit a CCM but a CRAC motif. They not only showed a raft association of gp41 at the plasma membrane but also within the Golgi [262]. By using a chimeric protein of YFP N-terminally fused to gp41, therefore replacing gp120 by YFP, they performed FLIM-FRET experiments with gp41-YFP as acceptor and GPI-CFP as raft marker. When measuring FRET efficiencies of this pair within the Golgi, *a CRAC motif dependent clustering of gp41 with the raft marker was observed, which was similar to the results obtained for the plasma membrane.* This data provides prove of a cholesterol-binding motif dependent association with raft-like structures already emerging in the Golgi, that support our indirect findings of a cholesterol-binding motif dependent transport within the Golgi. The results presented in this study regarding the CCM can be interpreted in the context of the rapid portioning model in the following manner:
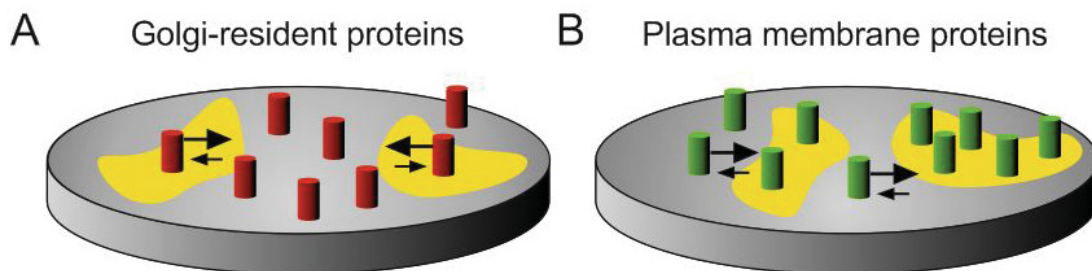
Figure 4-4: Rapid-Partitioning Model. (A) Golgi- resident proteins and CCM mutants (red) are more probably in the processing domains (grey) **(B)** transmembranal plasma membrane proteins like HA WT (green) are more likely to be found in the export domains (yellow). (Adapted from [151])

The wild type HA and CCM variants differ in their probability to be found in processing or export domains. While the wild type protein has a higher probability to diffuse into export domains, stay there and to finally being transported to the plasma membrane, the CCM mutant variants behave more like Golgi-resident proteins with a higher probability to diffuse out of the export domains (see Figure 4-4). Nevertheless, constant diffusion in and out of the two domains still enables the CCM mutant variants to be transported to the plasma membrane, just with a delayed kinetic.

Another reason for the differential affinity of the wild type HA compared to the altered versions could be the different availability of cholesterol in the two domains. Not only is the cholesterol content enriched within the export domains compared to the processing domains allowing for more interactions of HA molecules, but also the incorpo-

ration of cholesterol between lipids in its surrounding differs, thereby potentially leading to a changing accessibility of the binding site. Cholesterol has two faces due to the aliphatic groups at the end of the planar sterane backbone, the α- and β-face (reviewed in [277]) (see Figure 4-5). When embedded in a phospholipid-rich environment as it would be present in the processing domains, cholesterol is neither bound by the α- nor the β-face but the side of the molecule and therefore has both faces available for interaction with TMRs of proteins, while when embedded in a sphingolipid-rich environment the sphingolipids interact with the cholesterol via its α-face leaving the β-face available.
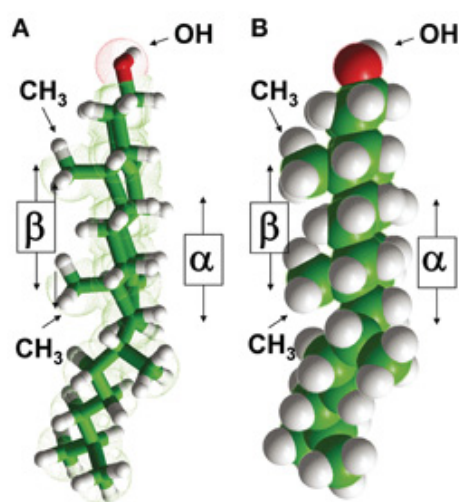
Figure 4-5: Structural properties of cholesterol. The symmetric distribution of aliphatic groups of the sterane backbone defines a smooth α-face and a rough β-face. Reprinted and modified from [277] with permission by the CC-BY license.

Consequently, it could be possible that for full binding of the CCM, sphingolipids are needed to ensure the right orientation of the cholesterol towards the TMR. When having a closer look at the structure of the CCM located in the β-adrenergic receptor binding the cholesterol (Figure 1-7 A), we can see that the TMR is binding the cholesterol via its β-face as the aliphatic groups of the planar sterane backbone are facing the TMR and the interacting amino acid side chains. The altered interaction with cholesterol in a phospholipid-rich membrane with both faces available, but in a different orientation, might additionally favor the incorporation of the wild type protein into the export domains over the processing domains. Therefore the wild type protein not only would be still able to bind to cholesterol in the export domains compared to the CCM mutant vari-

ants, but additionally might be more attracted to the export domains because they are providing the correct orientation of cholesterol for binding.

Comparing the models of Simons and Patterson with the results of this study, both have drawbacks. Simons only focuses on apical transport of proteins in polarized cells, which was not investigated here and Patterson investigated a basolateral protein (VSV-G) in non-polarized COS 7 cells claiming that cargo can leave from every stack of the Golgi, which was never detected in the case of HA. From studies on VSV-G protein and influenza HA in polarized MDCK cells, we know that basolateral and apical proteins are transported in different vesicles to the plasma membrane [278]. *The question arises if such a sorting system already exists in non-polarized cells.* Yoshimori and colleagues investigated the delivery routes of the basolateral proteins VSV-G and Semliki Forest virus spike glycoproteins compared to the apical HA of influenza virus in non-polarized BHK and CHO-K1 cells [279]. Their data demonstrates that basolateral and apical proteins use a similar transport mechanism in polarized and non-polarized cells to reach the plasma membrane. Different treatments interfering with the known basolateral pathway and its regulation in MDCK cells interfered as well with the transport of VSV-G, SVF glycoproteins and a HA mutant, which is retargeted to the basolateral membrane in polarized cells, but not wild type HA. These findings were supported by another study from the same year, coming to the same conclusion investigating the transport of VSV-G and influenza HA in two more non-polarized cell lines (3T3 and GH3) [280]. *Therefore, a combination of Simons and Patterson's theory could be possible.* Incorporation into more general raft lipid enriched export domains within the Golgi would be the prerequisite for a transport through the Golgi, in which then apical and basolateral proteins are sorted. Thereby HA would integrate into smaller raft-like patches, which then by clustering form vesicles due to their line tension not only at the TGN for transport to the plasma membrane but already within the Golgi.

4.2 Clustering of HA with a lipid raft maker is reduced by introduction of mutations in the putative cholesterol consensus motif

Finally, FLIM-FRET measurements were performed to examine whether the cholesterol consensus motif is crucial for raft association. Since Stephanie Engel established the method with HA-Cerulean as donor and Myr-Pal-YFP as acceptor, the first aim was to reproduce the results obtained for HA-Cer wt and HA-Cer VIL3A. FRET measurements are highly sensitive to changes in the equipment, which can result in different FRET efficiencies measured, but should not affect clustering of the investigated protein with the raft marker. While Stephanie Engel was able to reproducibly detect FRET efficiencies of around 50 % for HA-Cer wt and Myr-Pal-YFP, in this study only a median FRET efficiency of 17,6 % could be detected. But remarkably, the clustering was not changed, as the K_D of 1,6 x 10^{-16} was altered not significantly to 1,3 x 10^{-16}. Additionally, the loss of clustering when mutating the hydrophobic VIL motif was verified as the K_D of 1,3 x 10^{-16} rises to 7488 (see Figure 3–16). Even though the actual measured FRET efficiencies changed between the here presented study and the study of Stephanie Engel, the interpretation of the data still remains the same: *Mutation of the hydrophobic raft-targeting signal in the beginning of the TMR leads to a loss in lipid raft association.*

To ensure a correct measurement, the values measured were compared with published data in the literature. The lifetime of the donor is the limiting factor in the calculation of FRET efficiencies by using the following equation:

$$E = \left(1 - \frac{\overline{\tau}_{DA}}{\overline{\tau}_D}\right) * 100$$

In case $\overline{\tau}_D$ (the lifetime of the donor in absence of an acceptor) is too high or too low, E will result accordingly in an incorrect value. The lifetime of a fluorophore is dependent on the environment of the chromophore. The chromophore of Cerulean is build by three amino acids: serine 65, tryptophan 66 and glycine 67, whereby the tryptophan is creating the cyan fluorescence [296]. These three amino acids are embedded into the β-barrel structure of the fluorophore (Figure 4-6) and consequently

shielded from the surrounding. Therefore the lifetime of Cerulean should be a measurable constant.
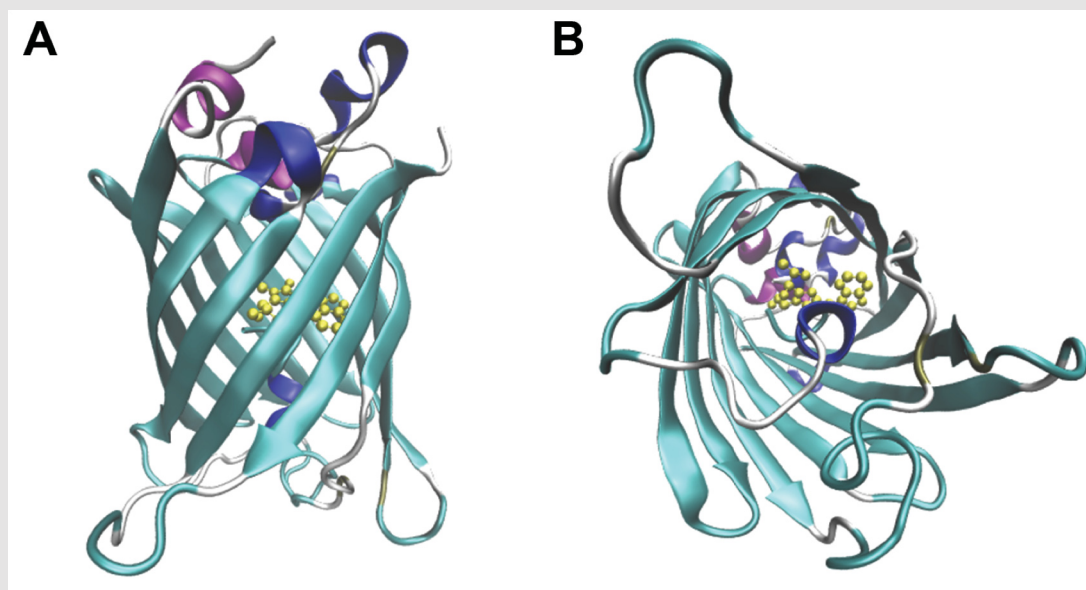
Figure 4-6: Structure of Cerulean. Chromophore (Ser65, Trp66 and Gly67 in yellow) is embedded in β-barrel structure (cyan) **(A)** Side view **(B)** View from below. Created with Visual molecular dynamics (VMD) 1.9.1 and POV-Ray 3.7.0 from PDB code 2Q57.

Cerulean expressed individually in HeLa cells exhibits a lifetime of 2.3 ns [297,298], which was true as well when the lifetime of purified recombinant protein was determined using time-correlated single photon counting spectroscopy [247]. When CFP was attached to a GPI anchor to function as a raft marker, lifetimes of 2.3-2.5 ns [223,262] were detected. During this study lifetimes of 184 HA-Cerulean expressing cells in absence of a FRET acceptor were measured for calculation of the FRET efficiency. The calculation of the average lifetime yielded 2.52 ns ± 0.01 (SEM was used due to the high number of measurements), which is in accordance to the published data. When interpreting FRET efficiencies one has to keep in mind the preconditions for energy transfer:

3   The overlap of the donor's emission spectrum and the acceptor's excitation spectrum

4   The orientation of the dipoles

5   The quantum yield (QY) $\Phi = \dfrac{number\ of\ photons\ emitted}{number\ of\ photons\ absorbed}$

6   The distance of the donor and acceptor

For ECFP and EYFP a FRET efficiency of 25 % was measured [297], when both proteins were expressed as fusion protein. The same was true for Cerulean as the FRET donor and mVenus as FRET acceptor, an enhanced version of mYFP with the same excitation and emission spectrum and quantum yield, but a better stability regarding pH and Cl$^-$ [299], with FRET efficiencies of 25 % [300] and 26 % [298], respectively. Both groups also used direct fusion proteins of Cerulean and mVenus. As no fusion of the fluorophores to other proteins takes place changing the distance of the fluorophores, *we can assume that this is the maximal FRET efficiency, which can be achieved with this FRET pair and the according quantum yield of Cerulean.* According to **(3)** improvement in the quantum yield of the donor, like in the case of mTurquoise, a fluorophore with an increased QY of 0.84 instead of 0.48 [301], can yield higher FRET efficiencies of 30 % [300] and 33 % [298], respectively. *These publications support my finding of only about 18 % FRET efficiency for HA-mCer and Myr-Pal-YFP instead of about 50 % detected by Stephanie Engel, which seems to be in a more natural range of energy transfer of this specific FRET pair of Cerulean.* If Cerulean or CFP is coupled to proteins the distance of the fluorophores can change, which is why each FRET pair has to be evaluated on its own, only mutants of the same construct can be compared with each other. According to **(4)** the increased distance of the fluorophores, when coupled to proteins can lead to different FRET efficiencies being measured. For HA, another different system was used, as the fluorophore was not attached to the cytoplasmic tail but rather N-terminally replacing the ectodomain. Under those conditions a GPI anchor can be used as raft marker, C-terminally fused to a fluorophore [223], whereby a medium FRET efficiency of 10 % was measured. The same system was used elucidating the lateral organisation of HIV gp41 and yielded a FRET efficiency of 18 % [262], showing the influence of the protein attached to the fluorophores on the energy transfer.

The above-mentioned findings demonstrate that the measurements made within this study are valid, and that further experiments regarding the role of the cholesterol consensus motif can be performed under the same conditions as the validation of the FLIM-FRET measurement.

Table 2: Summary of all results including FLIM-FRET

Mutant	Transport to medial Golgi ($t_{1/2}$)	Transport to TGN ($t_{1/2}$)	Transport Golgi to TGN	Surface expression	Clustering with raft (K_D)
wt	40 min	55 min	15 min	100%	$1{,}3 \times 10^{-16}$
VIL3A	40 min	55 min	15 min	ND	7488
IA	80 min	150 min	70 min	ND	ND
LA	40 min	70 min	30 min	95%	ND
WA	90 min	190 min	100 min	85%	474
YK2A	40 min	110 min	70 min	80%	3662
LW2A	40 min	120 min	80 min	80%	2630
KLW3A	100 min	290 min	190 min	50%	ND
YKLW4A	240 min	290 min	50 min	50%	ND

Half times for transport to the medial Golgi and to the TGN were compiled from Figures 3-2, 3-12 and 3-13. The time for transport between Golgi and TGN was calculated as the difference between the $t_{1/2}$ for transport to the TGN minus the $t_{1/2}$ for transport to the medial Golgi. Data for surface expression are from Figure 3-14. Clustering with rafts as determined by FLIM-FRET (Figure 3-16) is displayed as K_D. ND: not determined. Results are divided into three classes: Mutants with the strongest effect on the respective process are highlighted in dark gray, with an intermediate effect are highlighted in light gray and with no (or very little) effect are not highlighted.

For the analysis of the influence of the CCM on lipid raft association/clustering with the Myr-Pal raft marker, only a subset of the created mutants was used.

The mutation of the tryptophan (HA-Cer WA) has the least effect on clustering. Although the FRET efficiency is reduced in the same manner than all other mutants, the cluster analysis shows a less pronounced reduction in clustering. Therefore, the conclusion can be drawn that *the exchange of tryptophan in the CCM affects clustering with the raft marker but only in a marginal matter*. As seen in the before mentioned experiments, the remaining amino acids binding in the linker region and in the middle of the motif can partially compensate the missing binding, but not completely. For the other two measured mutants the results allow for a more complex analysis. While regarding transport and surface expression HA-Cer YK2A showed only an intermediate

effect comparable to HA-Cer WA and HA-Cer LW2A showed the strongest effect, the clustering is affected in the same range. Both have a reduction of FRET efficiency comparable as all other mutants investigated, but their K_{D}s are both in the range of the VIL mutant (7488, 3662 and 2630, respectively for VIL3A, YK2A and LW2A) and not HA-Cer WA. As the VIL mutant resembles the LA single mutant, as shown in the previous parts, it seems that the additional mutation of the tryptophan in the LW2A mutant does not act in an additive manner at the plasma membrane, as seen before for the transport. *Further, both the binding of the hydroxyl group of cholesterol in the linker region by the two outer amino acids lysine and arginine and the hydrophobic and aromatic amino acids binding the sterol rings seem to have the same effect on interaction with the raft marker.*

Supporting data for both parts being important for raft association at the plasma membrane comes from an electron spin resonance (ESR) analysis of an H3 HA with mutations of either the lysine (K) or leucine (L) of the putative CCM. Via ESR it is possible to measure the hydration/dehydration state of the headgroup of lipids and therefore the ordering state of the membrane. With increasing amount of HA TMR peptides incorporated into the membrane, the ordering of cholesterol rich membranes increases accordingly. Mutant peptides with lysine exchanged by glutamic acid, hence changing the polarity of the amino acid from positive to negative, and leucine exchanges against alanine were not able to induce ordering of the membrane [281].

4.3 Speculations on the role of cholesterol binding of HA for virus replication

Binding cholesterol can be advantageous for viruses in sense of a **higher stability**. Integration into lipid rafts at the plasma membrane leads to budding from higher ordered membrane domains resulting in a more densely packed viral envelope. This could be of advantage especially for transmission via aerosols.

For influenza viruses it was shown by a proton magic angle NMR study that the virus membrane has different physical states that are temperature dependent. At 41°C both liquid ordered and disordered phases could be detected, while at 22°C lipids were in a

gel phase [282]. This phase is even higher ordered than the liquid ordered phase [283] due to the fatty acid chains, which are elongated to their maximum, therefore forming a highly compact structure. This compact virus shell might be one reason for the higher transmission rates of influenza virus at lower temperatures. Lowen and colleagues performed transmission experiments in guinea pigs and were able to show that viral transmission is dependent on temperature and relative humidity [284]. Transmission at low temperatures (5°C) is most effective with low relative humidity. Shedding of virus is increased under those conditions probably due to higher stability of the virus residing in the cold upper respiratory tract, which then can be spread more easily. For transmission at more moderate temperature (20°C) two stable conditions of virus particles could be detected either at low or higher (65%) relative humidity.

Despite a more stable viral envelope deriving from assembling in lipid rafts and subsequent budding from them, viruses exploit the properties of lipid rafts for their **entry and fusion**, as mentioned in the introduction. The fusion process of influenza viruses is well studied and its dependence on lipid raft association and cholesterol content in the viral envelope was already investigated. For the WSN strain a cholesterol dependence in the viral membrane for fusion was shown by cholesterol extraction assays [285]. Manipulation of the cellular cholesterol content in the expressing cell line, in this case the increase of cholesterol content in otherwise low-cholesterol insect cells, revealed a positive correlation of cholesterol content and the amount of full fusion [286]. The same study also revealed the dependence of the presence of the TMR for fusion and a promotion of pore size extension by cholesterol during the fusion process. Cholesterol thereby induces intrinsic negative curvature to build the pre-pore [286,287]. The abovementioned results that cholesterol in needed in the viral envelope as well as in the cellular membrane can be explained by the theory of Ge and colleagues. They stated that two highly ordered membranes with negative curvature and negative charge on their surface induce a water capillary bridge between the membranes attracting them toward each other [281] facilitating hemifusion. Additionally, concentration and clustering of HA in lipid rafts seems to be important for the efficiency of the fusion. Non-raft HA is less clustered on the surface of infected cells and is less incorporated into new virus particles, leading to a reduction in fusion activity

and infectivity [220]. Supporting evidence is given by several studies reporting the number of HA trimers needed for fusion. The latest opinion is that at least 8 HA trimers aggregate at the fusion site, while 2 trimers are enough to perform the synchronized activation and refolding, inducing the fusion event [288–291]. Since for HIV the CRAC motif is crucial for fusion, the here described putative CCM comprising the TMR raft-targeting signal, might also be crucial for fusion, ensuring the right clustering of HA.

5 Outlook

So far, only a couple of possible mutants were used to assess the effect of the putative CCM on the transport and raft integration behavior of the influenza hemagglutinin. Especially, the positively charged K and aromatic Y at the water-lipid interface were only mutated together but not alone. The change in effect, from a medium effect on the intracellular transport to a comparable effect on clustering with a raft marker, is an aspect, which needs further investigation. New mutants with single exchange of lysine and arginine against alanine and double mutants with either leucine or trypto-phan were already designed and genes were synthesized. These mutants are now ready to be cloned into the expression plasmid to be used in further experiments.

For a complete insight of the function of the putative CCM, introduction of the muta-tions in the viral context would be advantageous. Some mutations can show an effect on the protein behavior, but may not lead to reduction in virus growth. After subclon-ing the mutated regions of HA into the reverse genetics system, recombinant viruses can be tested for propagation. Since the mutation of the VIL motif already reduced the titer of the Udorn virus by ~3 [220] logs, it might be possible that viruses with a com-plete mutation of the cholesterol-binding motif are not rescuable. For those viruses, which are rescuable, the classic characterization methods of growth behavior like con-ducting growth kinetics experiments and plaque size assays should be applied. The prepared viruses could then further be analyzed regarding their membrane ordering and hence their stability in the environment. Laurdan (6-dodecanoyl-2-dimethylaminonaph-talene) is a lipophilic fluorophore that is able to detect and dis-play the lateral ordering status of membranes [292,293].

1.1.1 Established method: Laurdan measurements to determine the lateral organization of viral membranes

Laurdan can integrate into lipid membranes, whereby its emission spectrum is de-pendent on the hydration state of the membrane. In ordered membranes water is repressed and Laurdan exhibits a blue shift in its emission spectrum from 440 nm

in liquid disordered (L_d) membranes to 490 nm in liquid ordered (L_o) membranes. From the intensity of the blue and red emission it is possible to calculate the general polarization (GP) according to:

$$GP = \frac{I(440nm) - I(490nm)}{I(440nm) + I(490nm)}$$

GP values can range between +1 (most ordered) and -1 (least ordered), whereby GP values under +0.25 and between 0.25 and 0.5 correspond to L_d phases and L_o phases, as determined for model membranes [302]. However, cellular membranes have a more complex composition as model membranes. The determination of the membrane ordering status of giant plasma membrane vesicles (GMPVs), vesicles which are prepared from the plasma membrane of cells, yielded values of 0.67 for L_d phases and 0.80 for L_o phase. Therefore the difference of lipid rafts and the regular plasma membrane is less prominent [293]. Since these experiments were performed only at 10°C, the low temperature can influence the outcome of the measurement as ordering of membranes increases with decreasing temperature. At physical temperatures of about 37°C the differences should be higher and better discernable.

The method was established by me during the time of this study by measuring the lateral organization of FPV as a raft budding virus and Semliki Forest virus as a non-raft virus with a lipidome resembling the regular plasma membrane. According to Lorizate et al. [304], purified virus particles containing 20 μg of protein were incubated in a 5 μM Laurdan solution in 100 μl TE buffer, to allow incorporation, whereupon non-integrating Laurdan was removed by ultracentrifugation through a 20 % sucrose cushion. The pelleted virus was resuspended in buffer containing 150 mM NaCl and 10 mM Hepes (pH7,4) and investigated by fluorescence spectroscopy. After excitation with 355 nm the emission spectrum between 400 and 550 nm was recorded. Values for 440 and 490 nm were used to calculate the GP value. As seen in Figure 5-1 the discrimination between the lateral membrane organization of raft and non-raft viruses is possible, since a significant difference between the GP values was detected. Even though the difference is quite small, the method is sensitive enough to differentiate between the two ordering states (Figure 5-1)
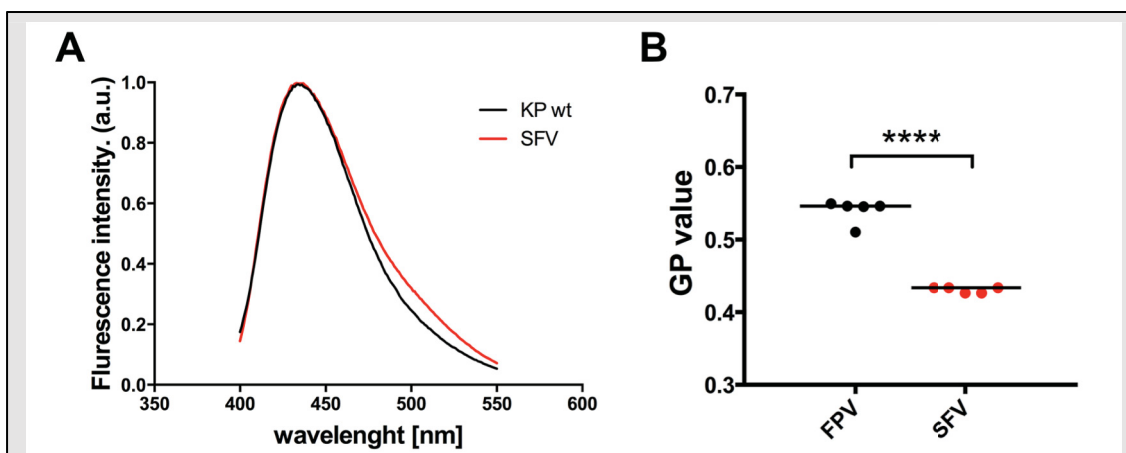
Figure 5-1: Laurdan measurement of fowl plaque virus (FPV, black) and Semliki Forest virus (SFV, red). (A) Recorded fluorescence emission spectrum between 400 and 550 nm **(B)** Calculated GP values. Results are median GP value. P> 0,0001 by unpaired two-tailed student's t-test.

The method is also applicable to investigate the increasing and decreasing stability, respectively, under changing temperature conditions (Figure 5-2). Higher temperature lead to an increases hydration state of the membrane, which is reflected in a decreasing GP value that is measured by Laurdan.
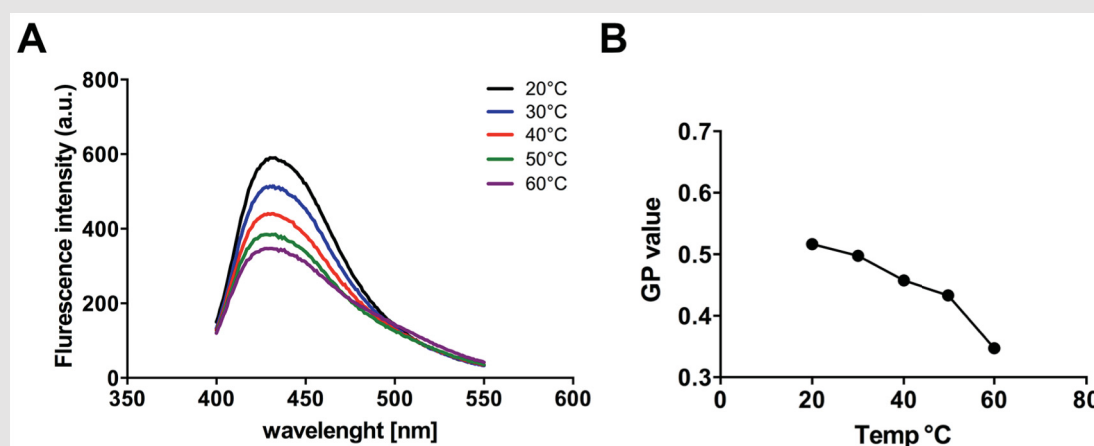
Figure 5-2**: Temperature dependence of the lateral organization of the viral envelope.**
(A) Recorded fluorescence emission spectrum between 400 and 550 nm at temperatures varying from 20°C to 60°C. **(B)** Calculated GP values.

Not only can Laurdan be used to investigate purified viruses, but also to visualize the lateral organization of the plasma membrane in infected cells. A combination of Laurdan measurements of the hydration state of the cellular membrane with high resolution microscopy (established so far for widefield microscopy [294]) might make it even possible to monitor the assembly of newly formed viruses. Clusters build by HA on the

cell surface are detectable by high-resolution microscopy like FPALM (fluorescence photoactivation localization microscopy) [216]. Using this technique in combination with Laurdan, it would be possible to not only identify clusters build by HA at the assembly site, but also additionally measure the lateral organization to prove directly the involvement of lipid rafts in the assembly of influenza A viruses. Mutations in the CCM might also lead to an unclustered distribution of HA as seen by electron microscopy for the mutation of the VIL domain [220], which could then be visualized in living cells.

Performing fusion assays of viruses with labeled ghost erythrocytes could give an insight in the role of the CCM or a virus membrane enriched in raft lipid, respectively in the fusion process of influenza viruses. Two fusion assays can be used to investigate the fusion capacities of the hemagglutinin. Either one investigates the fusion of purified virus with ghost erythrocytes or the fusion of infected cells with regular red blood cells.

Finally, the most important question needs to be answered. Is the putative CCM really able to bind cholesterol? So far all the data hint towards binding, but it has not been proven directly. Computational modeling of HA within a cholesterol-containing membrane might give further insight into the binding capacity of HA. For every computational modeling a structure of the protein or peptide of interest is a prerequisite. As the structure of the TMR of influenza HA is still not solved, further studies on this topic are needed. Collaborators of our laboratory, Larissa Kordyukova and colleagues, published an article in 2010 including a computational model of the TMRs of a group 1 and group 2 HA, subtypes H6 and H14, respectively [246]. This method of modeling could be used in cooperation to create a model of the TMR of H7 HA including the amino acids building the CCM, whereupon further MD simulations could be run to model in cholesterol binding [295]. The binding properties could be based on the insights of known structures of the CCM bound to cholesterol or using programs like AutoDock. Experimentally, new collaborators being expert in studying membrane proteins could perform NMR studies in micelles containing cholesterol to solve the structure of the TMR, which then in turn could be used to model trimers in a membrane to gain further insights of the possible cholesterol binding or association.

Addendum

Bibliography

1   Webster, R. G., Bean, W. J., Gorman, O. T., Chambers, T. M. and Kawaoka, Y. (1992) Evolution and ecology of influenza A viruses. Microbiol. Rev. **56**, 152–79.

2   Keawcharoen, J., Amonsin, A., Oraveerakul, K., Wattanodorn, S., Papravasit, T., Karnda, S., Lekakul, K., Pattanarangsan, R., Noppornpanth, S., Fouchier, R. A. M., et al. (2005) Characterization of the hemagglutinin and neuraminidase genes of recent influenza virus isolates from different avian species in Thailand. Acta Virol. **49**, 277–80.

3   Tong, S., Li, Y., Rivailler, P., Conrardy, C., Castillo, D. A. A., Chen, L.-M., Recuenco, S., Ellison, J. A., Davis, C. T., York, I. A., et al. (2012) A distinct lineage of influenza A virus from bats. Proc. Natl. Acad. Sci. U. S. A. **109**, 4269–74.

4   Tong, S., Zhu, X., Li, Y., Shi, M., Zhang, J., Bourgeois, M., Yang, H., Chen, X., Recuenco, S., Gomez, J., et al. (2013) New world bats harbor diverse influenza A viruses. PLoS Pathog. **9**, e1003657.

5   Horimoto, T. and Kawaoka, Y. (2001) Pandemic threat posed by avian influenza A viruses. Clin. Microbiol. Rev. **14**, 129–49.

6   Osterhaus, A. D., Rimmelzwaan, G. F., Martina, B. E., Bestebroer, T. M. and Fouchier, R. A. (2000) Influenza B virus in seals. Science **288**, 1051–3.

7   Glezen, W. P. (1980) Influenza C Virus Infection. Arch. Intern. Med., American Medical Association **140**, 1278.

8   Guo, Y. J., Jin, F. G., Wang, P., Wang, M. and Zhu, J. M. (1983) Isolation of influenza C virus from pigs and experimental infection of pigs with influenza C virus. J. Gen. Virol. **64 (Pt 1)**, 177–82.

9   Skehel, J. J. and Wiley, D. C. (1995) Influenza viruses and cell membranes. Am. J. Respir. Crit. Care Med. **152**, S13–5.

10   Wiley, D. C., Skehel, J. J. and Waterfield, M. (1977) Evidence from studies with a cross-linking reagent that the haemagglutinin of influenza virus is a trimer. Virology **79**, 446–8.

11   Wilson, I. A., Skehel, J. J. and Wiley, D. C. (1981) Structure of the haemagglutinin membrane glycoprotein of influenza virus at 3 A resolution. Nature **289**, 366–73.

12   White, J., Kartenbeck, J. and Helenius, A. (1982) Membrane fusion activity of influenza virus. EMBO J. **1**, 217–22.

13   Varghese, J. N., McKimm-Breschkin, J. L., Caldwell, J. B., Kortt, A. A. and Colman, P. M. (1992) The structure of the complex between influenza virus neuraminidase and sialic acid, the viral receptor. Proteins **14**, 327–32.

14   Siegl, G., Pette, J. and Mahnel, H. (1968) [On the structure of equine influenza virus. A contribution on the ultrastructure of influenza viruses]. Arch. Gesamte Virusforsch. **24**, 299–311.

15   Herrler, G., Rott, R., Klenk, H. D., Müller, H. P., Shukla, A. K. and Schauer, R. (1985) The receptor-destroying enzyme of influenza C virus is neuraminate-O-acetylesterase. EMBO J. **4**, 1503–6.

16   Herrler, G., Dürkop, I., Becht, H. and Klenk, H. D. (1988) The glycoprotein of influenza C virus is the haemagglutinin, esterase and fusion factor. J. Gen. Virol. **69 (Pt 4)**, 839–46.

17   Holsinger, L. J. and Lamb, R. A. (1991) Influenza virus M2 integral membrane protein is a homotetramer stabilized by formation of disulfide bonds. Virology **183**, 32–43.

18   Sugrue, R. J. and Hay, A. J. (1991) Structural characteristics of the M2 protein of influenza A viruses: evidence that it forms a tetrameric channel. Virology **180**, 617–24.

19   Pinto, L. H., Holsinger, L. J. and Lamb, R. A. (1992) Influenza virus M2 protein has ion channel activity. Cell **69**, 517–528.

20   Brassard, D. L., Leser, G. P. and Lamb, R. A. (1996) Influenza B virus NB glycoprotein is a component of the virion. Virology **220**, 350–60.

21 Tada, Y., Hongo, S., Muraki, Y., Matsuzaki, Y., Sugawara, K., Kitame, F. and Nakamura, K. (1998) Phosphorylation of influenza C virus CM2 protein. Virus Res. **58**, 65–72.

22 Pons, M. W., Schulze, I. T., Hirst, G. K. and Hauser, R. (1969) Isolation and characterization of the ribonucleoprotein of influenza virus. Virology **39**, 250–9.

23 Area, E., Martín-Benito, J., Gastaminza, P., Torreira, E., Valpuesta, J. M., Carrascosa, J. L. and Ortín, J. (2004) 3D structure of the influenza virus polymerase complex: localization of subunit domains. Proc. Natl. Acad. Sci. U. S. A. **101**, 308–13.

24 Medina, R. a and García-Sastre, A. (2011) Influenza A viruses: new research developments. Nat. Rev. Microbiol., Nature Publishing Group **9**, 590–603.

25 Hale, B. G., Randall, R. E., Ortín, J. and Jackson, D. (2008) The multifunctional NS1 protein of influenza A viruses. J. Gen. Virol. **89**, 2359–76.

26 Chen, W., Calvo, P. A., Malide, D., Gibbs, J., Schubert, U., Bacik, I., Basta, S., O'Neill, R., Schickli, J., Palese, P., et al. (2001) A novel influenza A virus mitochondrial protein that induces cell death. Nat. Med. **7**, 1306–12.

27 Gibbs, J. S., Malide, D., Hornung, F., Bennink, J. R. and Yewdell, J. W. (2003) The influenza A virus PB1-F2 protein targets the inner mitochondrial membrane via a predicted basic amphipathic helix that disrupts mitochondrial function. J. Virol. **77**, 7214–24.

28 Yamada, H., Chounan, R., Higashi, Y., Kurihara, N. and Kido, H. (2004) Mitochondrial targeting sequence of the influenza A virus PB1-F2 protein and its function in mitochondria. FEBS Lett. **578**, 331–6.

29 Henkel, M., Mitzner, D., Henklein, P., Meyer-Almes, F.-J., Moroni, A., Difrancesco, M. L., Henkes, L. M., Kreim, M., Kast, S. M., Schubert, U., et al. (2010) The proapoptotic influenza A virus protein PB1-F2 forms a nonselective ion channel. PLoS One **5**, e11112.

30 Conenello, G. M., Tisoncik, J. R., Rosenzweig, E., Varga, Z. T., Palese, P. and Katze, M. G. (2011) A single N66S mutation in the PB1-F2 protein of influenza A virus increases virulence by inhibiting the early interferon response in vivo. J. Virol. **85**, 652–62.

31 Varga, Z. T., Ramos, I., Hai, R., Schmolke, M., García-Sastre, A., Fernandez-Sesma, A. and Palese, P. (2011) The influenza virus protein PB1-F2 inhibits the

induction of type I interferon at the level of the MAVS adaptor protein. PLoS Pathog. **7**, e1002067.

32 Mazur, I., Anhlan, D., Mitzner, D., Wixler, L., Schubert, U. and Ludwig, S. (2008) The proapoptotic influenza A virus protein PB1-F2 regulates viral polymerase activity by interaction with the PB1 protein. Cell. Microbiol. **10**, 1140–52.

33 McAuley, J. L., Zhang, K. and McCullers, J. A. (2010) The effects of influenza A virus PB1-F2 protein on polymerase activity are strain specific and do not impact pathogenesis. J. Virol. **84**, 558–64.

34 McCullers, J. A. (2006) Insights into the interaction between influenza virus and pneumococcus. Clin. Microbiol. Rev. **19**, 571–82.

35 Coleman, J. R. (2007) The PB1-F2 protein of Influenza A virus: increasing pathogenicity by disrupting alveolar macrophages. Virol. J. **4**, 9.

36 McAuley, J. L., Hornung, F., Boyd, K. L., Smith, A. M., McKeon, R., Bennink, J., Yewdell, J. W. and McCullers, J. A. (2007) Expression of the 1918 influenza A virus PB1-F2 enhances the pathogenesis of viral and secondary bacterial pneumonia. Cell Host Microbe **2**, 240–9.

37 Wise, H. M., Foeglein, A., Sun, J., Dalton, R. M., Patel, S., Howard, W., Anderson, E. C., Barclay, W. S. and Digard, P. (2009) A complicated message: Identification of a novel PB1-related protein translated from influenza A virus segment 2 mRNA. J. Virol. **83**, 8021–31.

38 Wise, H. M., Barbezange, C., Jagger, B. W., Dalton, R. M., Gog, J. R., Curran, M. D., Taubenberger, J. K., Anderson, E. C. and Digard, P. (2011) Overlapping signals for translational regulation and packaging of influenza A virus segment 2. Nucleic Acids Res. **39**, 7775–90.

39 Muramoto, Y., Noda, T., Kawakami, E., Akkina, R. and Kawaoka, Y. (2013) Identification of novel influenza A virus proteins translated from PA mRNA. J. Virol. **87**, 2455–62.

40 Wise, H. M., Hutchinson, E. C., Jagger, B. W., Stuart, A. D., Kang, Z. H., Robb, N., Schwartzman, L. M., Kash, J. C., Fodor, E., Firth, A. E., et al. (2012) Identification of a novel splice variant form of the influenza A virus M2 ion channel with an antigenically distinct ectodomain. PLoS Pathog. **8**, e1002998.

41 Jagger, B. W., Wise, H. M., Kash, J. C., Walters, K., Wills, N. M., Xiao, Y.-L., Dunfee, R. L., Schwartzman, L. M., Ozinsky, a, Bell, G. L., et al. (2012) An

overlapping protein-coding region in influenza A virus segment 3 modulates the host response. Science **337**, 199–204.

42 Firth, a E., Jagger, B. W., Wise, H. M., Nelson, C. C., Parsawar, K., Wills, N. M., Napthine, S., Taubenberger, J. K., Digard, P. and Atkins, J. F. (2012) Ribosomal frameshifting used in influenza A virus expression occurs within the sequence UCC_UUU_CGU and is in the +1 direction. Open Biol. **2**, 120109.

43 Rogers, G. N., Paulson, J. C., Daniels, R. S., Skehel, J. J., Wilson, I. A. and Wiley, D. C. Single amino acid substitutions in influenza haemagglutinin change receptor binding specificity. Nature **304**, 76–8.

44 Matrosovich, M. N., Gambaryan, A. S., Teneberg, S., Piskarev, V. E., Yamnikova, S. S., Lvov, D. K., Robertson, J. S. and Karlsson, K. A. (1997) Avian influenza A viruses differ from human viruses by recognition of sialyloligosaccharides and gangliosides and by a higher conservation of the HA receptor-binding site. Virology **233**, 224–34.

45 Rust, M. J., Lakadamyali, M., Zhang, F. and Zhuang, X. (2004) Assembly of endocytic machinery around individual influenza viruses during viral entry. Nat. Struct. Mol. Biol. **11**, 567–73.

46 De Vries, E., Tscherne, D. M., Wienholts, M. J., Cobos-Jiménez, V., Scholte, F., García-Sastre, A., Rottier, P. J. M. and de Haan, C. A. M. (2011) Dissection of the influenza A virus endocytic routes reveals macropinocytosis as an alternative entry pathway. PLoS Pathog. **7**, e1001329.

47 Lakadamyali, M., Rust, M. J., Babcock, H. P. and Zhuang, X. (2003) Visualizing infection of individual influenza viruses. Proc. Natl. Acad. Sci. U. S. A. **100**, 9280–5.

48 Carr, C. M. and Kim, P. S. (1993) A spring-loaded mechanism for the conformational change of influenza hemagglutinin. Cell **73**, 823–832.

49 Bullough, P. A., Hughson, F. M., Skehel, J. J. and Wiley, D. C. (1994) Structure of Influenza haemagglutinin at the pH of membrane fusion. Nature **371**, 37–43.

50 Zhirnov, O. P. (1990) [The effect of pH on in vitro deproteinization in orthomyxo- and paramyxoviruses]. Mol. Gen. Mikrobiol. Virusol. 11–5.

51 Helenius, A. (1992) Unpacking the incoming influenza virus. Cell **69**, 577–578.

52   Wang, P., Palese, P. and O'Neill, R. E. (1997) The NPI-1/NPI-3 (karyopherin alpha) binding site on the influenza a virus nucleoprotein NP is a nonconventional nuclear localization signal. J. Virol. **71**, 1850–6.

53   Weber, F., Kochs, G., Gruber, S. and Haller, O. (1998) A classical bipartite nuclear localization signal on Thogoto and influenza A virus nucleoproteins. Virology **250**, 9–18.

54   Bullido, R., Gómez-Puertas, P., Albo, C. and Portela, A. (2000) Several protein regions contribute to determine the nuclear and cytoplasmic localization of the influenza A virus nucleoprotein. J. Gen. Virol. **81**, 135–42.

55   Blaas, D., Patzelt, E. and Kuechler, E. (1982) Cap-recognizing protein of influenza virus. Virology **116**, 339–48.

56   Blaas, D., Patzelt, E. and Kuechler, E. (1982) Identification of the cap binding protein of influenza virus. Nucleic Acids Res. **10**, 4803–12.

57   Dias, A., Bouvier, D., Crépin, T., McCarthy, A. a, Hart, D. J., Baudin, F., Cusack, S. and Ruigrok, R. W. H. (2009) The cap-snatching endonuclease of influenza virus polymerase resides in the PA subunit. Nature **458**, 914–8.

58   Braam, J., Ulmanen, I. and Krug, R. M. (1983) Molecular model of a eucaryotic transcription complex: functions and movements of influenza P proteins during capped RNA-primed transcription. Cell **34**, 609–18.

59   Luo, G. X., Luytjes, W., Enami, M. and Palese, P. (1991) The polyadenylation signal of influenza virus RNA involves a stretch of uridines followed by the RNA duplex of the panhandle structure. J. Virol. **65**, 2861–7.

60   Li, X. and Palese, P. (1994) Characterization of the polyadenylation signal of influenza virus RNA. J. Virol. **68**, 1245–9.

61   Veit, M., Kretzschmar, E., Kuroda, K., Garten, W., Schmidt, M. F., Klenk, H. D. and Rott, R. (1991) Site-specific mutagenesis identifies three cysteine residues in the cytoplasmic tail as acylation sites of influenza virus hemagglutinin. J. Virol. **65**, 2491–2500.

62   Sugrue, R. J., Belshe, R. B. and Hay, A. J. (1990) Palmitoylation of the influenza A virus M2 protein. Virology **179**, 51–6.

63   Veit, M., Klenk, H. D., Kendal, A. and Rott, R. (1991) The M2 protein of influenza A virus is acylated. J. Gen. Virol. **72 (Pt 6)**, 1461–5.

64 Perez, J. T., Varble, A., Sachidanandam, R., Zlatev, I., Manoharan, M., García-Sastre, A. and tenOever, B. R. (2010) Influenza A virus-generated small RNAs regulate the switch from transcription to replication. Proc. Natl. Acad. Sci. U. S. A. **107**, 11525–30.

65 Umbach, J., Yen, H., Poon, L. and Cullen, B. (2010) Influenza A virus expresses high levels of an unusual class of small viral leader RNAs in infected cells. MBio **1**.

66 O'Neill, R. E., Talon, J. and Palese, P. (1998) The influenza virus NEP (NS2 protein) mediates the nuclear export of viral ribonucleoproteins. EMBO J. **17**, 288–96.

67 Neumann, G., Hughes, M. T. and Kawaoka, Y. (2000) Influenza A virus NS2 protein mediates vRNP nuclear export through NES-independent interaction with hCRM1. EMBO J. **19**, 6751–8.

68 Bui, M., Wills, E. G., Helenius, A. and Whittaker, G. R. (2000) Role of the influenza virus M1 protein in nuclear export of viral ribonucleoproteins. J. Virol. **74**, 1781–6.

69 Akarsu, H., Burmeister, W. P., Petosa, C., Petit, I., Müller, C. W., Ruigrok, R. W. H. and Baudin, F. (2003) Crystal structure of the M1 protein-binding domain of the influenza A virus nuclear export protein (NEP/NS2). EMBO J. **22**, 4646–55.

70 Jo, S., Kawaguchi, A., Takizawa, N., Morikawa, Y., Momose, F. and Nagata, K. (2010) Involvement of vesicular trafficking system in membrane targeting of the progeny influenza virus genome. Microbes Infect. **12**, 1079–84.

71 Amorim, M. J., Bruce, E. a, Read, E. K. C., Foeglein, A., Mahen, R., Stuart, A. D. and Digard, P. (2011) A Rab11- and microtubule-dependent mechanism for cytoplasmic transport of influenza A virus viral RNA. J. Virol. **85**, 4143–56.

72 Momose, F., Sekimoto, T., Ohkura, T., Jo, S., Kawaguchi, A., Nagata, K. and Morikawa, Y. (2011) Apical transport of influenza A virus ribonucleoprotein requires Rab11-positive recycling endosome. PLoS One **6**, e21123.

73 Avilov, S. V, Moisy, D., Naffakh, N. and Cusack, S. (2012) Influenza A virus progeny vRNP trafficking in live infected cells studied with the virus-encoded fluorescently tagged PB2 protein. Vaccine **30**, 7411–7.

74   Scheiffele, P., Roth, M. G. and Simons, K. (1997) Interaction of influenza virus haemagglutinin with sphingolipid-cholesterol membrane domains via its transmembrane domain. EMBO J. **16**, 5501–8.

75   Scheiffele, P., Rietveld, a, Wilk, T. and Simons, K. (1999) Influenza viruses select ordered lipid domains during budding from the plasma membrane. J. Biol. Chem. **274**, 2038–44.

76   Barman, S. and Nayak, D. P. (2000) Analysis of the transmembrane domain of influenza virus neuraminidase, a type II transmembrane glycoprotein, for apical sorting and raft association. J. Virol. **74**, 6538–45.

77   Barman, S., Adhikary, L., Chakrabarti, A. K., Bernas, C., Kawaoka, Y. and Nayak, D. P. (2004) Role of transmembrane domain and cytoplasmic tail amino acid sequences of influenza a virus neuraminidase in raft association and virus budding. J. Virol. **78**, 5258–69.

78   Gómez-Puertas, P., Mena, I., Castillo, M., Vivo, A., Pérez-Pastrana, E. and Portela, A. (1999) Efficient formation of influenza virus-like particles: dependence on the expression levels of viral proteins. J. Gen. Virol. **80 (Pt 7)**, 1635–45.

79   Gómez-Puertas, P., Albo, C., Pérez-Pastrana, E., Vivo, A. and Portela, A. (2000) Influenza virus matrix protein is the major driving force in virus budding. J. Virol. **74**, 11538–47.

80   Barman, S., Ali, A., Hui, E. K.-W., Adhikary, L. and Nayak, D. P. (2001) Transport of viral proteins to the apical membranes and interaction of matrix protein with glycoproteins in the assembly of influenza viruses. Virus Res. **77**, 61–69.

81   Fujii, Y., Goto, H., Watanabe, T., Yoshida, T. and Kawaoka, Y. (2003) Selective incorporation of influenza virus RNA segments into virions. Proc. Natl. Acad. Sci. U. S. A. **100**, 2002–7.

82   Inagaki, A., Goto, H., Kakugawa, S., Ozawa, M. and Kawaoka, Y. (2012) Competitive incorporation of homologous gene segments of influenza A virus into virions. J. Virol. **86**, 10200–2.

83   Goto, H., Muramoto, Y., Noda, T. and Kawaoka, Y. (2013) The genome-packaging signal of the influenza A virus genome comprises a genome incorporation signal and a genome-bundling signal. J. Virol. **87**, 11316–22.

84   Schroeder, C., Heider, H., Möncke-Buchner, E. and Lin, T.-I. (2005) The influenza virus ion channel and maturation cofactor M2 is a cholesterol-binding protein. Eur. Biophys. J. **34**, 52–66.

85   Rossman, J. S., Jing, X., Leser, G. P. and Lamb, R. a. (2010) Influenza virus M2 protein mediates ESCRT-independent membrane scission. Cell, Elsevier Ltd **142**, 902–13.

86   Matrosovich, M. N., Matrosovich, T. Y., Gray, T., Roberts, N. A. and Klenk, H.-D. (2004) Neuraminidase is important for the initiation of influenza virus infection in human airway epithelium. J. Virol. **78**, 12665–7.

87   Klenk, H. D., Rott, R., Orlich, M. and Blödorn, J. (1975) Activation of influenza A viruses by trypsin treatment. Virology **68**, 426–39.

88   Kido, H., Yokogoshi, Y., Sakai, K., Tashiro, M., Kishino, Y., Fukutomi, A. and Katunuma, N. (1992) Isolation and characterization of a novel trypsin-like protease found in rat bronchiolar epithelial Clara cells. A possible activator of the viral fusion glycoprotein. J. Biol. Chem. **267**, 13573–9.

89   Gotoh, B., Ogasawara, T., Toyoda, T., Inocencio, N. M., Hamaguchi, M. and Nagai, Y. (1990) An endoprotease homologous to the blood clotting factor X as a determinant of viral tropism in chick embryo. EMBO J. **9**, 4189–95.

90   Gotoh, B., Yamauchi, F., Ogasawara, T. and Nagai, Y. (1992) Isolation of factor Xa from chick embryo as the amniotic endoprotease responsible for paramyxovirus activation. FEBS Lett. **296**, 274–8.

91   Böttcher, E., Matrosovich, T., Beyerle, M., Klenk, H.-D., Garten, W. and Matrosovich, M. (2006) Proteolytic activation of influenza viruses by serine proteases TMPRSS2 and HAT from human airway epithelium. J. Virol. **80**, 9896–8.

92   Horimoto, T., Nakayama, K., Smeekens, S. P. and Kawaoka, Y. (1994) Proprotein-processing endoproteases PC6 and furin both activate hemagglutinin of virulent avian influenza viruses. J. Virol. **68**, 6074–8.

93   Xiang, Y., Molloy, S. S., Thomas, L. and Thomas, G. (2000) The PC6B cytoplasmic domain contains two acidic clusters that direct sorting to distinct trans-Golgi network/endosomal compartments. Mol. Biol. Cell **11**, 1257–73.

94   Wang, Q., Tian, X., Chen, X. and Ma, J. (2007) Structural basis for receptor specificity of influenza B virus hemagglutinin. Proc. Natl. Acad. Sci. U. S. A. **104**, 16874–9.

95   Herfst, S., Schrauwen, E. J. a, Linster, M., Chutinimitkul, S., de Wit, E., Munster, V. J., Sorrell, E. M., Bestebroer, T. M., Burke, D. F., Smith, D. J., et al. (2012) Airborne transmission of influenza A/H5N1 virus between ferrets. Science **336**, 1534–41.

96   Webster, R. G., Wright, S. M., Castrucci, M. R., Bean, W. J. and Kawaoka, Y. (1993) Influenza--a model of an emerging virus disease. Intervirology **35**, 16–25.

97   Chang, D.-K., Cheng, S.-F., Kantchev, E. A. B., Lin, C.-H. and Liu, Y.-T. (2008) Membrane interaction and structure of the transmembrane domain of influenza hemagglutinin and its fusion peptide complex. BMC Biol. **6**, 2.

98   Kornfeld, R. and Kornfeld, S. (1985) Assembly of asparagine-linked oligosaccharides. Annu. Rev. Biochem. **54**, 631–664.

99   Roberts, P. C., Garten, W. and Klenk, H. D. (1993) Role of conserved glycosylation sites in maturation and transport of influenza A virus hemagglutinin. J. Virol. **67**, 3048–60.

100   Keil, W., Geyer, R., Dabrowski, J., Dabrowski, U., Niemann, H., Stirm, S. and Klenk, H. D. (1985) Carbohydrates of influenza virus. Structural elucidation of the individual glycans of the FPV hemagglutinin by two-dimensional 1H n.m.r. and methylation analysis. EMBO J. **4**, 2711–20.

101   Wagner, R., Heuer, D., Wolff, T., Herwig, A. and Klenk, H.-D. (2002) N-Glycans attached to the stem domain of haemagglutinin efficiently regulate influenza A virus replication. J. Gen. Virol. **83**, 601–9.

102   Copeland, C. S., Doms, R. W., Bolzau, E. M., Webster, R. G. and Helenius, A. (1986) Assembly of influenza hemagglutinin trimers and its role in intracellular transport. J. Cell Biol. **103**, 1179–1191.

103   Brett, K., Kordyukova, L. V, Serebryakova, M. V, Mintaev, R. R., Alexeevski, A. V and Veit, M. (2014) Site-specific S-acylation of influenza virus hemagglutinin: the location of the acylation site relative to the membrane border is the decisive factor for attachment of stearate. J. Biol. Chem. **289**, 34978–89.

104   Kordyukova, L. V, Serebryakova, M. V, Baratova, L. a and Veit, M. (2008) S acylation of the hemagglutinin of influenza viruses: mass spectrometry reveals site-specific attachment of stearic acid to a transmembrane cysteine. J. Virol. **82**, 9288–92.

105   Veit, M. and Schmidt, M. F. G. (1993) Timing of palmitoylation of influenza virus hemagglutinin. FEBS Lett. **336**, 243–247.

106   Vey, M., Schäfer, W., Berghöfer, S., Klenk, H. D. and Garten, W. (1994) Maturation of the trans-Golgi network protease furin: compartmentalization of propeptide removal, substrate cleavage, and COOH-terminal truncation. J. Cell Biol. **127**, 1829–42.

107   Schäfer, W., Stroh, A., Berghöfer, S., Seiler, J., Vey, M., Kruse, M. L., Kern, H. F., Klenk, H. D. and Garten, W. (1995) Two independent targeting signals in the cytoplasmic domain determine trans-Golgi network localization and endosomal trafficking of the proprotein convertase furin. EMBO J. **14**, 2424–35.

108   Walker, J. A., Sakaguchi, T., Matsuda, Y., Yoshida, T. and Kawaoka, Y. (1992) Location and character of the cellular enzyme that cleaves the hemagglutinin of a virulent avian influenza virus. Virology **190**, 278–287.

109   Molloy, S. S., Thomas, L., VanSlyke, J. K., Stenberg, P. E. and Thomas, G. (1994) Intracellular trafficking and activation of the furin proprotein convertase: localization to the TGN and recycling from the cell surface. EMBO J. **13**, 18–33.

110   Chen, B. J., Leser, G. P., Morita, E. and Lamb, R. a. (2007) Influenza virus hemagglutinin and neuraminidase, but not the matrix protein, are required for assembly and budding of plasmid-derived virus-like particles. J. Virol. **81**, 7111–23.

111   Kretzschmar, E., Bui, M. and Rose, J. K. (1996) Membrane association of influenza virus matrix protein does not require specific hydrophobic domains or the viral glycoproteins. Virology **220**, 37–45.

112   Zhang, J. and Lamb, R. A. (1996) Characterization of the membrane association of the influenza virus matrix protein in living cells. Virology **225**, 255–66.

113   Thaa, B., Herrmann, A. and Veit, M. (2009) The polybasic region is not essential for membrane binding of the matrix protein M1 of influenza virus. Virology **383**, 150–5.

114 Enami, M. and Enami, K. (1996) Influenza virus hemagglutinin and neuraminidase glycoproteins stimulate the membrane association of the matrix protein. J. Virol. **70**, 6653–7.

115 Ali, A., Avalos, R. T., Ponimaskin, E. and Nayak, D. P. (2000) Influenza virus assembly: effect of influenza virus glycoproteins on the membrane association of M1 protein. J. Virol. **74**, 8709–19.

116 McCown, M. F. and Pekosz, A. (2006) Distinct domains of the influenza a virus M2 protein cytoplasmic tail mediate binding to the M1 protein and facilitate infectious virus production. J. Virol. **80**, 8178–89.

117 Chen, B. J., Leser, G. P., Jackson, D. and Lamb, R. a. (2008) The influenza virus M2 protein cytoplasmic tail interacts with the M1 protein and influences virus assembly at the site of virus budding. J. Virol. **82**, 10059–70.

118 Thaa, B., Herrmann, A. and Veit, M. (2010) Intrinsic cytoskeleton-dependent clustering of influenza virus M2 protein with hemagglutinin assessed by FLIM-FRET. J. Virol. **84**, 12445–9.

119 Rossman, J. S., Jing, X., Leser, G. P., Balannik, V., Pinto, L. H. and Lamb, R. a. (2010) Influenza virus m2 ion channel protein is necessary for filamentous virion formation. J. Virol. **84**, 5078–88.

120 Singer, S. J. and Nicolson, G. L. (1972) The fluid mosaic model of the structure of cell membranes. Science **175**, 720–31.

121 Yee, A. G., Fischbach, G. D. and Karnovsky, M. J. (1978) Clusters of intramembranous particles on cultured myotubes at sites that are highly sensitive to acetylcholine. Proc. Natl. Acad. Sci. U. S. A. **75**, 3004–8.

122 Bell, R. M., Ballas, L. M. and Coleman, R. A. (1981) Lipid topogenesis. J. Lipid Res. **22**, 391–403.

123 Reinhart, M. P., Billheimer, J. T., Faust, J. R. and Gaylor, J. L. (1987) Subcellular localization of the enzymes of cholesterol biosynthesis and metabolism in rat liver. J. Biol. Chem. **262**, 9649–55.

124 Van Meer, G., Voelker, D. R. and Feigenson, G. W. (2008) Membrane lipids: where they are and how they behave. Nat. Rev. Mol. Cell Biol. **9**, 112–24.

125   Liscum, L., Vance, D. E. and Vance, J. E. (2008) Cholesterol biosynthesis. In Biochemistry of Lipids, Lipoproteins and Membranes (Fifth Edition) Fith Editi., pp 399–421, Elsevier.

126   Lange, Y. (1991) Disposition of intracellular cholesterol in human fibroblasts. J. Lipid Res. **32**, 329–39.

127   Kaplan, M. R. and Simoni, R. D. (1985) Transport of cholesterol from the endoplasmic reticulum to the plasma membrane. J. Cell Biol. **101**, 446–53.

128   Van Meer, G. (1989) Lipid traffic in animal cells. Annu. Rev. Cell Biol., Annual Reviews 4139 El Camino Way, P.O. Box 10139, Palo Alto, CA 94303-0139, USA **5**, 247–275.

129   Lev, S. (2012) Nonvesicular lipid transfer from the endoplasmic reticulum. Cold Spring Harb. Perspect. Biol. **4**, a013300–.

130   Futerman, A. H., Stieger, B., Hubbard, A. L. and Pagano, R. E. (1990) Sphingomyelin synthesis in rat liver occurs predominantly at the cis and medial cisternae of the Golgi apparatus. J. Biol. Chem. **265**, 8650–7.

131   Jeckel, D., Karrenbauer, A., Birk, R., Schmidt, R. R. and Wieland, F. (1990) Sphingomyelin is synthesized in the cis Golgi. FEBS Lett. **261**, 155–7.

132   Futerman, A. H. and Riezman, H. (2005) The ins and outs of sphingolipid synthesis. Trends Cell Biol. **15**, 312–8.

133   Mariño, G. and Kroemer, G. (2013) Mechanisms of apoptotic phosphatidylserine exposure. Cell Res., Shanghai Institutes for Biological Sciences, Chinese Academy of Sciences **23**, 1247–8.

134   Pomorski, T. and Menon, A. K. (2006) Lipid flippases and their biological functions. Cell. Mol. Life Sci. **63**, 2908–21.

135   Devaux, P. F. and Morris, R. (2004) Transmembrane asymmetry and lateral domains in biological membranes. Traffic **5**, 241–6.

136   Daleke, D. L. (2007) Phospholipid flippases. J. Biol. Chem. **282**, 821–5.

137   Burger, K. N., van der Bijl, P. and van Meer, G. (1996) Topology of sphingolipid galactosyltransferases in ER and Golgi: transbilayer movement of monohexosyl sphingolipids is required for higher glycosphingolipid biosynthesis. J. Cell Biol. **133**, 15–28.

138   Pomorski, T., Hrafnsdóttir, S., Devaux, P. F. and van Meer, G. (2001) Lipid distribution and transport across cellular membranes. Semin. Cell Dev. Biol. **12**, 139–48.

139   Van Meer, G. (2011) Dynamic transbilayer lipid asymmetry. Cold Spring Harb. Perspect. Biol. **3**.

140   Simons, K. and van Meer, G. (1988) Lipid sorting in epithelial cells. Biochemistry **27**, 6197–202.

141   Simons, K. and Ikonen, E. (1997) Functional rafts in cell membranes. Nature, Macmillan Magazines Ltd. **387**, 569–72.

142   Eeman, M. and Deleu, M. (2010, December 3) From biological membranes to biomimetic model membranes. Base.

143   Pike, L. J. (2006) Rafts defined: a report on the Keystone Symposium on Lipid Rafts and Cell Function. J. Lipid Res. **47**, 1597–8.

144   Simons, K. and Toomre, D. (2000) Lipid rafts and signal transduction. Nat. Rev. Mol. Cell Biol. **1**, 31–9.

145   Surma, M. A., Klose, C. and Simons, K. (2012) Lipid-dependent protein sorting at the trans-Golgi network. Biochim. Biophys. Acta **1821**, 1059–67.

146   Simons, K. and Sampaio, J. L. (2011) Membrane organization and lipid rafts. Cold Spring Harb. Perspect. Biol. **3**, a004697.

147   Vetrivel, K. S., Cheng, H., Lin, W., Sakurai, T., Li, T., Nukina, N., Wong, P. C., Xu, H. and Thinakaran, G. (2004) Association of gamma-secretase with lipid rafts in post-Golgi and endosome membranes. J. Biol. Chem. **279**, 44945–54.

148   Brügger, B., Sandhoff, R., Wegehingel, S., Gorgas, K., Malsam, J., Helms, J. B., Lehmann, W. D., Nickel, W. and Wieland, F. T. (2000) Evidence for segregation of sphingomyelin and cholesterol during formation of COPI-coated vesicles. J. Cell Biol. **151**, 507–18.

149   Glick, B. S. and Luini, A. (2011) Models for Golgi traffic: a critical assessment. Cold Spring Harb. Perspect. Biol. **3**, a005215.

150   Klemm, R. W., Ejsing, C. S., Surma, M. a, Kaiser, H.-J., Gerl, M. J., Sampaio, J. L., de Robillard, Q., Ferguson, C., Proszynski, T. J., Shevchenko, A., et al. (2009)

Segregation of sphingolipids and sterols during formation of secretory vesicles at the trans-Golgi network. J. Cell Biol. **185**, 601–12.

151 Patterson, G. H., Hirschberg, K., Polishchuk, R. S., Gerlich, D., Phair, R. D. and Lippincott-Schwartz, J. (2008) Transport through the Golgi apparatus by rapid partitioning within a two-phase membrane system. Cell **133**, 1055–67.

152 Brown, D. A. and Rose, J. K. (1992) Sorting of GPI-anchored proteins to glycolipid-enriched membrane subdomains during transport to the apical cell surface. Cell **68**, 533–544.

153 Varma, R. and Mayor, S. (1998) GPI-anchored proteins are organized in submicron domains at the cell surface. Nature **394**, 798–801.

154 Wang, J., Gunning, W., Kelley, K. M. M. and Ratnam, M. (2002) Evidence for segregation of heterologous GPI-anchored proteins into separate lipid rafts within the plasma membrane. J. Membr. Biol. **189**, 35–43.

155 Resh, M. D. (1999) Fatty acylation of proteins: new insights into membrane targeting of myristoylated and palmitoylated proteins. Biochim. Biophys. Acta **1451**, 1–16.

156 Roy, S., Luetterforst, R., Harding, a, Apolloni, a, Etheridge, M., Stang, E., Rolls, B., Hancock, J. F. and Parton, R. G. (1999) Dominant-negative caveolin inhibits H-Ras function by disrupting cholesterol-rich plasma membrane domains. Nat. Cell Biol. **1**, 98–105.

157 Parton, R. G. and Hancock, J. F. (2004) Lipid rafts and plasma membrane microorganization: insights from Ras. Trends Cell Biol. **14**, 141–7.

158 Benslimane, N., Hassan, G. S., Yacoub, D. and Mourad, W. (2012) Requirement of transmembrane domain for CD154 association to lipid rafts and subsequent biological events. PLoS One **7**, e43070.

159 Fernández-Muñoz, B., Yurrita, M. M., Martín-Villar, E., Carrasco-Ramírez, P., Megías, D., Renart, J. and Quintanilla, M. (2011) The transmembrane domain of podoplanin is required for its association with lipid rafts and the induction of epithelial-mesenchymal transition. Int. J. Biochem. Cell Biol. **43**, 886–896.

160 Russ, W. P. and Engelman, D. M. (2000) The GxxxG motif: a framework for transmembrane helix-helix association. J. Mol. Biol. **296**, 911–9.

161 Barrett, P. J., Song, Y., Van Horn, W. D., Hustedt, E. J., Schafer, J. M., Hadziselimovic, A., Beel, A. J. and Sanders, C. R. (2012) The amyloid precursor protein has a flexible transmembrane domain and binds cholesterol. Science **336**, 1168–71.

162 Rossin, A., Kral, R., Lounnas, N., Chakrabandhu, K., Mailfert, S., Marguet, D. and Hueber, A.-O. (2010) Identification of a lysine-rich region of Fas as a raft nanodomain targeting signal necessary for Fas-mediated cell death. Exp. Cell Res. **316**, 1513–22.

163 Contreras, F.-X., Ernst, A. M., Haberkant, P., Björkholm, P., Lindahl, E., Gönen, B., Tischer, C., Elofsson, A., von Heijne, G., Thiele, C., et al. (2012) Molecular recognition of a single sphingolipid species by a protein's transmembrane domain. Nature **481**, 525–9.

164 Björkholm, P., Ernst, A. M., Hacke, M., Wieland, F., Brügger, B. and von Heijne, G. (2014) Identification of novel sphingolipid-binding motifs in mammalian membrane proteins. Biochim. Biophys. Acta, Elsevier B.V. **1838**, 2066–70.

165 Strandberg, E. and Killian, J. A. (2003) Snorkeling of lysine side chains in transmembrane helices: how easy can it get? FEBS Lett. **544**, 69–73.

166 Li, H. and Papadopoulos, V. (1998) Peripheral-type benzodiazepine receptor function in cholesterol transport. Identification of a putative cholesterol recognition/interaction amino acid sequence and consensus pattern. Endocrinology, Endocrine Society **139**, 4991–7.

167 Chini, B. (2004) G-protein coupled receptors in lipid rafts and caveolae: how, when and why do they go there? J. Mol. Endocrinol. **32**, 325–338.

168 Sengupta, D. and Chattopadhyay, A. (2012) Identification of cholesterol binding sites in the serotonin1A receptor. J. Phys. Chem. B, American Chemical Society **116**, 12991–6.

169 Vincent, N. (2002) Identification of a conserved domain of the HIV-1 transmembrane protein gp41 which interacts with cholesteryl groups. Biochim. Biophys. Acta - Biomembr. **1567**, 157–164.

170 Schroeder, C. (2010) Cholesterol Binding and Cholesterol Transport Proteins: (Harris, J. R., ed.), Springer Netherlands, Dordrecht.

171 Baier, C. J., Fantini, J. and Barrantes, F. J. (2011) Disclosure of cholesterol recognition motifs in transmembrane domains of the human nicotinic acetylcholine receptor. Sci. Rep. **1**, 69.

172 Hanson, M. A., Cherezov, V., Griffith, M. T., Roth, C. B., Jaakola, V.-P., Chien, E. Y. T., Velasquez, J., Kuhn, P. and Stevens, R. C. (2008) A specific cholesterol binding site is established by the 2.8 A structure of the human beta2-adrenergic receptor. Structure **16**, 897–905.

173 Song, Y., Kenworthy, A. K. and Sanders, C. R. (2014) Cholesterol as a co-solvent and a ligand for membrane proteins. Protein Sci. **23**, 1–22.

174 Barrett, P. J., Song, Y., Van Horn, W. D., Hustedt, E. J., Schafer, J. M., Hadziselimovic, A., Beel, A. J. and Sanders, C. R. (2012) The amyloid precursor protein has a flexible transmembrane domain and binds cholesterol. Science **336**, 1168–71.

175 Panchal, R. G., Ruthel, G., Kenny, T. a, Kallstrom, G. H., Lane, D., Badie, S. S., Li, L., Bavari, S. and Aman, M. J. (2003) In vivo oligomerization and raft localization of Ebola virus protein VP40 during vesicular budding. Proc. Natl. Acad. Sci. U. S. A. **100Panchal**, 15936–15941.

176 Bavari, S., Bosio, C. M., Wiegand, E., Ruthel, G., Will, A. B., Geisbert, T. W., Hevey, M., Schmaljohn, C., Schmaljohn, A. and Aman, M. J. (2002) Lipid raft microdomains: a gateway for compartmentalized trafficking of Ebola and Marburg viruses. J. Exp. Med. **195**, 593–602.

177 Schlie, K., Maisa, A., Lennartz, F., Ströher, U., Garten, W. and Strecker, T. (2010) Characterization of Lassa virus glycoprotein oligomerization and influence of cholesterol on virus replication. J. Virol. **84**, 983–92.

178 Cordo, S. M., Valko, A., Martinez, G. M. and Candurra, N. a. (2013) Membrane localization of Junín virus glycoproteins requires cholesterol and cholesterol rich membranes. Biochem. Biophys. Res. Commun. **430**, 912–917.

179 Clemente, R., de Parseval, A., Perez, M. and de la Torre, J. C. (2009) Borna disease virus requires cholesterol in both cellular membrane and viral envelope for efficient cell entry. J. Virol. **83**, 2655–2662.

180 Vincent, S., Gerlier, D. and Manié, S. N. (2000) Measles virus assembly within membrane rafts. J. Virol. **74**, 9911–5.

181   Manié, S. N., de Breyne, S., Vincent, S. and Gerlier, D. (2000) Measles virus structural components are enriched into lipid raft microdomains: a potential cellular location for virus assembly. J. Virol. **74**, 305–311.

182   Henderson, G., Murray, J. and Yeo, R. P. (2002) Sorting of the respiratory syncytial virus matrix protein into detergent-resistant structures is dependent on cell-surface expression of the glycoproteins. Virology **300**, 244–54.

183   Marty, a, Meanger, J., Mills, J., Shields, B. and Ghildyal, R. (2004) Association of matrix protein of respiratory syncytial virus with the host cell membrane of infected cells. Arch. Virol. **149**, 199–210.

184   Chang, T.-H., Segovia, J., Sabbah, A., Mgbemena, V. and Bose, S. (2012) Cholesterol-rich lipid rafts are required for release of infectious human respiratory syncytial virus particles. Virology **422**, 205–13.

185   Ali, A. and Nayak, D. P. (2000) Assembly of Sendai virus: M protein interacts with F and HN proteins and with the cytoplasmic tail and transmembrane domain of F protein. Virology **276**, 289–303.

186   Laliberte, J. P., McGinnes, L. W., Peeples, M. E. and Morrison, T. G. (2006) Integrity of membrane lipid rafts is necessary for the ordered assembly and release of infectious Newcastle disease virus particles. J. Virol. **80**, 10652–10662.

187   Laliberte, J. P., McGinnes, L. W. and Morrison, T. G. (2007) Incorporation of functional HN-F glycoprotein-containing complexes into newcastle disease virus is dependent on cholesterol and membrane lipid raft integrity. J. Virol. **81**, 10636–48.

188   Barnard, D. L. (2004) Inhibitors of measles virus. Antivir. Chem. Chemother. **15**, 111–9.

189   Robinzon, S., Dafa-Berger, A., Dyer, M. D., Paeper, B., Proll, S. C., Teal, T. H., Rom, S., Fishman, D., Rager-Zisman, B. and Katze, M. G. (2009) Impaired cholesterol biosynthesis in a neuronal cell line persistently infected with measles virus. J. Virol. **83**, 5495–504.

190   Gosselin-Grenet, A.-S., Mottet-Osman, G. and Roux, L. (2006) From assembly to virus particle budding: pertinence of the detergent resistant membranes. Virology **344**, 296–303.

191 Martín, J. J., Holguera, J., Sánchez-Felipe, L., Villar, E. and Muñoz-Barroso, I. (2012) Cholesterol dependence of Newcastle Disease Virus entry. Biochim. Biophys. Acta **1818**, 753–61.

192 Shi, S. T., Lee, K.-J., Aizaki, H., Hwang, S. B. and Lai, M. M. C. (2003) Hepatitis C virus RNA replication occurs on a detergent-resistant membrane that cofractionates with caveolin-2. J. Virol. **77**, 4160–8.

193 Aizaki, H., Morikawa, K., Fukasawa, M., Hara, H., Inoue, Y., Tani, H., Saito, K., Nishijima, M., Hanada, K., Matsuura, Y., et al. (2008) Critical role of virion-associated cholesterol and sphingolipid in hepatitis C virus infection. J. Virol. **82**, 5715–24.

194 Hirata, Y., Ikeda, K., Sudoh, M., Tokunaga, Y., Suzuki, A., Weng, L., Ohta, M., Tobita, Y., Okano, K., Ozeki, K., et al. (2012) Self-enhancement of hepatitis C virus replication by promotion of specific sphingolipid biosynthesis. PLoS Pathog. **8**, e1002860.

195 Xie, N., Huang, K., Zhang, T., Lei, Y., Liu, R., Wang, K., Zhou, S., Li, J., Wu, J., Wu, H., et al. (2012) Comprehensive proteomic analysis of host cell lipid rafts modified by HBV infection. J. Proteomics **75**, 725–739.

196 Kawabata, A., Tang, H., Huang, H., Yamanishi, K. and Mori, Y. (2009) Human herpesvirus 6 envelope components enriched in lipid rafts: evidence for virion-associated lipid rafts. Virol. J. **6**, 127.

197 Carro, A. C. and Damonte, E. B. (2013) Requirement of cholesterol in the viral envelope for dengue virus infection. Virus Res. **174**, 78–87.

198 Pratelli, A. and Colao, V. (2015) Role of the lipid rafts in the life cycle of canine coronavirus. J. Gen. Virol. **96**, 331–7.

199 Cui, J., Fu, X., Xie, J., Gao, M., Hong, M., Chen, Y., Su, S. and Li, S. (2014) Critical role of cellular cholesterol in bovine rotavirus infection. Virol. J. **11**, 98.

200 Aloia, R. C., Jensen, F. C., Curtain, C. C., Mobley, P. W. and Gordon, L. M. (1988) Lipid composition and fluidity of the human immunodeficiency virus. Proc. Natl. Acad. Sci. U. S. A. **85**, 900–4.

201 Nguyen, D. H. and Hildreth, J. E. K. (2000) Evidence for Budding of Human Immunodeficiency Virus Type 1 Selectively from Glycolipid-Enriched Membrane Lipid Rafts Evidence for Budding of Human Immunodeficiency Virus Type 1 Selectively from Glycolipid-Enriched Membrane Lipid Rafts.

202   Ono, a and Freed, E. O. (2001) Plasma membrane rafts play a critical role in HIV-1 assembly and release. Proc. Natl. Acad. Sci. U. S. A. **98**, 13925–13930.

203   Hogue, I. B., Grover, J. R., Soheilian, F., Nagashima, K. and Ono, A. (2011) Gag induces the coalescence of clustered lipid rafts and tetraspanin-enriched microdomains at HIV-1 assembly sites on the plasma membrane. J. Virol. **85**, 9749–66.

204   Alfadhli, A. and Barklis, E. (2014) The roles of lipids and nucleic acids in HIV-1 assembly. Front. Microbiol. **5**, 253.

205   Brügger, B., Glass, B., Haberkant, P., Leibrecht, I., Wieland, F. T. and Kräusslich, H.-G. (2006) The HIV lipidome: a raft with an unusual composition. Proc. Natl. Acad. Sci. U. S. A. **103**, 2641–6.

206   Van 't Wout, A. B., Lehrman, G. K., Mikheeva, S. A., O'Keeffe, G. C., Katze, M. G., Bumgarner, R. E., Geiss, G. K. and Mullins, J. I. (2003) Cellular gene expression upon human immunodeficiency virus type 1 infection of CD4(+)-T-cell lines. J. Virol. **77**, 1392–402.

207   Van 't Wout, A. B., Swain, J. V., Schindler, M., Rao, U., Pathmajeyan, M. S., Mullins, J. I. and Kirchhoff, F. (2005) Nef induces multiple genes involved in cholesterol synthesis and uptake in human immunodeficiency virus type 1-infected T cells. J. Virol. **79**, 10053–8.

208   Brügger, B., Krautkrämer, E., Tibroni, N., Munte, C. E., Rauch, S., Leibrecht, I., Glass, B., Breuer, S., Geyer, M., Kräusslich, H.-G., et al. (2007) Human immunodeficiency virus type 1 Nef protein modulates the lipid composition of virions and host cell membrane microdomains. Retrovirology **4**, 70.

209   Alfsen, A., Iniguez, P., Bouguyon, E. and Bomsel, M. (2001) Secretory IgA Specific for a Conserved Epitope on gp41 Envelope Glycoprotein Inhibits Epithelial Transcytosis of HIV-1. J. Immunol., American Association of Immunologists **166**, 6257–6265.

210   Van Wilgenburg, B., Moore, M. D., James, W. S. and Cowley, S. A. (2014) The productive entry pathway of HIV-1 in macrophages is dependent on endocytosis through lipid rafts containing CD4. PLoS One **9**, e86071.

211   Liao, Z., Graham, D. R. and Hildreth, J. E. K. (2003) Lipid rafts and HIV pathogenesis: virion-associated cholesterol is required for fusion and infection of susceptible cells. AIDS Res. Hum. Retroviruses **19**, 675–687.

212 Salzwedel, K., West, J. T. and Hunter, E. (1999) A conserved tryptophan-rich motif in the membrane-proximal region of the human immunodeficiency virus type 1 gp41 ectodomain is important for Env-mediated fusion and virus infectivity. J. Virol. **73**, 2469–80.

213 Vishwanathan, S. A., Thomas, A., Brasseur, R., Epand, R. F., Hunter, E. and Epand, R. M. (2008) Large changes in the CRAC segment of gp41 of HIV do not destroy fusion activity if the segment interacts with cholesterol. Biochemistry **47**, 11869–76.

214 Hess, S. T., Kumar, M., Verma, A., Farrington, J., Kenworthy, A. and Zimmerberg, J. (2005) Quantitative electron microscopy and fluorescence spectroscopy of the membrane distribution of influenza hemagglutinin. J. Cell Biol. **169**, 965–76.

215 Leser, G. P. and Lamb, R. a. (2005) Influenza virus assembly and budding in raft-derived microdomains: a quantitative analysis of the surface distribution of HA, NA and M2 proteins. Virology **342**, 215–27.

216 Hess, S. T., Gould, T. J., Gudheti, M. V, Maas, S. a, Mills, K. D. and Zimmerberg, J. (2007) Dynamic clustered distribution of hemagglutinin resolved at 40 nm in living cell membranes discriminates between raft theories. Proc. Natl. Acad. Sci. U. S. A. **104**, 17370–5.

217 Gudheti, M. V, Curthoys, N. M., Gould, T. J., Kim, D., Gunewardene, M. S., Gabor, K. A., Gosse, J. A., Kim, C. H., Zimmerberg, J. and Hess, S. T. (2013) Actin mediates the nanoscale membrane organization of the clustered membrane protein influenza hemagglutinin. Biophys. J. **104**, 2182–92.

218 Gerl, M. J., Sampaio, J. L., Urban, S., Kalvodova, L., Verbavatz, J.-M., Binnington, B., Lindemann, D., Lingwood, C. a, Shevchenko, A., Schroeder, C., et al. (2012) Quantitative analysis of the lipidomes of the influenza virus envelope and MDCK cell apical membrane. J. Cell Biol. **196**, 213–21.

219 Wagner, R., Herwig, A., Azzouz, N. and Klenk, H. D. (2005) Acylation-mediated membrane anchoring of avian influenza virus hemagglutinin is essential for fusion pore formation and virus infectivity. J. Virol. **79**, 6449–58.

220 Takeda, M., Leser, G. P., Russell, C. J. and Lamb, R. a. (2003) Influenza virus hemagglutinin concentrates in lipid raft microdomains for efficient viral fusion. Proc. Natl. Acad. Sci. U. S. A. **100**, 14610–7.

221 Lichtenberg, D., Goñi, F. M. and Heerklotz, H. (2005) Detergent-resistant membranes should not be identified with membrane rafts. Trends Biochem. Sci. **30**, 430–6.

222 Engel, S., Scolari, S., Thaa, B., Krebs, N., Korte, T., Herrmann, A. and Veit, M. (2010) FLIM-FRET and FRAP reveal association of influenza virus haemagglutinin with membrane rafts. Biochem. J. **425**, 567–73.

223 Scolari, S., Engel, S., Krebs, N., Plazzo, A. P., De Almeida, R. F. M., Prieto, M., Veit, M. and Herrmann, A. (2009) Lateral distribution of the transmembrane domain of influenza virus hemagglutinin revealed by time-resolved fluorescence imaging. J. Biol. Chem. **284**, 15708–16.

224 Gimpl, G. (2010) Cholesterol-protein interaction: methods and cholesterol reporter molecules. Subcell. Biochem. **51**, 1–45.

225 Zidovetzki, R. and Levitan, I. (2007) Use of cyclodextrins to manipulate plasma membrane chlolesterol content: evidence, misconceptions and control strategies. Biochim. Biophys. Acta - Biomembr. **1768**, 1311–1324.

226 Chamberlain, L. H. (2004) Detergents as tools for the purification and classification of lipid rafts. FEBS Lett. **559**, 1–5.

227 Liu, R., Lu, P., Chu, J. W. K. and Sharom, F. J. (2009) Characterization of fluorescent sterol binding to purified human NPC1. J. Biol. Chem. **284**, 1840–52.

228 Thaa, B., Levental, I., Herrmann, A. and Veit, M. (2011) Intrinsic membrane association of the cytoplasmic tail of influenza virus M2 protein and lateral membrane sorting regulated by cholesterol binding and palmitoylation. Biochem. J. **437**, 389–97.

229 Umashankar, M., Sánchez-San Martín, C., Liao, M., Reilly, B., Guo, A., Taylor, G. and Kielian, M. (2008) Differential cholesterol binding by class II fusion proteins determines membrane fusion properties. J. Virol. **82**, 9245–53.

230 Newby, Z. E. R., O'Connell, J. D., Gruswitz, F., Hays, F. A., Harries, W. E. C., Harwood, I. M., Ho, J. D., Lee, J. K., Savage, D. F., Miercke, L. J. W., et al. (2009) A general protocol for the crystallization of membrane proteins for X-ray structural investigation. Nat. Protoc. **4**, 619–637.

231 Caffrey, M. and Cherezov, V. (2009) Crystallizing membrane proteins using lipidic mesophases. Nat. Protoc. **4**, 706–31.

232 Cherezov, V. (2011) Lipidic cubic phase technologies for membrane protein structural studies. Curr. Opin. Struct. Biol. **21**, 559–66.

233 Wang, S., Munro, R. A., Shi, L., Kawamura, I., Okitsu, T., Wada, A., Kim, S.-Y., Jung, K.-H., Brown, L. S. and Ladizhansky, V. (2013) Solid-state NMR spectroscopy structure determination of a lipid-embedded heptahelical membrane protein. Nat. Methods, Nature Publishing Group, a division of Macmillan Publishers Limited. All Rights Reserved. **10**, 1007–12.

234 Forster, T. (1946) Energiewanderung und Fluoreszenz. Naturwissenschaften **33**, 166–175.

235 Lakowicz, J. R. (2006) Principles of Fluorescence Spectroscopy Third edit., Springer, Berlin.

236 Ward, M. E., Wu, J. Y. and Rao, Y. (2004) Visualization of spatially and temporally regulated N-WASP activity during cytoskeletal reorganization in living cells. Proc. Natl. Acad. Sci. U. S. A. **101**, 970–4.

237 Llères, D., James, J., Swift, S., Norman, D. G. and Lamond, A. I. (2009) Quantitative analysis of chromatin compaction in living cells using FLIM-FRET. J. Cell Biol. **187**, 481–96.

238 Gambin, Y. and Deniz, A. A. (2010) Multicolor single-molecule FRET to explore protein folding and binding. Mol. Biosyst. **6**, 1540–7.

239 Keller, B. G., Kobitski, A., Jäschke, A., Nienhaus, G. U. and Noé, F. (2014) Complex RNA folding kinetics revealed by single-molecule FRET and hidden Markov models. J. Am. Chem. Soc. **136**, 4534–43.

240 Zal, T. (2008) Visualization of protein interactions in living cells. Adv. Exp. Med. Biol. **640**, 183–97.

241 Padilla-Parra, S. and Tramier, M. (2012) FRET microscopy in the living cell: different approaches, strengths and weaknesses. Bioessays **34**, 369–76.

242 Becker, W. (2012) Fluorescence lifetime imaging--techniques and applications. J. Microsc. **247**, 119–36.

243 Luchowski, R., Gryczynski, Z., Sarkar, P., Borejdo, J., Szabelski, M., Kapusta, P. and Gryczynski, I. (2009) Instrument response standard in time-resolved fluorescence. Rev. Sci. Instrum., AIP Publishing **80**, 033109.

244   Zacharias, D. a, Violin, J. D., Newton, A. C. and Tsien, R. Y. (2002) Partitioning of lipid-modified monomeric GFPs into membrane microdomains of live cells. Science **296**, 913–6.

245   Keller, P. and Simons, K. (1998) Cholesterol is required for surface transport of influenza virus hemagglutinin. J. Cell Biol. **140**, 1357–67.

246   Kordyukova, L. V., Serebryakova, M. V., Polyansky, A. a., Kropotkina, E. a., Alexeevski, A. V., Veit, M., Efremov, R. G., Filippova, I. Y. and Baratova, L. a. (2011) Linker and/or transmembrane regions of influenza A/Group-1, A/Group-2, and type B virus hemagglutinins are packed differently within trimers. Biochim. Biophys. Acta - Biomembr., Elsevier B.V. **1808**, 1843–1854.

247   Rizzo, M. A., Springer, G. H., Granada, B. and Piston, D. W. (2004) An improved cyan fluorescent protein variant useful for FRET. Nat. Biotechnol. **22**, 445–9.

248   Ho, S. N., Hunt, H. D., Horton, R. M., Pullen, J. K. and Pease, L. R. (1989) Site-directed mutagenesis by overlap extension using the polymerase chain reaction. Gene **77**, 51–9.

249   Stockmann-Juvala, H. and Savolainen, K. (2008) A review of the toxic effects and mechanisms of action of fumonisin B1. Hum. Exp. Toxicol. **27**, 799–809.

250   Laemmli, U. K. and Quittner, S. F. (1974) Maturation of the head of bacteriophage T4. IV. The proteins of the core of the tubular polyheads and in vitro cleavage of the head proteins. Virology **62**, 483–99.

251   Dunn, K. W., Kamocka, M. M. and McDonald, J. H. (2011) A practical guide to evaluating colocalization in biological microscopy. Am. J. Physiol. Cell Physiol. **300**, C723–42.

252   Engel, S., de Vries, M., Herrmann, A. and Veit, M. (2012) Mutation of a raft-targeting signal in the transmembrane region retards transport of influenza virus hemagglutinin through the Golgi. FEBS Lett. **586**, 277–82.

253   Engel, S. V. (2008) Assembly von Influenzaviren : Analyse von Protein-Protein- und Protein-Lipid- Interaktionen mittels biochemischer und biophysikalischer Methoden, Humboldt-Universität zu Berlin.

254   Lowe, S. L., Peter, F., Subramaniam, V. N., Wong, S. H. and Hong, W. (1997) A SNARE involved in protein transport through the Golgi apparatus. Nature **389**, 881–4.

255 Hay, J. C., Klumperman, J., Oorschot, V., Steegmaier, M., Kuo, C. S. and Scheller, R. H. (1998) Localization, dynamics, and protein interactions reveal distinct roles for ER and Golgi SNAREs. J. Cell Biol. **141**, 1489–502.

256 Tatulian, S. A. and Tamm, L. K. (2000) Secondary structure, orientation, oligomerization, and lipid interactions of the transmembrane domain of influenza hemagglutinin. Biochemistry **39**, 496–507.

257 Mineev, K. S., Lyukmanova, E. N., Krabben, L., Serebryakova, M. V, Shulepko, M. A., Arseniev, A. S., Kordyukova, L. V and Veit, M. (2013) Structural investigation of influenza virus hemagglutinin membrane-anchoring peptide. Protein Eng. Des. Sel. **26**, 547–52.

258 De Vries, M., Herrmann, A. and Veit, M. (2015) A cholesterol consensus motif is required for efficient intracellular transport and raft association of a group 2 HA from influenza virus. Biochem. J. **465**, 305–14.

259 Nobusawa, E., Aoyama, T., Kato, H., Suzuki, Y., Tateno, Y. and Nakajima, K. (1991) Comparison of Complete Amino Acid Sequences among 13 Serotypes of Hemagglutinins and Receptor-Binding Properties of Influenza A Viruses Indirect immunofluorescence. Virology **485**, 475–485.

260 Jou, W., Verhoeyen, M., Devos, R., Saman, E., Fang, R., Huylebroeck, D., Fiers, W., Threlfall, G., Barber, C. and Carey, N. (1980) Complete structure of the hemagglutinin gene from the human influenza A/Victoria/3/75 (H3N2) strain as determined from cloned DNA. Cell **19**, 683–696.

261 Lin, S. (1998) Mutations in the Middle of the Transmembrane Domain Reverse the Polarity of Transport of the Influenza Virus Hemagglutinin in MDCK Epithelial Cells. J. Cell Biol. **142**, 51–57.

262 Schwarzer, R., Levental, I., Gramatica, A., Scolari, S., Buschmann, V., Veit, M. and Herrmann, A. (2014) The cholesterol-binding motif of the HIV-1 glycoprotein gp41 regulates lateral sorting and oligomerization. Cell. Microbiol.

263 Garten, W., Will, C., Buckard, K., Kuroda, K., Ortmann, D., Munk, K., Scholtissek, C., Schnittler, H., Drenckhahn, D. and Klenk, H. D. (1992) Structure and assembly of hemagglutinin mutants of fowl plague virus with impaired surface transport. J. Virol. **66**, 1495–505.

264 Simpson, D. A. and Lamb, R. A. (1991) Influenza virus ts61S hemagglutinin is significantly defective in polypeptide folding and intracellular transport at the permissive temperature. Virology **185**, 477–483.

265   Rodriguez-Boulan, E., Paskiet, K. T., Salas, P. J. and Bard, E. (1984) Intracellular transport of influenza virus hemagglutinin to the apical surface of Madin-Darby canine kidney cells. J. Cell Biol. **98**, 308–19.

266   Tafesse, F. G., Sanyal, S., Ashour, J., Guimaraes, C. P., Hermansson, M., Somerharju, P. and Ploegh, H. L. (2013) Intact sphingomyelin biosynthetic pathway is essential for intracellular transport of influenza virus glycoproteins. Proc. Natl. Acad. Sci. U. S. A. **110**, 6406–11.

267   Yamaoka, S., Miyaji, M., Kitano, T., Umehara, H. and Okazaki, T. (2004) Expression cloning of a human cDNA restoring sphingomyelin synthesis and cell growth in sphingomyelin synthase-defective lymphoid cells. J. Biol. Chem. **279**, 18688–93.

268   Carette, J. E., Guimaraes, C. P., Wuethrich, I., Blomen, V. A., Varadarajan, M., Sun, C., Bell, G., Yuan, B., Muellner, M. K., Nijman, S. M., et al. (2011) Global gene disruption in human cells to assign genes to phenotypes by deep sequencing. Nat. Biotechnol. **29**, 542–6.

269   Bonnon, C., Wendeler, M. W., Paccaud, J.-P. and Hauri, H.-P. (2010) Selective export of human GPI-anchored proteins from the endoplasmic reticulum. J. Cell Sci. **123**, 1705–1715.

270   Sharpe, H. J., Stevens, T. J. and Munro, S. (2010) A comprehensive comparison of transmembrane domains reveals organelle-specific properties. Cell **142**, 158–69.

271   Munro, S. (1995) An investigation of the role of transmembrane domains in Golgi protein retention. EMBO J. **14**, 4695–704.

272   Sampaio, J. L., Gerl, M. J., Klose, C., Ejsing, C. S., Beug, H., Simons, K. and Shevchenko, A. (2011) Membrane lipidome of an epithelial cell line. Proc. Natl. Acad. Sci. U. S. A. **108**, 1903–7.

273   Zacchetti, D., Peränen, J., Murata, M., Fiedler, K. and Simons, K. (1995) VIP17/MAL, a proteolipid in apical transport vesicles. FEBS Lett. **377**, 465–9.

274   Cheong, K. H., Zacchetti, D., Schneeberger, E. E. and Simons, K. (1999) VIP17/MAL, a lipid raft-associated protein, is involved in apical transport in MDCK cells. Proc. Natl. Acad. Sci. U. S. A. **96**, 6241–8.

275   Schuck, S. and Simons, K. (2004) Polarized sorting in epithelial cells: raft clustering and the biogenesis of the apical membrane. J. Cell Sci. **117**, 5955–64.

276   Guerriero, C. J., Lai, Y. and Weisz, O. A. (2008) Differential Sorting and Golgi Export Requirements for Raft-associated and Raft-independent Apical Proteins along the Biosynthetic Pathway. J. Biol. Chem. **283**, 18040–18047.

277   Fantini, J. and Barrantes, F. J. (2013) How cholesterol interacts with membrane proteins: an exploration of cholesterol-binding sites including CRAC, CARC, and tilted domains. Front. Physiol., Frontiers **4**, 31.

278   Wandinger-Ness, A., Bennett, M. K., Antony, C. and Simons, K. (1990) Distinct transport vesicles mediate the delivery of plasma membrane proteins to the apical and basolateral domains of MDCK cells. J. Cell Biol. **111**, 987–1000.

279   Yoshimori, T., Keller, P., Roth, M. G. and Simons, K. (1996) Different biosynthetic transport routes to the plasma membrane in BHK and CHO cells. J. Cell Biol. **133**, 247–56.

280   Müsch, A., Xu, H., Shields, D. and Rodriguez-Boulan, E. (1996) Transport of vesicular stomatitis virus G protein to the cell surface is signal mediated in polarized and nonpolarized cells. J. Cell Biol. **133**, 543–58.

281   Ge, M. and Freed, J. H. (2011) Two conserved residues are important for inducing highly ordered membrane domains by the transmembrane domain of influenza hemagglutinin. Biophys. J. **100**, 90–7.

282   Polozov, I. V, Bezrukov, L., Gawrisch, K. and Zimmerberg, J. (2008) Progressive ordering with decreasing temperature of the phospholipids of influenza virus. Nat. Chem. Biol. **4**, 248–55.

283   Eeman, M. and Deleu, M. (2010) From biological membranes to biomimetic model membranes **14**, 719–736.

284   Lowen, A. C., Mubareka, S., Steel, J. and Palese, P. (2007) Influenza virus transmission is dependent on relative humidity and temperature. PLoS Pathog. **3**, 1470–6.

285   Sun, X. and Whittaker, G. R. (2003) Role for influenza virus envelope cholesterol in virus entry and infection. J. Virol. **77**, 12543–51.

286   Biswas, S., Yin, S.-R., Blank, P. S. and Zimmerberg, J. (2008) Cholesterol promotes hemifusion and pore widening in membrane fusion induced by influenza hemagglutinin. J. Gen. Physiol. **131**, 503–13.

287   Kuzmin, P. I., Zimmerberg, J., Chizmadzhev, Y. A. and Cohen, F. S. (2001) A quantitative model for membrane fusion based on low-energy intermediates. Proc. Natl. Acad. Sci. U. S. A. **98**, 7235–40.

288   Danieli, T., Pelletier, S. L., Henis, Y. I. and White, J. M. (1996) Membrane fusion mediated by the influenza virus hemagglutinin requires the concerted action of at least three hemagglutinin trimers. J. Cell Biol. **133**, 559–69.

289   Blumenthal, R., Sarkar, D. P., Durell, S., Howard, D. E. and Morris, S. J. (1996) Dilation of the influenza hemagglutinin fusion pore revealed by the kinetics of individual cell-cell fusion events. J. Cell Biol. **135**, 63–71.

290   Markovic, I., Leikina, E., Zhukovsky, M., Zimmerberg, J. and Chernomordik, L. V. (2001) Synchronized activation and refolding of influenza hemagglutinin in multimeric fusion machines. J. Cell Biol. **155**, 833–44.

291   Bentz, J. and Mittal, A. (2003) Architecture of the influenza hemagglutinin membrane fusion site. Biochim. Biophys. Acta - Biomembr. **1614**, 24–35.

292   Parasassi, T., De Stasio, G., d'Ubaldo, a and Gratton, E. (1990) Phase fluctuation in phospholipid membranes revealed by Laurdan fluorescence. Biophys. J. **57**, 1179–86.

293   Kaiser, H.-J., Lingwood, D., Levental, I., Sampaio, J. L., Kalvodova, L., Rajendran, L. and Simons, K. (2009) Order of lipid phases in model and plasma membranes. Proc. Natl. Acad. Sci. U. S. A. **106**, 16645–50.

294   Wheeler, G. and Tyler, K. M. (2011) Widefield microscopy for live imaging of lipid domains and membrane dynamics. Biochim. Biophys. Acta, Elsevier B.V. **1808**, 634–41.

295   Grouleff, J., Irudayam, S. J., Skeby, K. K. and Schiøtt, B. (2015) The influence of cholesterol on membrane protein structure, function, and dynamics studied by molecular dynamics simulations. Biochim. Biophys. Acta **1848**, 1783–1795.

296   Sarkisyan, K. S., Yampolsky, I. V, Solntsev, K. M., Lukyanov, S. A., Lukyanov, K. A. and Mishin, A. S. (2012) Tryptophan-based chromophore in fluorescent proteins can be anionic. Sci. Rep., Nature Publishing Group **2**, 608.

297   Kremers, G.-J., Goedhart, J., van Munster, E. B. and Gadella, T. W. J. (2006) Cyan and yellow super fluorescent proteins with improved brightness, protein folding, and FRET Förster radius. Biochemistry, American Chemical Society **45**, 6570–80.

298 Goedhart, J., van Weeren, L., Hink, M. A., Vischer, N. O. E., Jalink, K. and Gadella, T. W. J. (2010) Bright cyan fluorescent protein variants identified by fluorescence lifetime screening. Nat. Methods, Nature Publishing Group **7**, 137–9.

299 Nagai, T., Ibata, K., Park, E. S., Kubota, M., Mikoshiba, K. and Miyawaki, A. (2002) A variant of yellow fluorescent protein with fast and efficient maturation for cell-biological applications. Nat. Biotechnol. **20**, 87–90.

300 Markwardt, M. L., Kremers, G.-J., Kraft, C. A., Ray, K., Cranfill, P. J. C., Wilson, K. A., Day, R. N., Wachter, R. M., Davidson, M. W. and Rizzo, M. A. (2011) An improved cerulean fluorescent protein with enhanced brightness and reduced reversible photoswitching. PLoS One **6**, e17896.

301 Goedhart, J., von Stetten, D., Noirclerc-Savoye, M., Lelimousin, M., Joosen, L., Hink, M. A., van Weeren, L., Gadella, T. W. J. and Royant, A. (2012) Structure-guided evolution of cyan fluorescent proteins towards a quantum yield of 93%. Nat. Commun. **3**, 751.

302 Dietrich, C., Bagatolli, L. a, Volovyk, Z. N., Thompson, N. L., Levi, M., Jacobson, K. and Gratton, E. (2001) Lipid rafts reconstituted in model membranes. Biophys. J. **80**, 1417–28.

303 Kalvodova, L., Sampaio, J. L., Cordo, S., Ejsing, C. S., Shevchenko, A. and Simons, K. (2009) The lipidomes of vesicular stomatitis virus, semliki forest virus, and the host plasma membrane analyzed by quantitative shotgun mass spectrometry. J. Virol. **83**, 7996–8003.

304 Lorizate, M., Brügger, B., Akiyama, H., Glass, B., Müller, B., Anderluh, G., Wieland, F. T., Kräusslich, H.-G., Bru, B., Mu, B., et al. (2009) Probing HIV-1 membrane liquid order by Laurdan staining reveals producer cell-dependent differences. J. Biol. Chem. **284**, 22238–47.

Publications

de Vries M., Herrmann A. & Veit M.; A cholesterol consensus motif is required for efficient intracellular transport and raft association of a group 2 HA of influenza virus. Biochem. J. (2014) Immediate Publication, doi:10.1042/BJ20141114

de Vries M.*, Engel S.*, Herrmann A. & Veit M.; Mutation of a raft-targeting signal in the transmembrane region retards transport of influenza virus hemagglutinin through the Golgi. * Both authors contributed equally to this work. FEBS Lett. (2012), doi:10.1016/j.febslet.2012.01.002

Damiani AM., **de Vries M.**, Reimers G., Winkler S., Osterrieder N.; A severe equine herpesvirus type 1 (EHV-1) abortion outbreak caused by a neuropathogenic strain at a breeding farm in northern Germany. Vet Microbiol. (2014) Aug 27;172(3-4):555-62. doi: 10.1016/j.vetmic.2014.06.023.

Lang A., **de Vries M.**, Feineis S., Müller E., Osterrieder N., Damiani AM.; Development of a peptide ELISA for discrimination between serological responses to equine herpesvirus type 1 and 4. Journal of Virological Methods *193 (2013) 667– 673*

Talks

de Vries M., Engel S., Herrmann A. & Veit M.; Deletion of a raft targeting signal in the transmembrane region retards transport of influenza virus HA through the Golgi; 21st Annual meeting of the Society for Virology, Freiburg, Germany, 2011

de Vries M., Klenk H.D. & Veit M.; The use of Laurdan to analyze the fluidity of viral membranes with fluorescence spectroscopy, Young scientist workshop "Methods to study influenza virus", FU Berlin as part of the german-russion year of science, 2011

Poster

de Vries M., Herrmann A. & Veit M.; Mutation of a putative Cholesterol Consensus Motif (CCM) of Influenza virus HA retards transport through the Golgi and affects association with membrane rafts; 25th Annual meeting of the Society for Virology, 2014

de Vries M., Engel S., Herrmann A. & Veit M.; Studying association of Influenza Hemagglutinin with membrane rafts, International symposium: 4th European Congress of Virology, 2010

de Vries M., Engel S., Herrmann A. & Veit M.; Studying association of influenza virus HA with membrane-rafts in the Golgi and at the cell surface; International symposium: Membranes and Modules, Berlin, Deutschland, 2009

_____   _____
(Ort, Datum)   (Maren de Vries)

Eidesstattliche Erklärung

Hiermit erkläre ich, die vorliegende Arbeit selbstständig und ohne fremde Hilfe verfasst und nur die angegebene Literatur verwendet zu haben. Alle Stellen, die dem Wortlaut oder dem Sinn nach anderen Werken entnommen sind, sind nach bestem Wissen und Gewissen durch Angabe der Quellen kenntlich gemacht worden.

Die Ergebnisse, die durch Stepahnie Engel erzielt wurden, sind entsprechend gekennzeichnet.

Ich besitze keinen entsprechenden Doktorgrad und hab mich nicht anderwärts um einen solchen beworben.

Die dem Promotionsverfahren zugrunde liegende Promotionsordnung ist mir bekannt.

_____   _____
(Ort, Datum)   (Maren de Vries)